Design of an evacuated flat plate collector driven double effect solar absorption chiller for Automobile Lab of IUT, Gazipur, Bangladesh.

Department of Mechanical and Chemical Engineering

Islamic University of Technology (IUT)

Adnan Saif, Faisal Jamil, Md Munzir Khan

Abstract

Conventional vapor compression air conditioning systems are notorious for their greenhouse gas emissions and ozone depletion effect along with high energy consumption rate. Implementing new environment friendly and sustainable technologies in this field has become an area of interest for researchers across the globe. Solar absorption cooling(SAC) systems have the potential to be considered as the leading technologies for air conditioning today, as they utilize harmless working fluids and can be used alongside conventional systems for better economic performance. In the recent studies, SAC systems have proved to be environment friendly, economically viable and energy efficient.

In this study, an absorption air conditioning system has been designed and simulated for one of our laboratories in IUT (Islamic University of Technology), which is situated in Gazipur, Bangladesh. Analyzing the hourly solar radiation data and the overall climatic conditions of Bangladesh, and following the recent literature, the combination of Double-effect absorption chiller and Evacuated Flat Plate Collector was selected. By conducting regression analysis on a commercially available chiller, a double effect system was designed to meet the cooling demands of the laboratory. Python code was developed for simulating the results of the designed system, which indicated that 75% of the annual cooing demand could be supplied solely by solar energy if the system is incorporated, while relying on an auxiliary source for fulfilling the remaining 25%.

Despite moderate amount of solar irradiation throughout the calendar year, there has been very limited research for the prospects of SAC systems in Bangladesh. The objective of this study was to design an overall system that is well suited for the existing conditions in Bangladesh and pave the way for future research in this field for further improvements and modifications.

Contents

List of Figures

List of Tables

Nomenclature

Re Reynold number
Nu_{cf} Nusselt number for laminar flow, constant heat flux boundy
Po Poiseulle number
f friction coefficient
L passage length
B breadth of collector plate
A_c collector top surface area
$\dot{m}$ total mass flow rate
Q_u rate of heat extraction by fluid
G_T total (beam and diffuse) irradiance from Sun
S solar power absorbed by the collector, per square meter
U_L overall collector heat loss coefficient
T_a ambient temperature
T_i fluid temperature at inlet to collector
T_o fluid temperature at outlet from collector
T_{pm} collector plate mean surface temperature
ΔT_h temperature deifference driving convective heat transfer
$\Delta \bar{T}_f$ temperature rise of fluid (mean along the passage)
W_p fluid pumping power(frictional dissipation through the collector)
D_h hydraulic diameter
P pitch of circular passages
R hydraulic diameter to pitch ratio for circular passages
F_R heat recovery factor
μ fluid dynamic viscosity
ρ fluid density
η_i efficiency of collector
$\tau\alpha$ effective transmittance-absorptance product
τ tansmittance value
α absorptance value
β solar collector tilt angle
b subscript represent beam
d subscript represent diffuse
g subscript represent ground
ρ_g ground reflectance
I total (beam and diffuse) radiation
I_b beam radiation

I_d diffuse radiation
R_b ration of beam isotropic radiation on tilted surface to that on horizontal surface
ϕ latitude
δ declination
γ surface azimuth angle
ω hour angle
θ angle of incidence
θ_z zenith angle
α_s solar altitude angle
γ_s solar azimuth angle
F_l Load Factor
n Number of lights
q_iTotal lamp wattage
F_u raction of $q_i inuse$
F_s Special ballast allowance factor for fluorescent fixtures CLF Cooling load factor
m_v Mass flow rate of ventilated air
h_{fg} latent heat of vaporization of water
Cp_m Average specific heat of moist air
$T_o Outdoordrybulbtemperature$
$T_i Indoordrybulbtemperature$
$W_o OutdoorHumidityRatio$
$W_i IndoorHumidityRatio$
V_o Volumetric flow rate of outdoor air
ρ_o Specific Volume of outdoor air
U Design Heat Transmission Coefficients
K Color adjustment factor
LM Latitude-month correction
f Factor for atic fan and ducts

Chapter 1

Introduction

1.1 Problem Statement

In today's world, as human beings have started to become more aware of the environmental hazard caused by non-renewable sources of energy, the global energy market is still widely dependent on fossil fuel based energy production. Harmful emissions in form of greenhouse gases and chlorine based refrigerants are being taken into account for their disastrous impact on the climate and have led the scientists and researchers to work on developing new ways of cleaner energy production. However, renewable sources only contribute about 7% of the global energy generation, while 87% still relies on fossil fuels like coal, oil and natural gas. The increasing global energy demand and CO_2 emission is expected to increase almost 60% by 2030 in comparison to the beginning of this century. The European Union (EU) energy import dependency is expected to increase approximately 70% by 2030 which was 50% in 2000 [1]

Conventional refrigeration and air-conditioning are two of the systems, which have been identified to have a large impact on the environment in terms of its contribution to global warming. This is because of three main reasons. Firstly, they account for no less than 15% of world energy consumption[2] due to their widespread use. Secondly, the type of refrigerant gases such as CFC, which are used for the purpose of cooling, will be harmful to the environment in case of leakage and this aggravates the depletion of the ozone layer. Thirdly, the utilization of a large amount of energy by these systems makes them a major contributor to the emission of high amount of carbon dioxide in the air. Till now the biggest contributor is the electrical energy being generated by generators, which utilizes fossil fuel.

For these reasons, many organizations around the world such as International Institute of Refrigeration have come to conclude that an immediate action has to be taken to reduce direct emission of greenhouse gases introduced by cooling and refrigerant plants to 50% in the year 2020 and a new system should be designed and employed in the aim of reduction of energy consumption of refrigerant plants by 30-50% during the same period.

1.2 Motivation

Nowadays, the most common air conditioning systems are based on the vapour compression cycle using electrically driven compressors which are responsible for the highest proportion of the total consumption of HVAC system. Electricity consumption of an HVAC system is strongly related to the intensity of solar radiation, as the demand for cooling obviously increases in proportion to irradiation. Due to the carbon content of the fuel used to produce the electricity, this electricity consumption in the end increases the CO_2 emission in the air, which is one of the main causes of global warming.

A system that relates the cooling output to the heating input is well suited to be used as an alternative to current cooling technologies. Research is therefore being carried out on solar cooling air conditioning systems that use mostly solar thermal power to drive the cooling cycle instead of electricity.
In a solar cooling system the thermal energy from the sun is transformed into cooling. This can be done in two different ways:

- by using an adsorption cycle through a solid adsorber [3], which adsorbs water (refrigerant) at a lower temperature and releases heat by water desorption; or
- by an absorption cycle through a liquid absorber [4] which mixes with the refrigerant at a lower temperature and releases heat at a higher temperature.

The absorption and adsorption machines for purposes of refrigeration or air conditioning systems are currently the subjects of renewed interest after a period during which attention was directed mainly to vapour compression machines, characterized by a greater Coefficient Of Performance (COP). This interest is triggered especially by the limited availability of electric power in remote areas [5] [6]. Studies report that absorption systems are more suitable for air conditioning applications, while adsorption systems are more suitable for low temperature purposes.

Absorption cooling systems have been most frequently adopted for solar cooling for several reasons. First of all, it requires very low or no electric input. Secondly, for the same capacity, the physical dimension of an absorption machine is smaller than for solid sorption machines due to the high heat transfer coefficient of the liquid sorbent, i.e. absorbent. Besides, the fluidity of the absorbent gives greater flexibility in realizing a more compact and/or efficient machine. Finally and perhaps the most importantly, because absorption cooling had already established its position in air conditioning industry, the well developed sorption community supported its application in solar cooling by providing expertise in operation and manufacturing.

In this project, solar radiation is utilized in solar collectors to heat water. Thermal storage tanks can hold this high temperature water, similar to a domestic hot water tank, until needed by the system. This provides necessary heat during off-peak hours at night. The solar heated water provides the driving energy of a water-fired absorption chiller. This unit eliminates the need of a mechanical, electrical compressor. Instead the process is driven by heat

In designing and completing this project, the new application of existing technologies will reduce the need of fossil fuel generated power, and therefore, decrease the impact of energy consumption and the use of harmful materials and depleting energy sources. Due to the energy efficiency and reduction in consumption, the absorption chiller is an appropriate system to build on.

1.3 Solar Absorption Cooling

Absorption cooling is one of the first and oldest forms of air-conditioning and refrigeration systems used. The system uses thermal energy to produce cooling and thus solar energy, waste heat and other forms of low grate heat can be employed. As no CFCs are used, absorption systems are friendlier to the environment. Absorption is the process of attracting and holding moisture by substances called desiccants. Desiccants are sorbent materials that have an ability to attract and hold other gases or liquids and have a particular affinity for water. During absorption the desiccant undergoes a chemical change as it takes in the moisture, for example, table salt, which changes from a solid to a liquid as it absorbs the moisture. The characteristics of the binding of desiccants to moisture make the desiccants very useful in chemical separation processes [7]. Absorption air-conditioning systems are similar to vapor compression air-conditioning systems, but differ in the pressurization stages. In general an absorbent in the low pressure side absorbs an evaporating refrigerant (H_2O). The most usual combinations of chemical fluids used include lithium bromide–water ($LiBr$–H_2O), where water vapor is the refrigerant, and ammonia–water (NH_3–H_2O) system where ammonia is the refrigerant.

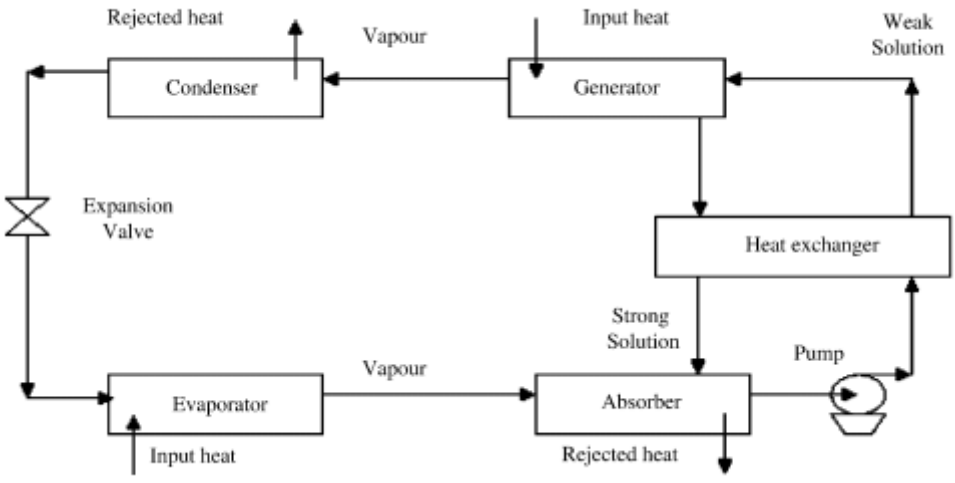

Figure 1.1: The basic principle of the absorption air-conditioning system

The basic energy flows of a solar-powered cooling system are shown schematically in Fig. 1.1. The collector receives energy from sunlight. The energy is then transferred through high temperature energy storage reservoir to the refrigeration system. In the

absorption system, heat is taken from the evaporator or cold storage reservoir (from the water that flows in the evaporator and comes out as chilled water), which evaporate the refrigerant as water vapor. The water vapor then passes into the absorber and is being absorbed by the lithium bromide in the absorber to form a weak solution. The weak solution is then pumped into the generator. In the generator, the water from the weak solution is separated to form water vapor and strong lithium bromide solution. The generator requires heat from the solar collector system to separate the water vapor from the solution. The water vapor thus generated is at high temperature and pressure. It is then passed to the condenser where heat is removed and the vapor cools down to form a liquid. The liquid water at high pressure is passed through the expansion valve to the low-pressure area in the evaporator where the water is turned into vapor again by drawing heat from the entering water in the tube heat exchanger. The vapor then passes to the absorber again and the process is repeated. The strong solution from the generator is pumped through a heat exchanger to the absorber and the weak solution from the absorber is passed through the same heat exchanger to the generator. The heat is removed from the system by cooling water, which passes through the condenser and the absorber to a cooling tower where the heat is dissipated to the environment. In the case that the sun is not shining, the generator heating energy may be supplied from an auxiliary heat source such as electricity or conventional boiler to run the system.

Chapter 2

Literature Review

The first absorption system was developed by Edmond Carre in 1850, which incorporated water and sulphuric acid [8]. The first commercial absorption unit was patented by Ferdinand Carre in 1860, soon after he discovered how to achieve refrigeration by using water and Ammonia together [8]. In the early 20th century, absorption systems started to get commercialized in the market, and $LiBr - H_2O$ chillers were mostly manufactured and marketed by Americans till the 1960's [9].

After the global consensus of scientists and researchers on using Renewable energy for tackling climate change and associated environmental factors, there has been an increasing trend of using solar cooling technologies for air conditioning demands. Since the correlation between the cooling demand and the availability of solar radiation are synchronous, more and more forms of solar cooling technologies have been introduced in the market since the eighties [10] and there are numerous options available commercially at present [2].

Solar cooling has been studied with great care by researchers across the globe, and almost 50 years of the past literature has marked significant improvements and innovations to move this technology forward. Absorption chillers are considered to be the most effective and reliable technology for using solar thermal energy in air conditioning applications, for their high efficiency, low cost compared to other technologies, and wide range of applications[11].Thermal sorption systems are concluded to be more economical compared to electric and thermo-mechanical systems. Although absorption and adsorption systems are close in terms of performance, absorption systems are significantly cheaper and less space-consuming compared to adsorption systems [12].

Among different types of working fluids used in absorption chillers, $LiBr - H_2O$ pair is most commonly used for air conditioning purposes, where $LiBr$ is the absorbent and H_2O is the refrigerant [11]. The other most widely used working pair is the $NH_3 - H_20$ which is mostly used for refrigeration purposes. At the same driving temperatures, $LiBr - H_2O$ pair achieves a higher Coefficient of Performance (COP) than $NH_3 - H_2O$ pair and the former is also preferable for it's non-volatile absorbent (LiBr) compared to highly volatile H_2O in the latter. $NH_3 - H_2O$ systems also require very high driving temperatures (125–170 °C) which is not always achievable solely from solar radiation for many loca-

tions [13] [14].

There are three types of $LiBr$ absorption chillers currently available on the market - half effect, single effect, double effect and triple effect chillers. Higher effect chillers have higher COP compared to single effect chillers, but they require higher driving temperatures. So, double and triple effect chillers are advantageous when a high temperature heat source is available [11]. Single effect chillers have a COP of around 0.7 and the driving heat source temperature is about 80-100°C . On the other hand double effect chillers require driving temperatures up to 180-200°C and can provide a COP of around 1.4 [15].

Single-effect $LiBr - H_2O$ chiller, the most popular machine in solar cooling for its low- temperature operability, has been incorporated in numerous studies including the following demonstration projects:

A research group started a series of researches on solar absorption cooling by designing and optimizing solar heating and cooling systems for several locations [7]. One of their conclusions was that a combined heating and cooling system was more economical than a heating alone system in most locations. A solar house with a combined cooling and heating system based on a single-effect $LiBr - H_2O$ chiller was investigated in a university campus[16]. Hattem and Dato [17] installed a solar absorption coolg system in Ispra, Italy, which consisted of a 4.6kW $LiBr - H_2O$ chiller and $36m^2$ flat plate collectors. They reported theoretical and experimental results were in good agreement and the measured seasonal average of the chiller COP and the overall cooling efficiency were 0.54 and 9.6% respectively.

Al-Karaghouli et al [18] reported the operation results of a solar cooling system installed at the Solar Energy Research Center in Iraq, which was considered the largest solar cooling system at the time. The system was equipped with two 60 ton $LiBr - H_2O$ chillers, 1577 evacuated tube collectors and various backup systems. They reported daily average collector efficiency of 49%, chiller COP 0.62 and solar fraction of 60.4%.

Best and Ortega[19] summarized the results of Sonntlan Mexicali Solar Cooling project from 1983 to 1986 in Mexico. The solar cooling system included six single-family houses, 316 m^2 flat plate collectors, $30m^3$ heat storage, a 90kW ARKLA-WFB 300 Solaire $LiBr - H_2O$ chiller and a 200 KW cooling tower. After a series of improvements on the solar collector system, the system managed to deliver enough cooling power that improved the yearly solar fraction up to 75%. COP of the absorption chiller varied from 0.53 to 0.73 when hot water was provided at the temperatures between 75 to 95 °C.

Izquierdo et al [20] reported the performance of a $LiBr - H_2O$ chiller with 35KW nominal cooling capacity driven by hot water from $49.9m^2$ flat plate collectors installed at a typical Spanish house in Madrid. Since the solar system was originally designed for 10 KW cooling capacity, the absorption chiller operated far away from its nominal working condition and yielded the maximum cooling capacity of only 7.5KW at the average COP

of 0.34.

Storkenmaier et al [21] reported the development of a 10KW water-cooled single-effect $LiBr - H_2O$ chiller. The machine was reported capable of producing 15°C chilled water from 85°C hot water with the COP 0.74 being cooled by cooling water at 27 °C. The design chilled water temperature was set rather high at 15°C for the use of chilled ceilings. The cooling capacity was reported to vary between 40 to 160% of the nominal capacity with the hot water temperature increasing from 56 to 105°C. The design was improved for launching in the market in 2007 by the German company Phönix.

Safarik et al (2005) presented the performance data of a water-cooled single-effect $LiBr - H_2O$ chiller. The machine produced about 16KW cooling at 15°C at the COP 0.75 with 90°C hot water and 32°C cooling water. With 27°C cooling water, COP increased to 0.8 and 80°C hot water was enough to produce the same cooling capacity. This machine is currently being field-tested in various locations in Europe by the German company EAW.

Double-effect $LiBr - H_2O$ machines were also used in a few solar cooling projects. Due to the requirement of a high driving temperature (ca. 150°C), in most cases, the hot water from solar collectors was fed to the low-temperature generator of a double-effect machine (Ishibashi, 1979; Lamp and Ziegler, 1998). This system has a merit of alternatively operating the system in a single-effect cycle with solar heat or in a double-effect cycle with the heat from fuel combustion so that it can achieve a high seasonal efficiency. It is also possible to drive a double-effect machine solely with solar heat when a concentrating solar collector is used. Lokurlu and Müller [22] reported a system installed at a hotel in Turkey, which consisted of a steam-driven double-effect machine, a trough type parabolic solar collector and a backup steam boiler. The trough collector with $180m^2$aperture area heated pressurized water up to 180°C and this water in turn generated 144°C steam (4bar) for a 140kW double-effect $LiBr - H_2O$ chiller.

The most commonly used solar thermal collectors in case of single effect systems are flat plate collectors (FPC) or evacuated tube collectors (ETC) [23] [24]. The main drawback in single effect systems is the low COP and the large collector area required for providing the thermal energy demand. That is why double effect chillers coupled with concentrating solar collectors are becoming more and more popular [25]. However, concentrating collectors are not always appropriate in climatic zones where the direct normal irradiance (DNI) is low [26]. Very recently, a new kind of collector, called Evacuated flat plate collectors (EFPC) have been invented that can capture both beam and diffuse radiation and generate temperatures up to 200°C without concentration [27] A recent study found out that the combination of Double effect chiller with Evacuated Flat plate collector (EFPC) achieves a good energetic and economic performance in a wide variety of climatic conditions. This is because it can simultaneously benefit from the relatively higher COP of double effect chiller and the utilization of diffuse radiation opposed to concentrating collectors that can only utilize beam radiation [28].

Chapter 3

Solar Collector

3.1 The Sun and The Solar Radiation

All the planets orbit, the only star of the solar system located at its center, the sun. Solar energy is the primary source of energy received by earth from the sun in the form of solar radiation. This energy supports almost all life on earth providing energy for photosynthesis and driving the earth's climate and weather.

The sun is an effective black body, with a temperature of approximately 5778 K or 5505 ^oC, made up of about 74% hydrogen, 25% helium and the rest is trace quantities of heavier elements. The temperature gives sun a visible range of white color, which, because of atmospheric scattering, appears yellow. The sun generates its energy by nuclear fusion of hydrogen nuclei to helium. Its structure and characteristics determine the nature of the energy it radiates into space. As seen from the earth, the sun, a sphere of intensely hot gaseous matter with a diameter of 1.39 x 109 m and is, on the average, 1.5 x 1011 m from the earth, rotates on its axis about once every 4 weeks.

Since prehistoric times, human realized that use of solar energy is remunerative and promising. The Greek historian Xenophon records some of the teachings of the Greek philosopher Socrates (470–399 BC), in his "memorabilia", regarding the correct orientation of dwellings to have houses that were cool in summer and warm in winter.

However, many historians believe that Archimedes(287 - 212 BC) did not use mirrors but the shields of soldiers, arranged in a large parabola, for focusing the sun's rays to a common point on a ship. This fact proved that solar radiation could be a powerful source of energy.

Many centuries later, scientists again considered solar radiation as a source of energy, trying to convert it into a usable form for direct utilization. During the eighteenth century, solar furnaces were constructed of polished iron, glass lenses and mirrors, which were capable of melting iron, copper, and other metals. The furnaces were in use throughout Europe and the Middle East. One of the first large-scale applications was the solar furnace built, around 1774, by the well-known French chemist Lavoisier, who constructed

powerful lenses to concentrate solar radiation.

During the past half century, many variations were designed and constructed using focusing collectors as a means of heating the heat-transfer or working fluid that powered mechanical equipment. The two primary solar technologies used are central receivers and distributed receivers employing various point and line focus optics to concentrate sunlight. Central receiver systems use fields of heliostats (two-axis tracking mirrors) to focus the sun's radiant energy onto a single tower-mounted receiver[29]. Distributed receiver technology includes parabolic dishes, Fresnel lenses, parabolic troughs, and special bowls. Parabolic dishes track the sun in two axes and use mirrors to focus radiant energy onto a point focus receiver. Troughs and bowls are line focus tracking reflectors that concentrate sunlight onto receiver tubes along their focal lines. Receiver temperatures range from 100 C in low-temperature troughs to close to 1500 C in dish and central receiver systems[29].

[30]Today, many large solar plants have output in the megawatt range to produce electricity or process heat. The first commercial solar plant was installed in Albuquerque, New Mexico, in 1979. It consisted of 220 heliostats and had an output of 5 MW. The second was erected at Barstow, California, with a total thermal output of 35 MW. Most of the solar plants produce electricity or process heat for industrial use and they provide superheated steam at 673 K. Thus, they can provide electricity or steam to drive small-capacity conventional desalination plants driven by thermal or electrical energy.

Another area of interest, hot water and house heating, appeared in the mid-1930s but gained interest in the last half of the 1940s. Until then, millions of houses were heated by coal-burning boilers. The idea was to heat water and feed it to the radiator system that was already installed.

However, human comfort in extreme or moderate climate regions has never been a ludicrous luxury. With the advent of the first modern air conditioner, in 1902, invented by Willis Haviland Carrier, a skilled engineer who began experimenting with the laws of humidity control to solve an application problem at a printing plant in Brooklyn, NY, the development on cooling technologies inside a closed space started to snowball. There were rapid developments and researches, in the following years, on solar heating and cooling due to their potential to reduce fossil fuel use and to extenuate greenhouse gas emissions in the building sector, which account for approximately 40% of the world energy use. [31]The technologies currently available on the market for thermally driven cooling systems are absorption and adsorption chillers, solid and liquid desiccant cooling systems, and ejector refrigeration cycles. Of these, absorption chillers are considered as the most desirable method for harnessing solar thermal energy due to their relative maturity, reliability, and higher efficiency. In addition, solar absorption chillers can take advantage of economies of scale in large buildings to obtain a relatively good levelized cost of cooling as compared to other thermally-driven air-conditioning systems[31].

3.2 Solar Collectors

Solar energy, being said the cleanest and cheapest form of all energies available on earth, is not certainly in a form that can be readily and easily utilized as desired. To make it available in forms, it is needed to be transferred and transformed, effectively and as efficiently as possible, to acquire the useful maximum output. It is possible to harness the energy from the sun and convert it into either electricity or heat using PV (photo-voltaic) or ST (solar thermal) technologies respectively.

3.2.1 PV (Photovoltaic) Technologies

PV technology uses photo-voltaic cells to receive sunlight and converts solar energy into electricity using a semiconductor material (normally silicon). When light strikes the cell a portion is absorbed within the semiconductor material knocking electrons loose and allowing them to flow. This results in an electric current and thus electricity production. PV panels primarily absorb the visible portion of the light spectrum.

Figure 3.1: Low price mini solar panel 5v 15W mono flexible small solar panel for mobile phone charge.

PV panels are normally connected to an inverter to convert from DC (Direct current) to AC (Alternating current) and subsequently the electricity is fed into the power grid. The PV panels may also directly run devices with DC power. These are commercially

available in different sizes starting from size small enough to power calculators using sunlight to providing electricity in domestic households. The DC electricity can also be stored in batteries.

Standard PV panels are able to convert available sunlight into electricity with optimal conversion efficiency of around 15%, with some panels able to reach as high as 20% (http://www.apricus.com/solar-collection.html.XYiyp0YzaUk).

Figure 3.1 shows commercially available mini solar panel of 5v $15W$ rating, mono flexible small solar panel for charging mobile phone and comes with a cost as high as $7.00 each.

3.2.2 ST (solar thermal) Technologies

Solar thermal panels are referred to by a number of different names such as Solar Water Heater, Solar Hot Water Panel, Solar Hot Water Collector, Solar Thermal Panel or Solar Thermal Collector. These terms all describe the same generic device.

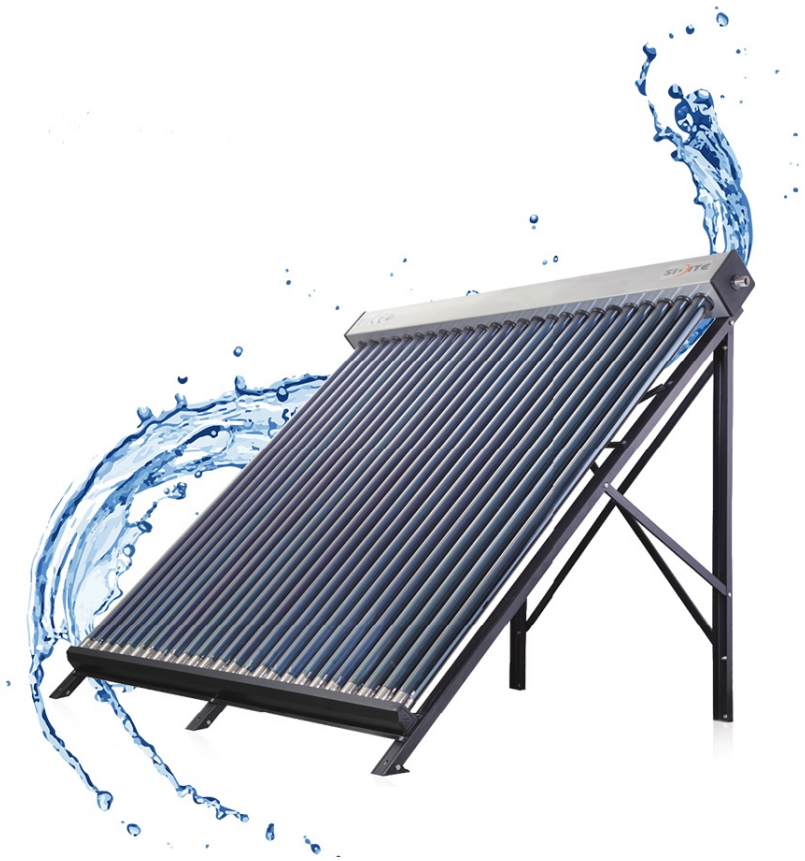

Figure 3.2: High pressurized Solar water heater / solar collector.

Solar water heaters work by absorbing sunlight and converting it into usable heat. A simply analogy is to think about a dark coloured object sitting in the summer sun. Over time it can become very hot from absorbing the sunlight. Solar water heaters work in the same way by using materials that are specially designed to maximise the efficiency of that absorption. High quality absorber coatings, as used by Apricus products, are able to absorb up to 95% of the energy in sunlight throughout the full spectral range while PV only absorbs a portion of the spectrum (http://www.apricus.com/solar-collection.html.XYiyp0YzaUk).

The price of solar collectors are usually a lot higher than PV panels, in the market. Figure 3.2 shows a commercially available high pressurized solar water heater or solar collector, with price as high as $400.00.

3.2.3 Solar Thermal Photovoltaic Working Together

Solar Thermal and PV should not be seen as competing technologies or products as they perform different functions and as shown below can be installed together to provide a well balanced solar energy harnessing system. Electricity can be used for almost any application, and so is a universal energy source (http://www.apricus.com/solar-collection.html.XYiyp0YzaUk). Figure 3.3 shows a system that incorporates a solar thermal system with a modest sized PV system is a great option.

Figure 3.3: A system that incorporates a solar thermal system with a modest sized PV system is a great option.

3.2.4 Solar thermal collector

A solar collector is a special kind of heat exchanger that transforms solar radiant energy into heat[32]. Heat exchangers usually accomplish a fluid-to-fluid exchange with high heat transfer rates and with radiation as an unimportant factor. In the solar collector, energy is transferred from a distant source of radiant energy to a fluid. The flux of incident radiation is, at best, approximately 1100 W/m2 (without optical concentration), and it is variable. The wavelength range is from 0.3 to 3 m, which is considerably shorter than that of the emitted radiation from most energy-absorbing surfaces[32]. Thus, the

analysis of solar collectors shows unique problems of low and variable energy fluxes and the relatively large importance of radiation.

3.2.5 Basic Working Principle

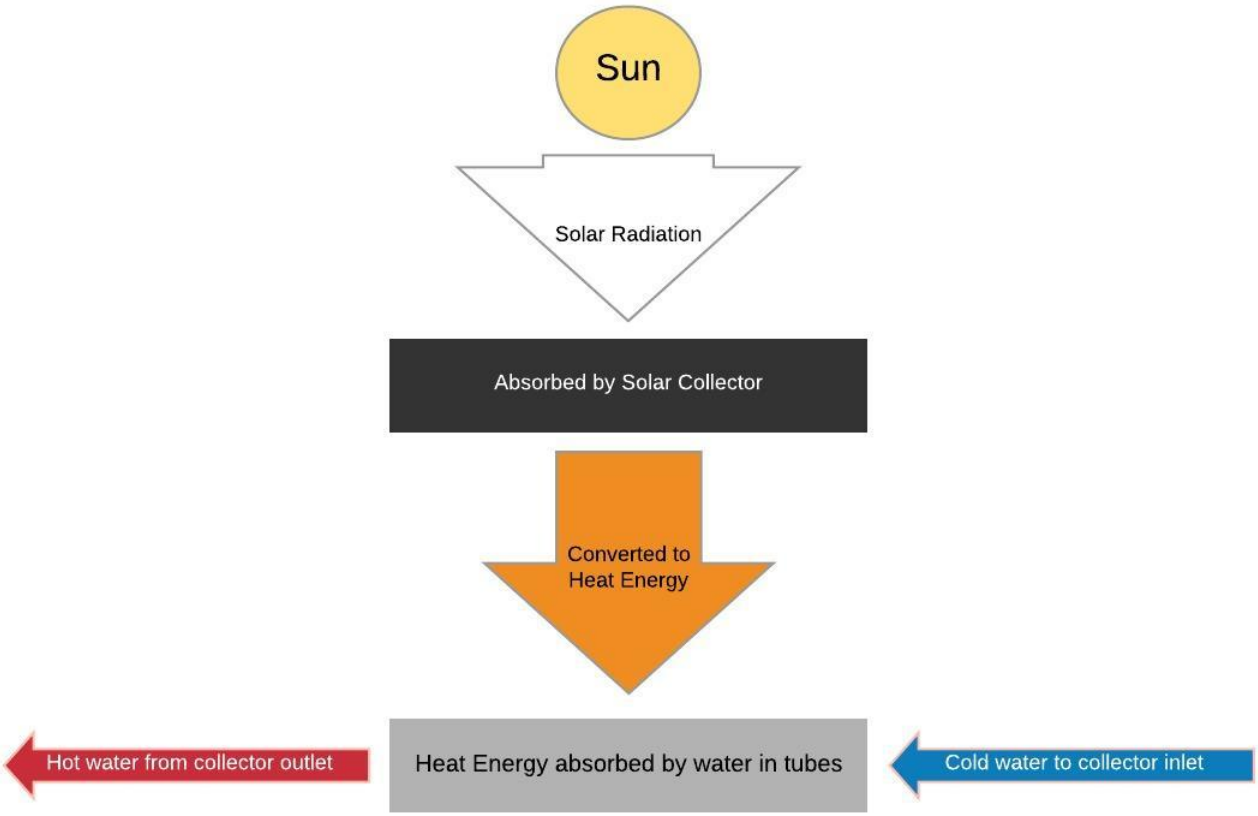

Figure 3.4: Energy flow from sun to fluid in collector.

The major component of any solar system is the solar collector. This is a device that absorbs the incoming solar radiation, converts it into heat, and transfers the heat to a fluid (usually air, water, or oil) flowing through the collector, as shown in Figure 3.4. The solar energy collected is carried from the circulating fluid either directly to the hot water or space conditioning equipment or to a thermal energy storage tank, from which it can be drawn for use at night or on cloudy days.

3.3 Types of Solar thermal Collectors

According to [30], there are basically two types of solar collectors: non-concentrating or stationary and concentrating. A non-concentrating collector has the same area for

intercepting and absorbing solar radiation, whereas a sun-tracking concentrating solar collector usually has concave reflecting surfaces to intercept and focus the sun's beam radiation to a smaller receiving area, thereby increasing the radiation flux. Concentrating collectors are suitable for high-temperature applications. Solar collectors can also be distinguished by the type of heat transfer liquid used (water, non-freezing liquid, air, or heat transfer oil) and whether they are covered or uncovered. A large number of solar collectors are available on the market. A summary of the types is shown in Table 3.1.

Motion	**Collector Type**	**Absorber Type**
Stationary	Flat-plate collector (FPC)	Flat
	Evacuated Flat Plate Collector (EFPC)	Flat
	Evacuated tube collector (ETC)	Flat
	Compound parabolic collector (CPC)	Tubular
Single-axis tracking	Compound parabolic collector (CPC)	Tubular
	Linear Fresnel reflector (LFR)	Tubular
	Cylindrical trough collector (CTC)	Tubular
	Parabolic trough collector (PTC)	Tubular
Two-axis tracking	Parabolic dish reflector (PDR)	Point
	Heliostat field collector (HFC)	Point

Table 3.1: Solar Energy Collectors

3.3.1 Flat Plate Collector (FPC)

Flat-plate collectors can be designed for applications requiring energy delivery at moderate temperatures, up to perhaps 100°C above ambient temperature. They use both beam and diffuse solar radiation, do not require tracking of the sun, and require little maintenance. They are mechanically simpler than concentrating collectors. The major applications of these units are in solar water heating, building heating, air conditioning, and industrial process heat.

The main components of an FPC, as shown in Figure 3.5 are the following [30]:

- **Cover.** One or more sheets of glass or other radiation-transmitting material.
- **Heat removal fluid passageways.** Tubes, fins, or passages that conduct or direct the heat transfer fluid from the inlet to the outlet.
- **Absorber plate.** Flat, corrugated, or grooved plates, to which the tubes, fins, or passages are attached. A typical attachment method is the embedded fixing shown in the detail of Figure 3.5. The plate is usually coated with a high-absorptance low-emittance layer.
- **Headers or manifolds.** Pipes and ducts to admit and discharge the fluid.
- **Insulation.** Used to minimize the heat loss from the back and sides of the collector.

- **Container.** The casing surrounds the aforementioned components and protects them from dust, moisture, and any other material.

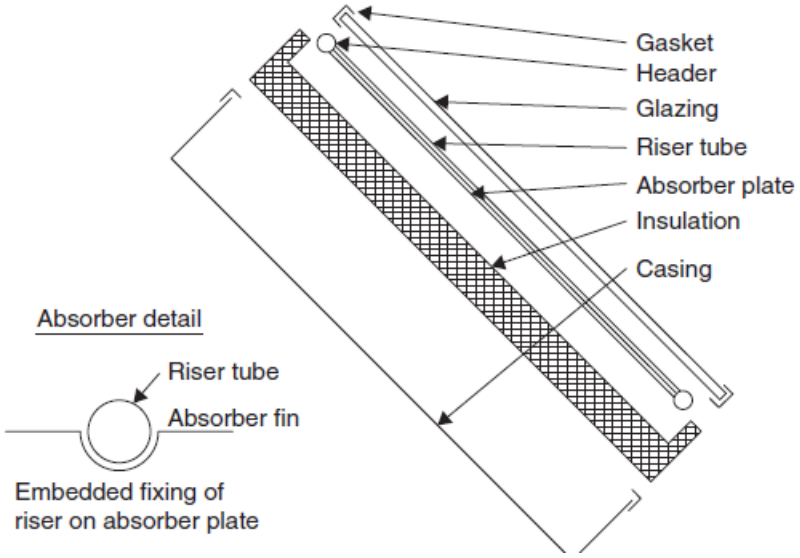

Figure 3.5: Exploded view of a flat-plate collector and absorber details [30]

Flat-plate collectors have been built in a wide variety of designs and from many different materials. They have been used to heat fluids such as water, water plus antifreeze additive, or air. Their major purpose isto collect as much solar energy as possible at the lowest possible total cost. The collector should also have a long effective life, despite the adverse effects of the sun's ultraviolet radiation and corrosion and clogging because of acidity, alkalinity, or hardness of the heat transfer fluid, freezing of water, or deposition of dust or moisture on the glazing and breakage of the glazing from thermal expansion, hail, vandalism, or other causes. These causes can be minimized by the use of tempered glass.

3.3.2 Compound parabolic collector (CPC)

Compound parabolic collectors (CPCs) are non-imaging concentrators. They have the capability of reflecting to the absorber all of the incident radiation within wide limits. Their potential as collectors of solar energy was pointed out by Winston [33]. Compound parabolic concentrators can accept incoming radiation over a relatively wide range of angles. By using multiple internal reflections, any radiation entering the aperture within the collector acceptance angle finds its way to the absorber surface located at the bottom of the collector.The necessity of moving the concentrator to accommodate the changing solar orientation can be reduced by using a trough with two sections of a parabola facing each other.

Two basic types of CPC collectors have been designed: symmetric and asymmetric. CPCs usually employ two main types of absorbers: the fin type with a pipe and tubular absorbers [30].

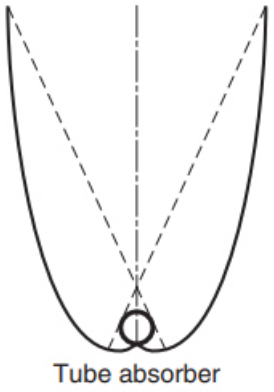

Figure 3.6: One opening and one receiver CPC [30].

CPCs should have a gap between the receiver and the reflector to prevent the reflector from acting as a fin conducting heat away from the absorber. Because the gap results in a loss of reflector area and a corresponding loss of performance, it should be kept small [30]. This is more important for flat receivers.

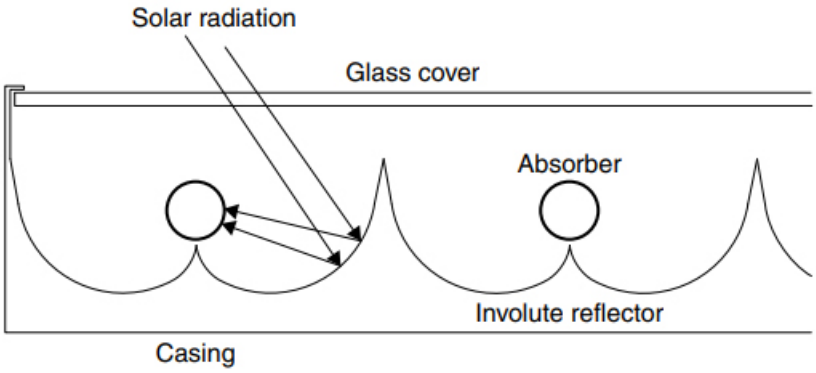

Figure 3.7: Schematic diagram of panel CPC collector with cylindrical absorbers [30]

For higher temperature applications a tracking CPC can be used. When tracking is used, this is very rough or intermittent, since the concentration ratio is usually small and radiation can be collected and concentrated by one or more reflections on the parabolic surfaces [30].

Figure 3.8: Photo of a CPC panel collector installation of panel CPC collector with cylindrical absorbers [30]

[30] CPCs can be manufactured either as one unit with one opening and one receiver (as shown in Figure 3.6) or as a panel (as shown in Figure 3.7). When constructed as a panel, the collector looks like an FPC, as shown in Figure 3.8.

3.3.3 Evacuated Tube Collector (ETC)

Evacuated heat pipe solar collectors (tubes) operate differently than the other collectors available on the market [30]. These solar collectors consist of a heat pipe inside a vacuum-sealed tube, as shown in Figure 3.9. In an actual installation, many tubes are connected to the same manifold as shown in Figure 3.10.

Evacuated tube collectors have shown that the combination of a selective surface and an effective convection suppressor can result in good performance at high temperatures. The vacuum envelope reduces convection and conduction losses, so the collectors can operate at higher temperatures than FPCs. Like FPCs, they collect both direct and diffuse radiation, but their efficiency is higher at low incidence angles. This gives ETCs an advantage over FPCs in terms of daylong performance.

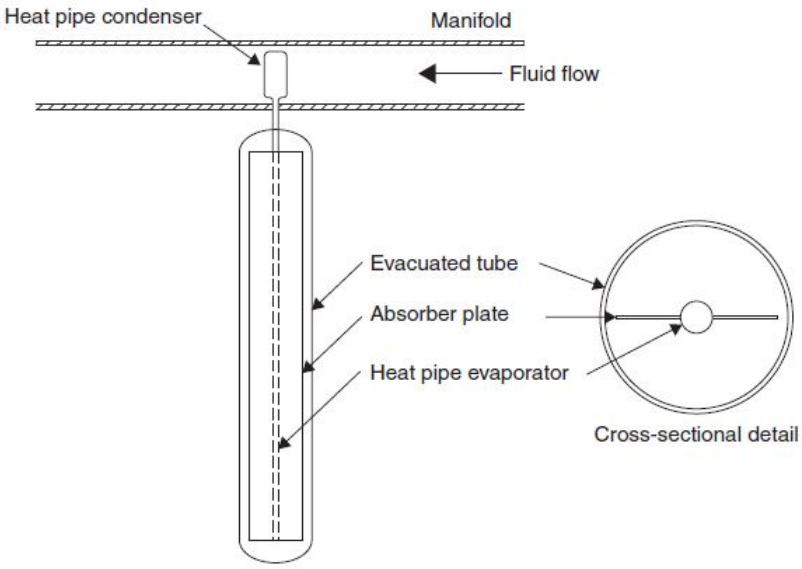

Figure 3.9: Schematic diagram of an evacuated tube collector [30].

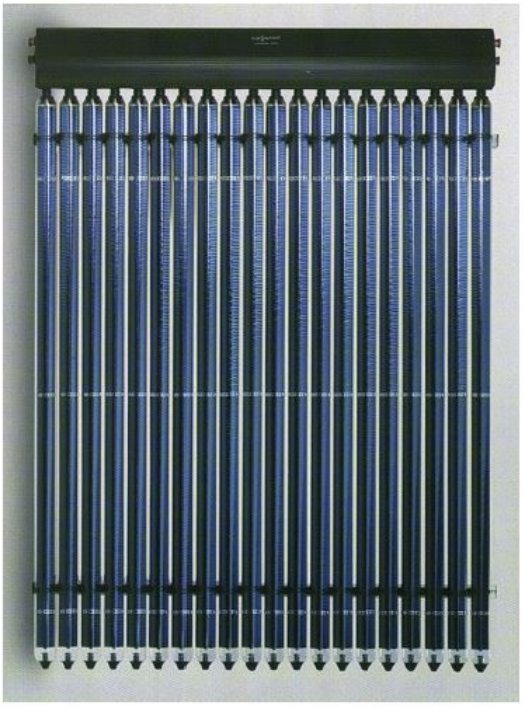

Figure 3.10: Actual ETC installation [30].

ETCs use liquid–vapor phase change materials to transfer heat at high efficiency. These collectors feature a heat pipe (a highly efficient thermal conductor) placed inside a vacuum-sealed tube. The pipe, which is a sealed copper pipe, is then attached to a black copper fin that fills the tube (absorber plate). Protruding from the top of each tube is a

metal tip attached to the sealed pipe (condenser). The heat pipe contains a small amount of fluid (e.g. methanol) that undergoes an evaporating–condensing cycle. In this cycle, solar heat evaporates the liquid and the vapor travels to the heat sink region, where it condenses and releases its latent heat. The condensed fluid returns to the solar collector and the process is repeated. When these tubes are mounted, the metal tip projects into a heat exchanger (manifold), as shown in Figure 3.9. Water or glycol flows through the manifold and picks up the heat from the tubes. The heated liquid circulates through another heat exchanger and gives off its heat to a process or water stored in a solar storage tank.

3.3.4 Evacuated Flat Plate Collector (EFPC)

One of the most widely used solar collector type in the world is a solar flat plate collector (FPC). Simple structure, high optical efficiency, low cost, and safe operation are its main features. However, FPC is generally designed for a low temperature level between 40°C and 60°C, which is mostly the case for the domestic hot water system. Any shifts to a higher temperature level could bring the extension of the applicability range of FPC. Hence, efforts aimed to improve the performance of flat plate solar collectors are ongoing. The performance of a flat plate solar collector is largely influenced by the thermal losses from the absorber to the ambient via the transparent cover. One way to reduce this heat loss is to reduce the natural convection heat transfer in the space between the absorber and the cover by its partitioning with the use of additional glass pane, plastic film, or transparent insulation materials (TIM). Another way to reduce this heat loss is to use gas with lower thermal conductivity rather than air or by evacuating the space.

Figure 3.11 shows a commercially available EFPC, designed to operate above 100°C in large-scale deployments, with highly active flat surface and high-vacuum for best performance. It has corrosion-proof all-metal casing for any environment, made with materials qualified for long-lasting high-vacuum operation. Most importantly, it is 100% recyclable.

The use of a moderate vacuum in flat plate collectors is known to reduce top heat losses since the work of Eaton and Blum [34]. The concept of an evacuated flat plate collector was commercially realized and is available on the market. Apart from the higher thermal output, these collectors have the advantage of longer lifetime compared to non-evacuated collectors, because no humidity and condensation problems occur within the casing. Typical interior pressures, which can be maintained economically, lie between 1 and 10 kPa. It means that although convection losses are suppressed, gas heat conduction remains fully developed. Further, Benz and Beikircher [35] constructed a prototype collector based on the commercially available flat plate collector. To implement high thermal efficiency in the medium temperature range, the thermal losses of the absorber have been reduced using a low emissive selective absorber, a low pressure krypton filling (5 kPa) in the collector casing. The prototype collector has been dynamically tested and has showed very high efficiencies of more than 60% at 100°C. Later, Benvenuti [36] presented a FPC, which is able to reach 300°C. That has become possible by ultrahigh vacuum (1 33 107 Pa) maintained by a getter pump powered by the sun. As for the

latest studies, Moss and Shire [37] indicate an improvement from 25% for a conventional FPC to 60–65% for vacuum FPC when operating at 140°C above ambient temperatures. More recently, Shire et al. [38] highlight that vacuum FPC collector could provide heat up to 200°C with efficiency greater than 50%.

Figure 3.11: TVP Solar evacuate flat plate collector (https://www.tvpsolar.com/newsinthemedia.html?id=27).

3.3.5 Parabolic Trough Collector (PTC)

PTC is a sun tracking, a high-performance, concentrating solar collectors, designed to deliver high temperatures with good efficiency. Systems with light structures and low-cost technology for process heat applications up to 400°C could be obtained with PTCs. PTCs can effectively produce heat at temperatures between 50°C and 400°C.

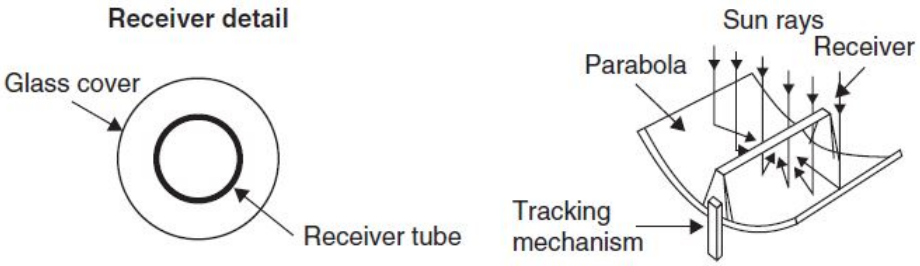

Figure 3.12: Schematic of a parabolic trough collector [30]

Parabolic trough collectors are made by bending a sheet of reflective material into a

parabolic shape. A black metal tube, covered with a glass tube to reduce heat losses, is placed along the focal line of the receiver, as shown in Figure 3.12. When the parabola is pointed toward the sun, parallel rays incident on the reflector are reflected onto the receiver tube. The concentrated radiation reaching the receiver tube heats the fluid that circulates through it, transforming the solar radiation into useful heat. It suffices to use a single-axis tracking of the sun; therefore, long collector modules are produced. According to [30], the collector can be oriented in an east–west direction, tracking the sun from north to south, or in a north–south direction, tracking the sun from east to west. The advantages of the former tracking mode is that little collector adjustment is required during the day and the full aperture always faces the sun at noon but the collector performance during the early and late hours of the day is greatly reduced, due to large incidence angles (cosine loss). North–south oriented troughs have their highest cosine loss at noon and the lowest in the mornings and evenings, when the sun is due east or due west.

Parabolic trough technology is the most advanced of the solar thermal technologies because of considerable experience with the systems and the development of a small commercial industry to produce and market these systems. PTCs are built-in modules that are supported from the ground by simple pedestals at either end.

3.3.6 Fresnel Collectors

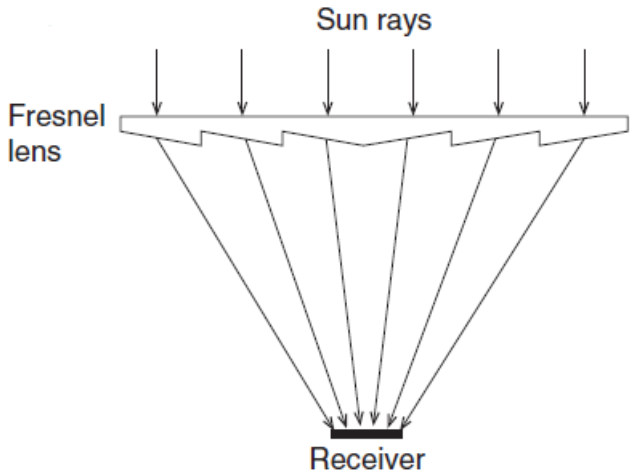

Figure 3.13: Fresnel lens collector (FLC) [30].

Fresnel collectors have two variations: the Fresnel lens collector (FLC), shown in Figure 3.13, and the linear Fresnel reflector (LFR), shown in Figure 3.14. The former is made from a plastic material and shaped in the way shown to focus the solar rays to a point receiver, whereas the latter relies on an array of linear mirror strips that concentrate light onto a linear receiver. The LFR collector can be imagined as a broken-up parabolic trough reflector, shown in Figure 3.14, but unlike parabolic troughs, the individual strips need not be of parabolic shape. The strips can also be mounted on flat ground (field)

and concentrate light on a linear fixed receiver mounted on a tower. A representation of an element of an LFR collector field is shown in Figure 3.15. In this case, large absorbers can be constructed and the absorber does not have to move. The greatest advantage of this type of system is that it uses flat or elastically curved reflectors, which are cheaper than parabolic glass reflectors. Additionally, these are mounted close to the ground, thus minimizing structural requirements.

The first to apply this principle was the great solar pioneer Giorgio Francia [39], who developed both linear and two-axis tracking Fresnel reflector systems at Genoa, Italy, in the 1960s. These systems showed that elevated temperatures could be reached using such systems, but he moved on to two-axis tracking, possibly because advanced selective coatings and secondary optics were not available [40].

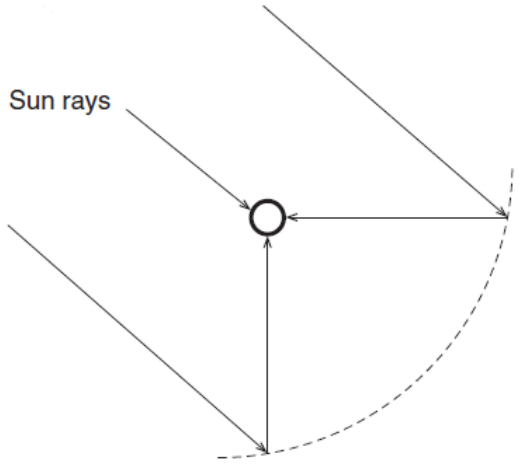

Figure 3.14: Linear Fresnel-type parabolic trough collector [30].

A good review of solar energy applications of Fresnel lenses is given by Xie et al. [41].

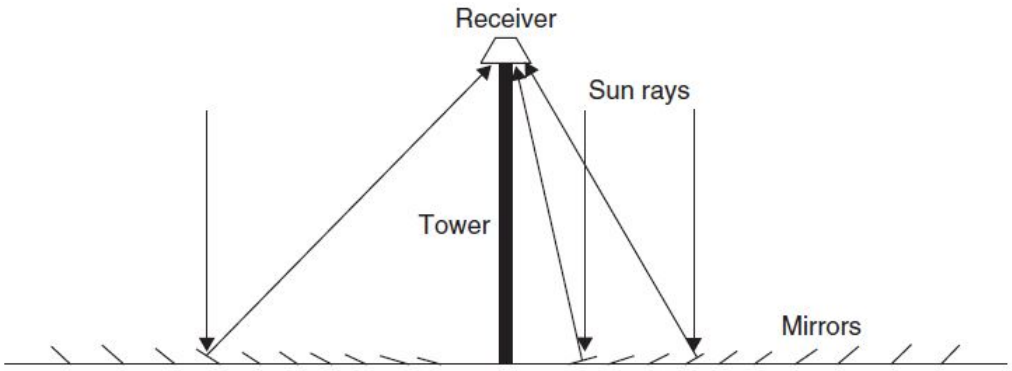

Figure 3.15: Schematic diagram of a downward-facing receiver illuminated from an LFR field [30].

3.3.7 Parabolic Dish Reflector (PDR)

A parabolic dish reflector (PDR), shown schematically in Figure 3.16, is a point-focus collector that tracks the sun in two axes, concentrating solar energy onto a receiver located at the focal point of the dish. The dish structure must fully track the sun to reflect the beam into the thermal receiver. For this purpose, tracking mechanisms similar to the ones described in the previous section are employed in double, so the collector is tracked in two axes.

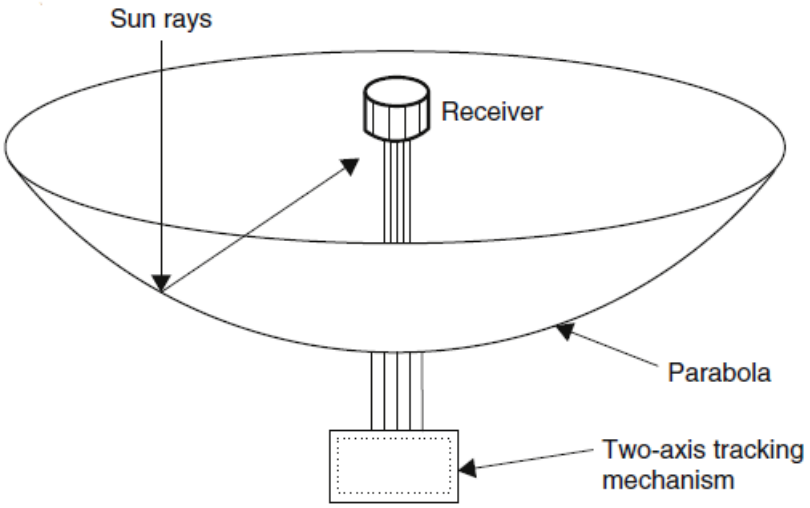

Figure 3.16: Schematic diagram of parabolic dish collector [30].

The receiver absorbs the radiant solar energy, converting it into thermal energy in a circulating fluid. The thermal energy can then be either converted into electricity using an engine–generator coupled directly to the receiver or transported through pipes to a central power conversion system. Parabolic dish systems can achieve temperatures in excess of 1500°C. Because the receivers are distributed throughout a collector field, like parabolic troughs, parabolic dishes are often called distributed receiver systems.

Parabolic dish systems that generate electricity from a central power converter collect the absorbed sunlight from individual receivers and deliver it via a heat transfer fluid to the power conversion systems. The need to circulate heat transfer fluid throughout the collector field raises design issues such as piping layout, pumping requirements, and thermal losses.

3.3.8 Heliostat Field Collector (HFC)

For extremely high inputs of radiant energy, a multiplicity of flat mirrors, or heliostats, using altazimuth mounts can be used to reflect their incident direct solar radiation onto a common target, as shown in Figure 3.17. This is called the heliostat field or central

receiver collector. By using slightly concave mirror segments on the heliostats, large amounts of thermal energy can be directed into the cavity of a steam generator to produce steam at high temperature and pressure.

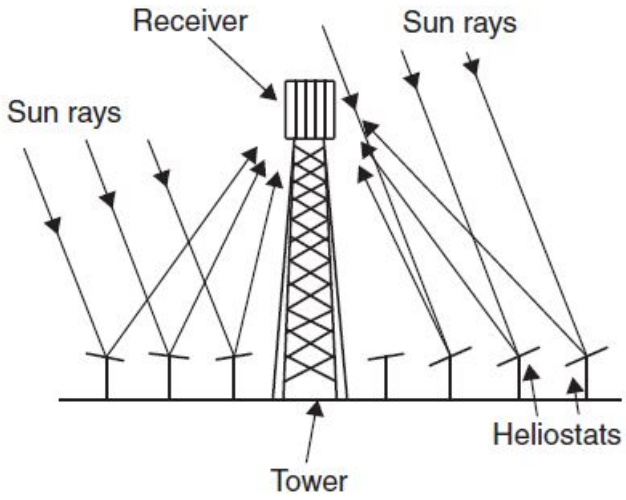

Figure 3.17: Schematic of central receiver system [30].

The collector and receiver systems come in three general configurations. In the first, heliostats completely surround the receiver tower, and the receiver, which is cylindrical, has an exterior heat transfer surface. In the second, the heliostats are located north of the receiver tower (in the Northern Hemisphere), and the receiver has an enclosed heat transfer surface. In the third, the heliostats are located north of the receiver tower, and the receiver, which is a vertical plane, has a north-facing heat transfer surface.

Each heliostat at a central receiver facility has from 50 to 150 m^2 of reflective surface, with four mirrors installed on a common pillar for economy. The heliostats collect and concentrate sunlight onto the receiver, which absorbs the concentrated sunlight, transferring its energy to a heat transfer fluid. The heat transport system, which consists primarily of pipes, pumps, and valves, directs the transfer fluid in a closed loop among the receiver, storage, and power conversion systems. A thermal storage system typically stores the collected energy as sensible heat for later delivery to the power conversion system. The storage system also decouples the collection of solar energy from its conversion to electricity. The power conversion system consists of a steam generator, turbine generator, and support equipment, which convert the thermal energy into electricity and supply it to the utility grid.

3.4 Selection of Solar Collector

Evacuated plate collector, constructed in stainless steel Figure 3.18, as discussed in literature[37], is chosen for the solar air conditioning system design. According to this literature, the 304 stainless plate had a few leaks and these were easily fixed; it has proved itself vacuum-tight over a period of several days (limited only by out-gassing of the test facility), and the welding of these one-off prototypes was performed manually using a pulsed laser but in a production environment with suitable jigs a stainless collector could be rapidly welded using a continuous laser. However, for the air conditioning system design certain assumptions have been made, such that the plate did not incurred any leaks, thus eliminating the nuisance of welding and its cost addition in operation and the plate is vacuum-tight through out the life time of its operation.

Figure 3.18: Stainless steel collector after laser welding[37]

3.5 Basic Energy Balance Equation

As defined by[32], the thermal energy lost from the collector to the surroundings by conduction, convection, and infrared radiation can be represented as the product of a heat transfer coefficient U_L times the difference between the mean absorber plate temperature T_{pm} and the ambient temperature T_a. In steady state, the useful energy output, Q_u, of a collector of area, $A_c = L$ x B, is the difference between the absorbed solar radiation and the thermal loss is:

$$Q_u = A_c\big[S - U_L(T_{pm} - T_a)\big] \tag{3.1}$$

The maximum useful energy output can be achieved if the absorber plate can be held at inlet fluid temperature, T_i, i.e., the difference between inlet fluid temperature and mean plate temperature is 'zero', $\Delta T = T_{pm}$ - $T_i = 0$. This effect can be described by Hottle-Whiller-Bliss equation by a heat recovery factor, F_R:

$$Q_u = F_R A_c\big[S - U_L(T_i - T_a)\big] \tag{3.2}$$

The heat energy output obtained by Equation 3.1 is less than that obtained by Equation 3.2. Generally, collector efficiency is defined by:

$$\eta_i = \frac{Q_u}{A_c G_T} = F_R \left[(\tau\alpha) - \frac{U_L(T_i - T_a)}{G_T} \right] \tag{3.3}$$

Measures to maximise $\tau\alpha$, include the use of a high clarity glass such as Pilkington's OptiWhite^{TM}, possibly with anti-reflection coatings; a selective coating (high absorptance at short wavelengths, low emittance at long wavelengths) such as black chrome[37].

3.6 Collector Overall Heat Loss Coefficient

In the conceptual design[42], a high vacuum enclosure eliminates gas conduction and convection losses; since there is no gas conduction, the collector spacing between collector and cover glass can be made small ($< 1\ cm$) without increasing the losses, thereby allowing a slim and architecturally attractive format. Gas pressures below 100 Pa start to eliminate convection; pressures below 0.1 Pa eliminate conduction too, for a typical glass-collector spacing[37]. The evacuated place collector design typically achieves $U_L = 1\ W/m^2K$ for $\frac{W_p}{L^2} = 0.1\ W/m^4$ as shown in Figure 3.21.

3.7 Plate Design

[37]A microchannel plate with rectangular channels, Figure 3.19 is considered to be equivalent to a virtual plate of length L with circular passages of hydraulic diameter D_h and size to pitch ratio $R = \frac{D_h}{P}$, where $R = \frac{2}{\pi}$ is equivalent in terms of low area and perimeter to square-section passages having width = 0.5 x pitch.

Figure 3.19: Definition of collector geometry parameters[37]

3.8 Manifold Design

The through-holes visible in the image below are for support pins that resist atmospheric pressure and hold the glass panes apart[42]. The pipe at 45^o was required to provide welding access to a manifold joint[37], shown in Figure 3.20.

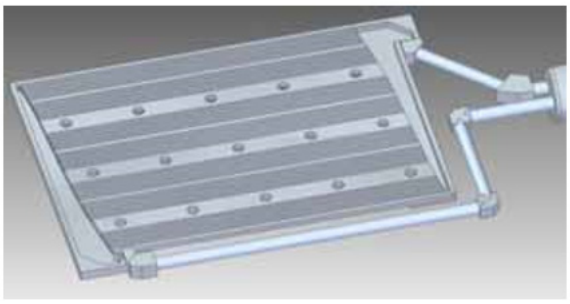

Figure 3.20: CAD rendering showing plate internal details.The pipe at 45 was required to provide welding access to a manifold joint[37].

3.9 Heat Transfer Fluid

Paratherm^{TM} MR is a mid-range heat transfer fluid rated for service from 36^oF to 550^oF and has boiling point greater than $650^oF/343^oC$. For temperature range 75^oC to 125^oC, variation in density, ρ, viscosity, μ, and specific heat, c, is shown in Table 3.2. Nevertheless, density, viscosity and specific heat are assumed to have constant values of 744 kg/m^3, 2.15 mm^2/sec and 2.536 kJ/kgK respectively, throughout the heat transfer process.

The fluid is efficient across the temperature range, thermally stable and cost-effective (www.paratherm.com/heat-transfer-fluids/paratherm-mr-heat-transfer-fluid).

^oC	**Density** kg/m^3	**Viscosity** mm^2/sec	**Specific Heat** kJ/kgK
0	821	25	2.32
25	795	8.6	2.374
50	778	4.3	2.429
75	761	2.7	2.483
100	744	2	2.536
125	727	1.6	2.589

Table 3.2: Thermal Properties of Paratherm^{TM} MR

3.10 Pumping Effects

To circulate the fluid required pumping power (per square meter of collector), W_p, is in range 0.1 to 1 W/m^2, for which hydraulic diameter lie in range 1.6 to 2.4 mm for Paratherm MR in a 1 m long plate[37]. Thus, a suitable hydraulic diameter, d_h, of 2 mm is selected for pumping power 0.1 W/m^2, achieving overall collector heat loss coefficient, U_L, of 1 W/m^2K and heat recovery factor, F_R, of 0.995 as approximated from Figure 3.21, for Paratherm MR at 120^oC.

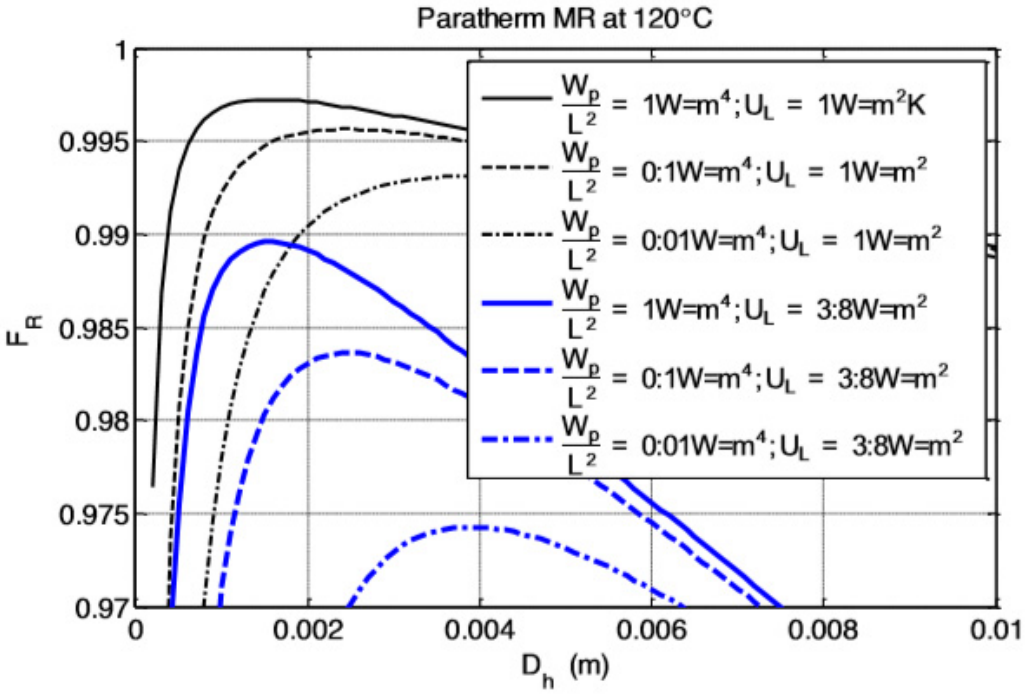

Figure 3.21: Effect of hydraulic diameter on heat recovery factor F_R[37]

It is to be assumed that flow through passages are laminar and for fully developed laminar flow having constant heat flux boundary condition, $Re < 2000$, $Nu_{cf} \approx 3.612$ [43] and $Po = 14.226$ [44] for square section duct. According to literature[37], friction coefficient, f can be calculated using $f = \frac{Po}{Re}$ and can be shown that the total mass flow rate, $\dot{m}$, is:

$$\dot{m} = \left(\frac{\rho B D_h^{1.5}}{4}\right)\sqrt{\frac{2\pi R W_p}{Po\mu}} \tag{3.4}$$

3.11 Mean Plate and Inlet Fluid Temperatures

For the calculation of ΔT and T_{pm}, literature[37] is being followed as described. ΔT has two components, the mean temperature rise of the fluid along the channels plus the temperature difference driving the convective heat transfer:

$$\Delta T = \frac{T_o - T_i}{2} + \Delta T_h = \Delta \bar{T}_f + \Delta T_h \tag{3.5}$$

One can see that reducing the passage size will reduce ΔT_h (because the heat transfer coefficient increases) but, for a constant W_p , reduce the mass flow rate and increase $\Delta \bar{T}_f$.

For any chosen R and W_p there will be an optimum D_h for a given fluid that balances these two effects to minimize ΔT (Figure 3.22).

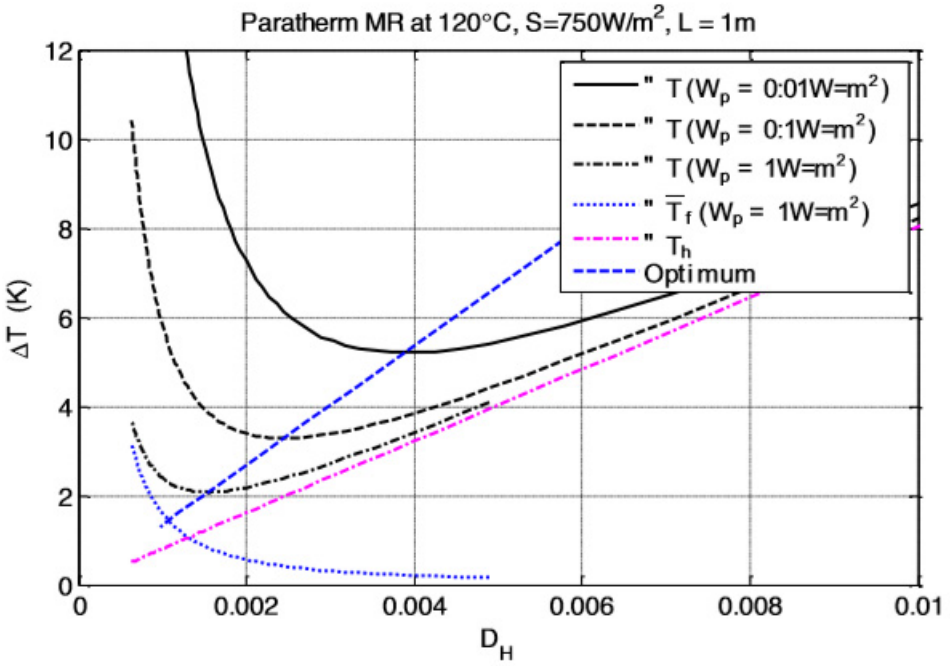

Figure 3.22: Effect of passage hydraulic diameter on ΔT. The curve ΔT ($W_p = 1\ W/m^2$) is the sum of the $\Delta \bar{T}_f$ ($W_p = 1\ W/m^2$) and the ΔT_h curves [37].

For pumping power 0.1 W/m^2 and selected hydraulic diameter 2 mm, ΔT of $7K$ can be estimated from the figure 3.5. Thus, under steady operation, for an assumed fluid inlet temperature T_i of 80^oC, mean fluid temperature can be calculated using the formulae described in literature[37]: $\Delta T = T_{pm} - T_i$

3.12 Absorbed Solar Radiation

The terminology defined by Duffie Beckman[32], using the isotropic diffuse concept on an hourly basis, has been adopted to calculate solar power, S, absorbed by the collector:

$$S = I_b R_b (\tau\alpha)_b + I_d (\tau\alpha)_d \frac{1+\cos\beta}{2} + \rho_g I (\tau\alpha)_g \frac{1-\cos\beta}{2} \tag{3.6}$$

where $(1 + \cos\ \beta)/2$ and $(1\ \cos\ \beta)/2$ are the view factors from the collector to the sky and from the collector to the ground, respectively, and total radiation, I, is summation of beam radiation, I_b, and diffuse radiation, I_d. The subscripts b, d, and g represent beam, diffuse, and ground. The hourly data of solar radiation, for latitude 23.94^o, is obtained for day 1 of each month for the year 2014 using Renewables.ninja (https:// www. renewables. ninja/). Hence, collector tilt angle is taken as 23.94^o and is to be kept constant.

3.12.1 Ground Reflectance

The flux of incident radiation is, at best, approximately 1100 W/m2 (without optical concentration), and the wavelength range is from 0.3 to 3 m, which is considerably shorter than that of the emitted radiation from most energy-absorbing surfaces[32]. It is assumed that the reflected wavelength from ground is 2.5 μm. A suitable place for the solar collectors to be placed, for the design of this solar air conditioning system, can on the roof top of the Automobile Laboratory. According to the literature[45], for an elevated target, case (b) as shown in Figure 3.23, an elevated height of 1.5 m is considered and, from Figure 3.24, for wavelength of 2.5 μm, a reflectance value of 0.24 is taken for soil in concrete background.

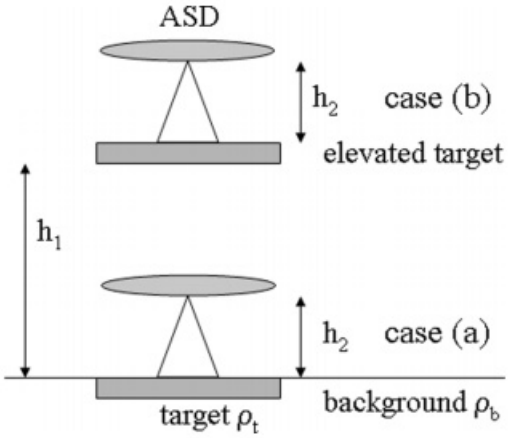

Figure 3.23: Geometric setup for ground reflectance measurements ($h_1 = 1.5\ m$, $h_2 = 22\ cm$)[45]

.

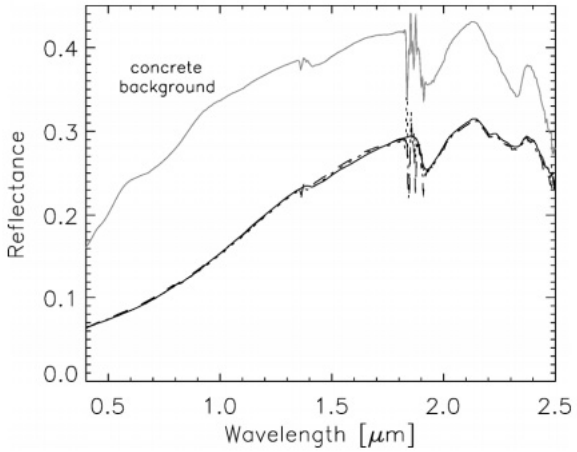

Figure 3.24: Soil in concrete background. The solid, dotted, and dashed curves represent measurements in the laboratory and those for cases (a) and (b), respectively[45]

3.12.2 Determination of Angle of Incidence and Zenith Angle

Figure 3.25 shows:

- G_{bn} is the beam radiation on surface.
- G_b is normal to horizontal surface.
- G_{bT} is normal to tilted surface.
- β is the slope, the angle between the plane of the surface and the horizontal.
- θ is the angle of incidence, the angle between the beam radiation on a surface and the normal to that surface.
- θ_z is the zenith angle, the angle of incidence of beam radiation on a horizontal surface.

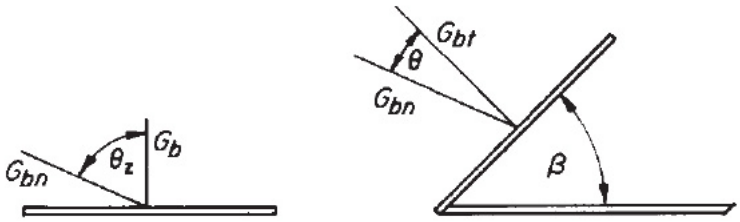

Figure 3.25: Beam radiation on horizontal and tilted surfaces[32]

Equation[32] relating the angle of incidence of beam radiation on a surface, θ, to the other angles is:

$$\begin{aligned}\cos\theta \;=\; \sin\delta\sin\phi\cos\beta \;-\; \sin\delta\cos\phi\sin\beta\cos\gamma \;+\; \cos\delta\cos\phi\cos\beta\cos\omega \\ +\; \cos\delta\sin\phi\sin\beta\cos\gamma\cos\omega \;+\; \cos\delta\sin\beta\sin\gamma\sin\omega \quad (3.7)\end{aligned}$$

where both latitude, ϕ, and slope, β, is considered to be 23.94^o, surface azimuth angle, γ, is 0^o for northern hemisphere.

The declination can be found from the approximate equation of Cooper[46]:

$$\delta = 23.45 \;\sin\left(360\;\frac{284+n}{365}\right) \quad (3.8)$$

Month	n for ith Day of Month	For Average Day of Month		
		Date	n	δ
January	i	17	17	−20.9
February	$31 + i$	16	47	−13.0
March	$59 + i$	16	75	−2.4
April	$90 + i$	15	105	9.4
May	$120 + i$	15	135	18.8
June	$151 + i$	11	162	23.1
July	$181 + i$	17	198	21.2
August	$212 + i$	16	228	13.5
September	$243 + i$	15	258	2.2
October	$273 + i$	15	288	−9.6
November	$304 + i$	14	318	−18.9
December	$334 + i$	10	344	−23.0

Figure 3.26: Recommended Average Days for Months and Values of n by Months[47]

From Klein[47], for $|\phi| < 66.5^o$, figure 3.9 shows the recommended average days for months, values of n by months and average value of δ to be used in further calculation.

In Equation 3.7, ω is the hour angle which is the angular displacement of the sun east or west of the local meridian due to rotation of the earth on its axis at 15^o per hour; with values negative in morning and positive in afternoon, as shown in Appendix A.

For the calculation of zenith angle, θ_z, the following equation[32] is used:

$$\cos\theta_z = \cos\phi\cos\delta\cos\omega \; + \; \sin\phi\sin\delta \tag{3.9}$$

Appendix B shows the values for angle of incidence, θ and zenith angle, θ_z for the year 2014.

3.12.3 Calculation of Geometry Factor R_b

The geometric factor R_b, the ratio of beam radiation on the tilted surface to that on a horizontal surface at any time, can be calculated using the ratio $\frac{G_{b,T}}{G_b}$ [32] :

$$R_b = \frac{G_{b,T}}{G_b} = \frac{G_{b,n}\cos\theta}{G_{b,n}\cos\theta_z} = \frac{\cos\theta}{\cos\theta_z} \tag{3.10}$$

Figure 3.25 shows the angle of incidence of beam radiation on the horizontal and tilted surfaces. The symbol G is used in Equation 3.10 to denote rates, while I is used for energy quantities integrated over an hour. The original development of R_b by Hottel and Woertz[48] was for hourly periods; for an hour (using angles at the midpoint of the hour), $R_b = I_{b,T} \; / \; I_b$. Appendix C shows the values for R_b.

3.12.4 Effective Transmittance-Absorptance Product

Transmittance is a measure of transmission expressed as the ratio of the intensity of the transmitted light to the intensity of the incident light, for a specified wavelength. It is usually given as a percentage. Absorptance of the surface of a material is its effectiveness in absorbing radiant energy. It is the ratio of the absorbed to the incident radiant power.

The product of the cover transmittance, τ, with the absorber-plate absorptance, α, is called the transmittance-absorptance product, $(\tau\alpha)$. The transmittance-absorptance product describes the properties of the glass and the absorber. According to the experimental analysis (http://energyprofessionalsymposium.com/?p=758) on the thermal performance of solar collectors as a function of transmittance-absorptance product in Nuussuaq, Greendland, the best performance is seen with a high transmittance-absorptance product. An increase in the transmittance-absorptance product from 0.83 to 0.9 will result in a increased performance of about 12% for all the collectors. The higher the product, the higher the thermal performance.

The terminology have been adopted, for the calculation of transmittance-absorptance product, as defined by Duffie and Beckman [32]:

$$(\tau\alpha) = \frac{\tau\alpha}{1 \; - \; (1-\alpha)\rho_d} \tag{3.11}$$

where τ, α and ρ_d, reflectance of glass, is calculated using Equations 3.12, 3.13 and 3.14, respectively:

$$\tau \cong \tau_a \tau_r \tag{3.12}$$

$$\alpha \cong 1 - \tau_a \tag{3.13}$$

$$\rho_d = \tau_a - \tau \tag{3.14}$$

Again, for single glass cover, τ_a and τ_r can be calculated using Equations 3.15 and 3.16, respectively:

$$\tau_a = exp\left(- \frac{KL}{\cos\theta_2} \right) \tag{3.15}$$

$$\tau_r = \frac{1}{2}\left(\frac{1 - r_{||}}{1 + r_{||}} + \frac{1 - r_{\perp}}{1 + r_{\perp}} \right) \tag{3.16}$$

where $r_{\perp}$ and $r_{||}$ is calculated by Equations 3.17 and 3.18, respectively:

$$r_{\perp} = \frac{\sin^2(\theta_2 - \theta_1)}{\sin^2(\theta_2 + \theta_1)} \tag{3.17}$$

$$r_{||} = \frac{\tan^2(\theta_2 - \theta_1)}{\tan^2(\theta_2 + \theta_1)} \tag{3.18}$$

In Equation 3.15, K is extinction coefficient, which K varies from approximately 4 m^{1} for 'water white' glass (which appears white when viewed on the edge) to approximately 32 m^{1} for high iron oxide content (greenish cast of edge) glass, and L is the thickness of a single glass cover, which is taken to be 2 mm.

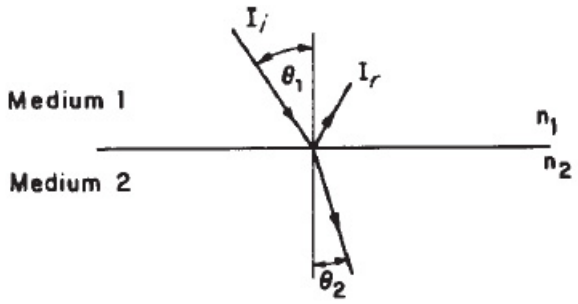

Figure 3.27: Angles of incidence and refraction in media with refractive indices n_1 and n_2.

The angles θ_1 and θ_2, shown in Figure 3.27, are related to the indices of refraction by Snell's law:

$$n_1 \ \sin\theta_1 = n_2 \ \sin\theta_2 \tag{3.19}$$

where medium 1 is air, so n_1 is taken to be 1.003 and medium 2 is glass, so n_2 is taken to be 1.526.

However, the value of $(\tau\alpha)$ is very nearly equal to 1.01 times the product of τ times α. According to [32], this is a reasonable approximation for most practical solar collectors. Thus, in place of Equation 3.11, Equation 3.20 can be used as an estimate of $(\tau\alpha)$:

$$(\tau\alpha) = 1.01\tau\alpha \tag{3.20}$$

where τ can be calculated using Equation 3.12 and α is calculated using the Equation 3.21:

$$\alpha = \left(\frac{\alpha}{\alpha_n}\right)(\alpha_n) \tag{3.21}$$

A glass with KL = 0.0370, and the absorptance of the plate at normal incidence, α_n, of 0.93 is selected. The directional absorptance for solar radiation of ordinary blackened surfaces (such as are used for solar collectors) is a function of the angle of incidence of the radiation on the surface as given by Equation 3.22:

$$\begin{aligned}\frac{\alpha}{\alpha_n} = 1 - 1.5879 \times 10^{-3}\,\theta + 2.7314 \times 10^{-4}\,\theta^2 - 2.3026 \times 10^{-5}\,\theta^3 + 9.0244 \times 10^{-7}\,\theta^4 \\ - \ 1.8000 \times 10^{-8}\,\theta^5 + 1.7734 \times 10^{-10}\,\theta^6 - 6.9937 \times 10^{-13}\,\theta^7\end{aligned} \tag{3.22}$$

For Beam Radiation

For angle of incidence, calculated using Equation 3.7, corresponding angle of refraction can be calculated using Equation 3.19. Hence Equation 3.20 can be used to calculate the value of transmittance-absorptance product for beam radiation, $(\tau\alpha)_b$.

For (Isotropic) Diffuse Radiation

Angle of incidence, for diffuse radiation, is given by [32]:

$$\theta_{e,d} = 59.7 - 0.1388\beta + 0.001497\beta^2 \tag{3.23}$$

The value of transmittance-absorptance product for diffuse radiation, $(\tau\alpha)_d$, can be calculated in similar manner to that used for the calculation of $(\tau\alpha)_b$.

For Ground-Reflected Radiation

Angle of incidence, for ground-reflected radiation, is given by [32]:

$$\theta_{e,g} = 90 - 0.5788\beta + 0.002693\beta^2 \tag{3.24}$$

The value of transmittance-absorptance product for ground-reflected radiation, $(\tau\alpha)_g$, can be calculated in similar manner to that used for the calculation of $(\tau\alpha)_b$.

3.13 Heat Extracted by HTF

The maximum heat energy can be extracted is given by Equation 3.2, with recovery factor, F_R, of 0.995, overall heat coefficient, U_L, of 1 $W/m^{2\circ}C$ and a collector surface area, A_c, of 1 m^2.

The basic method of measuring collector performance is to expose the operating collector to solar radiation and measure the fluid inlet and outlet temperatures and the fluid flow rate. The useful gain, by HTF, is:

$$Q_u = \dot{m} C_p (T_o - T_i) \tag{3.25}$$

3.14 Solar Collector Configuration

The literature [49], proposes two systemss: 1) Solar Direct Hot Water, which is composed of flat plate collectors and thermal storage tank, 2) Solar Indirect Hot Water in which an external heat exchanger, of constant effectiveness of 0.8, is added to the first system. We have selected the second system since two different fluid loops are being used to extract heat from the solar collectors. In the first loop, the mass flow rate of HTF through a collector is fixed to 0.04 Kgs^{-1} and the total number of collectors is adjusted to 60. In the second loop, water of varying flow rates have been used to extract heat from the heat exchanger and store it in the stratified tank, show in Figure 3.28.

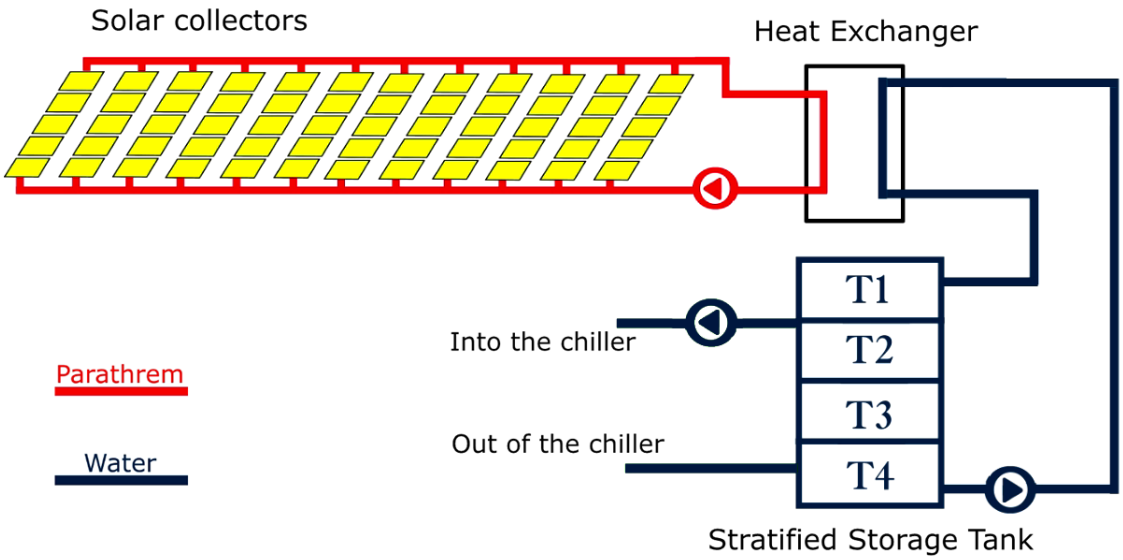

Figure 3.28: Solar Collector Configuration

The selection of the aforementioned configuration is adapted from the literature [49]. It shows, numerical results on a typical day in July. For all 60 collectors connected in parallel the total mass flow rate entering within the storage is the sum of those outgoing from collectors $\dot{m}_h = \sum_1^{60} \dot{m}_c = 2.4\ kgs^{-1}$ and the maximum temperature is 57°C at 5 pm. For a row of 2 collectors in series, the number of parallel rows is 30 and the mass flow rate entering is $\dot{m}_h = \sum_1^{30} \dot{m}_c = 1.2\ kgs^{-1}$ with the average temperature increasing from 57°C to 64°($\Delta T = 7$°C) as the mass flow rate decreases from 2.4 to 1.2 kgs^{-1}. For the case of 3 collectors by row, the number of parallel rows is 20 and the total mass

flow rate is $\dot{m}_h = \sum_1^{20} m_c = 0.\dot{8}\ kgs^{-1}$ with the average water temperature increasing from 64°C to 67°C as the mass flow rate decreased from 1.2 to 0.8 kgs^{-1}. When using 4 collectors by row, the number of parallel rows is 15, the total mass flow rate is $\dot{m}_h = \sum_1^{15} m_c = 0.\dot{6}\ kgs^{-1}$ and the storage average water temperature increased to 69°C. It is is observed that the temperature difference ΔT decreases if a collector in series is added and that from the 5th collector the average water temperature in the storage is the same, which explains that no output produced from the 6th. In this case, 5 is the maximum number has been selected to put in series.

3.15 Simulation Results of Heat Extraction Unit

A computer program was developed in Python 3.8.0, for the numerical calculation to determine the transient performance of the system. Various input parameter are used in the simulation program. All simulations, in this work are computed with a time step equal to one hour (60 minutes).

3.15.1 Available Solar Radiation

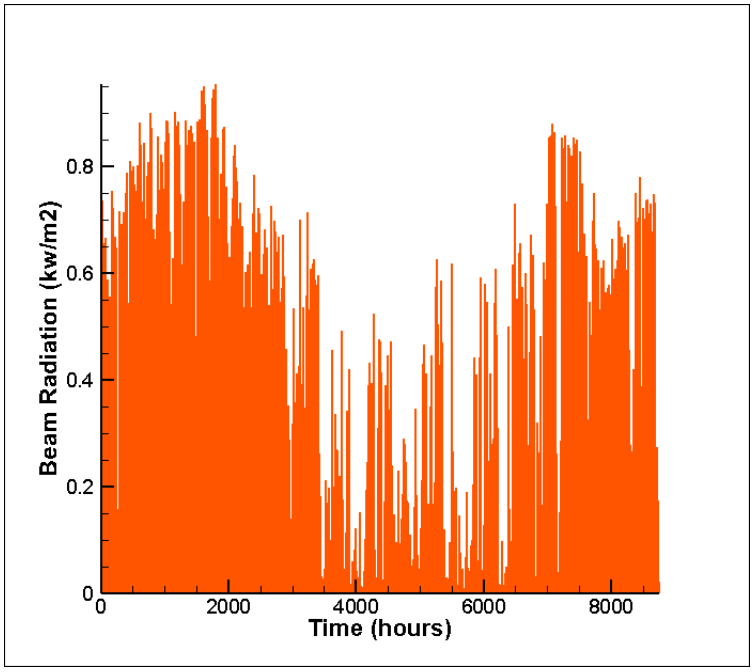

Figure 3.29: Available beam radiation for 8760 hours.

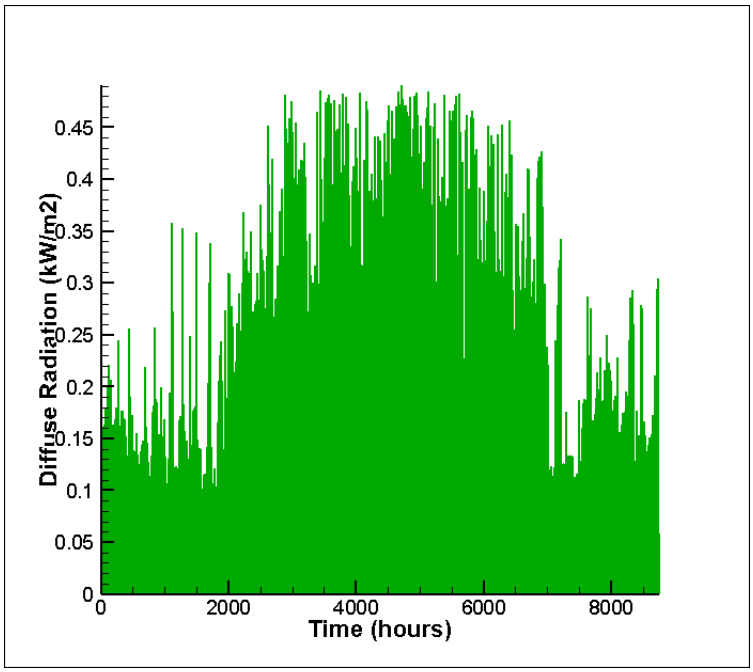

Figure 3.30: Available diffuse radiation for 8760 hours.

Figure 3.29 and 3.30 show the available beam and diffuse radiation, respectively, for the year 2014 and their sum gives the total available radiation for 8760 hours, shown in Figure 3.31.

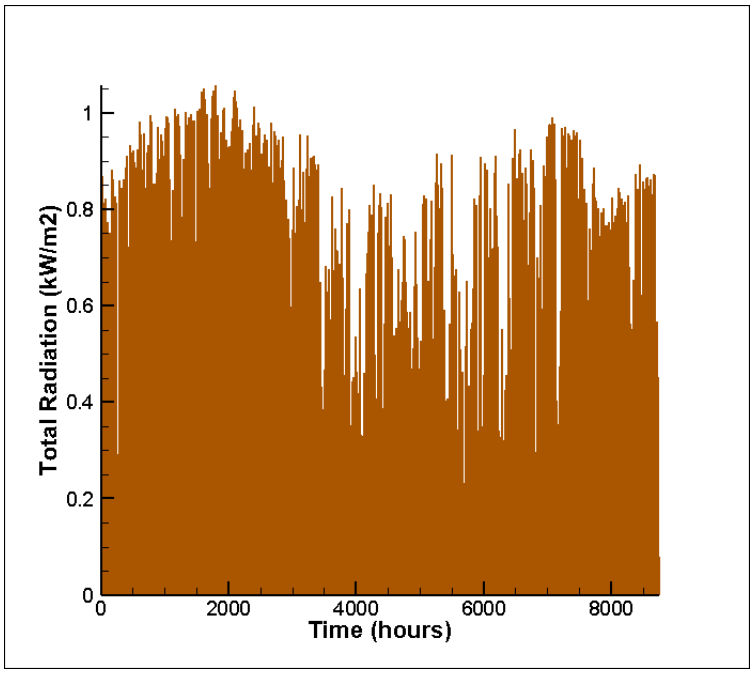

Figure 3.31: Total available radiation for 8760 hours.

3.15.2 Absorbed Solar Radiation

The use of evacuated flate plate collector having a heat recovery factor of 99.5%, yields a high absorption of solar radiation as can be seen in Figure 3.32, which is significantly close to the total available radiation, shown in Figure 3.31.

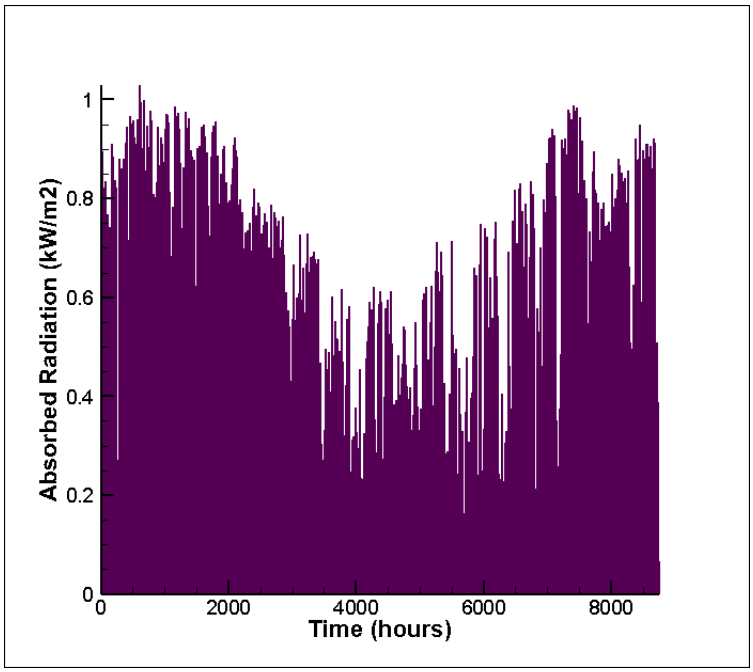

Figure 3.32: Absorbed radiation for 8760 hours using evacuated flat plate collector.

3.15.3 Heat Extraction by HTF

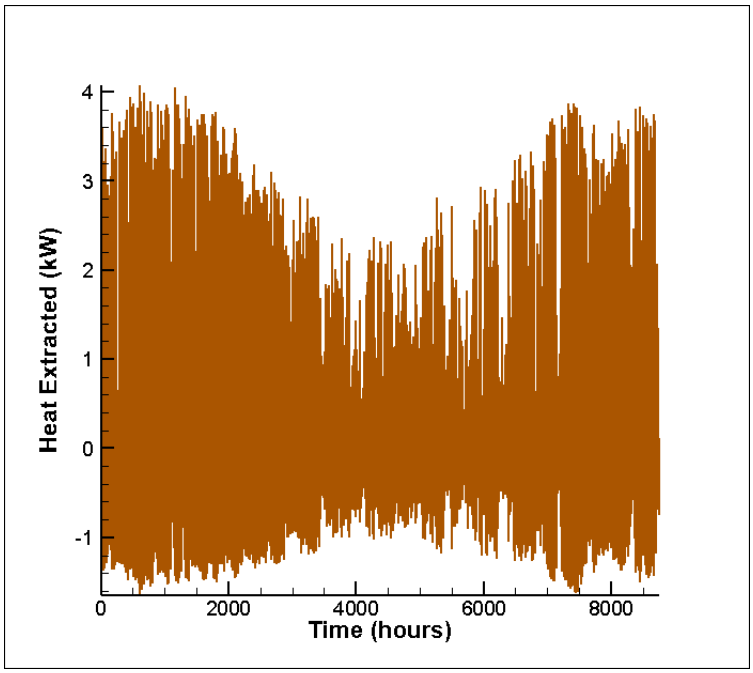

Figure 3.33: Heat energy that can be extracted by Paratherm for 8760 hours.

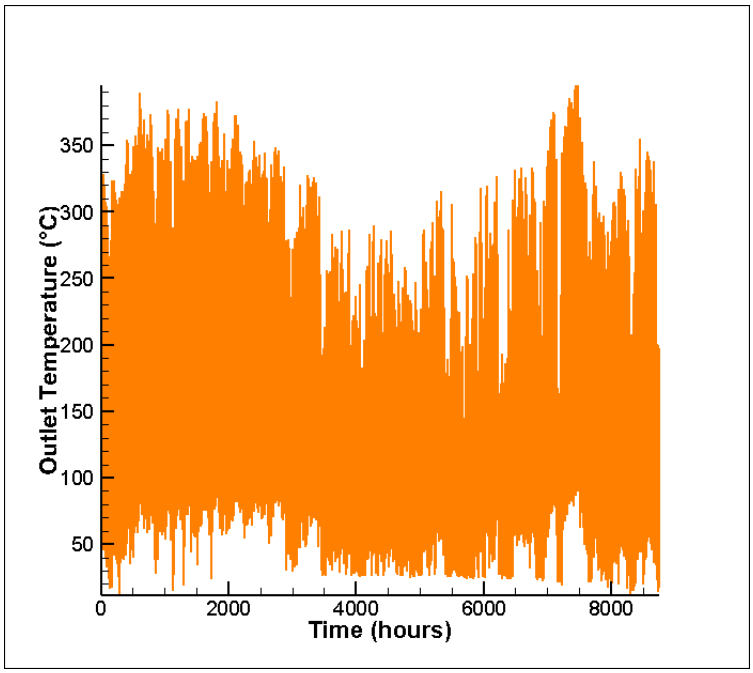

Figure 3.34: Hourly variation of temperature of Paratherm for 8760 hours.

In the first loop, Parathrem MR is used as HTF to extract heat from the solar collectors and transfer this heat to the second loop of water in the heat exchanger. Figure 3.33 and

3.34 shows the heat extracted by Parathrem MR and hourly temperatures, respectively, for 8760 hours. Since in day hours, surrounding temperature is higher than the HTF, heat extraction is positive and in night hours, since loop is run for 8760 hours, HTF temperature is higher than that of ambience, a negative temperature gradient results in negative heat extraction causing temperature drop of HTF.

3.15.4 Heat Transfer inside Heat Exchanger

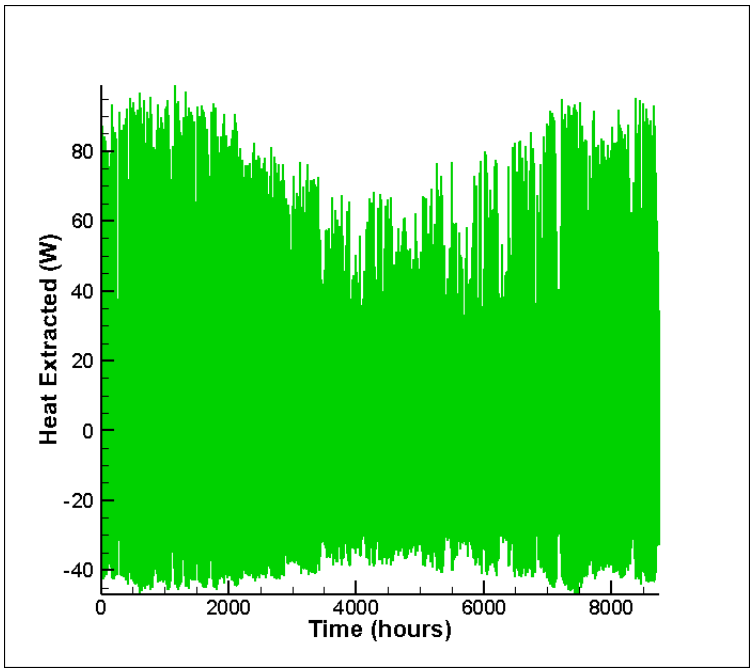

Figure 3.35: Heat transfer to feed water, into storage tank, from heat exchanger at a flow rate 0.5 kg/s.

Water is used as fluid in the second loop to extract heat from the first loop and store it in stratified storage tank for future use in the absorption chiller. Simulations have been carried out at varying flow rate of 0.5 kgs^{-1}(shown in Figure 3.35 and 3.36), 1.5 kgs^{-1}(shown in Figure 3.37 and 3.38) and 2.9 kgs^{-1} (shown in Figure 3.39 and 3.40) for 8760 hours. The positive temperature gradient signifies the heat transfer from first loop to second loop in day time, giving positive heat extraction and in night time, second loop being hotter than the first results in negative temperature gradient thus giving negative heat extraction and drop in temperature of second loop.

Figure 3.41 shows the heat extracted by second loop of water at different flow rates. It can be seen that with a flow rate of 0.5 kgs^{-1} heat extracted through our 8760 hours is more steady, having less negative value, whereas, with a flow rate of 2.9 kgS^{-1} heat extraction has high peak values, achieving high fluid temperature at centain postion of the years, shown in Figure 3.42.

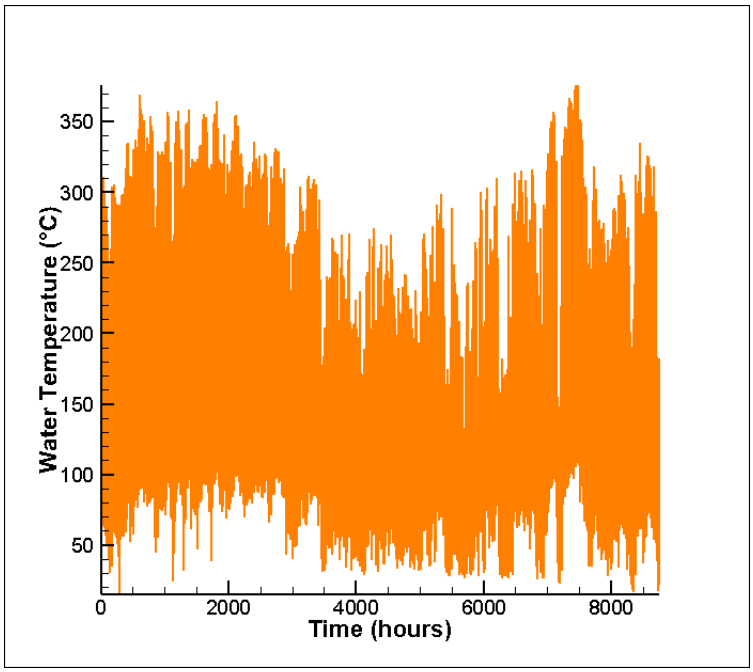

Figure 3.36: Temperature of feed water from heat exchanger to storage tank at a flow rate 0.5 kg/s.

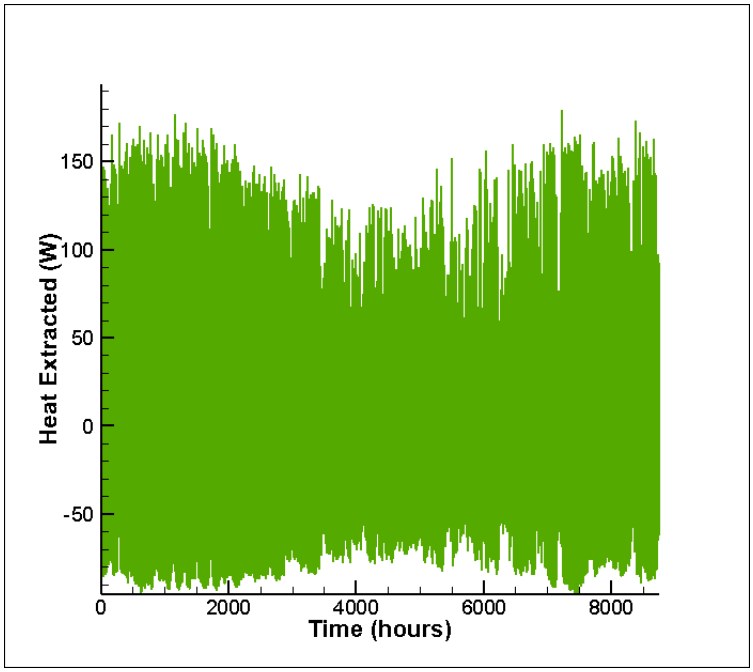

Figure 3.37: Heat transfer to feed water, into storage tank, from heat exchanger at a flow rate 1.5 kg/s.

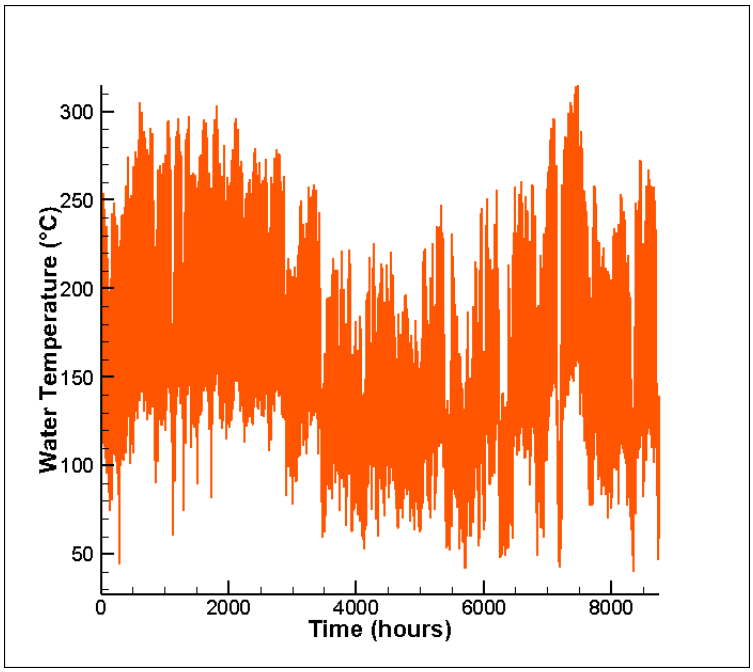

Figure 3.38: Temperature of feed water from heat exchanger to storage tank at a flow rate 1.5 kg/s.

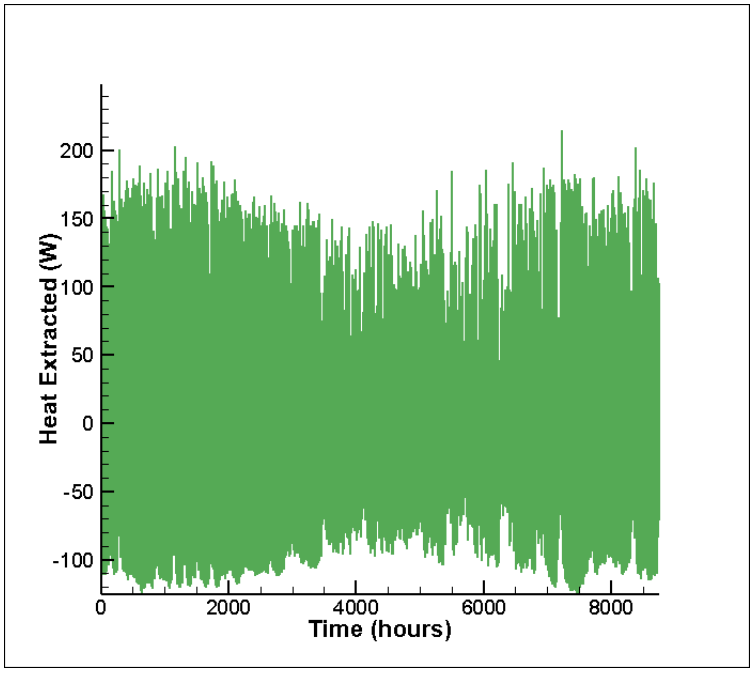

Figure 3.39: Heat transfer to feed water, into storage tank, from heat exchanger at a flow rate 2.9 kg/s.

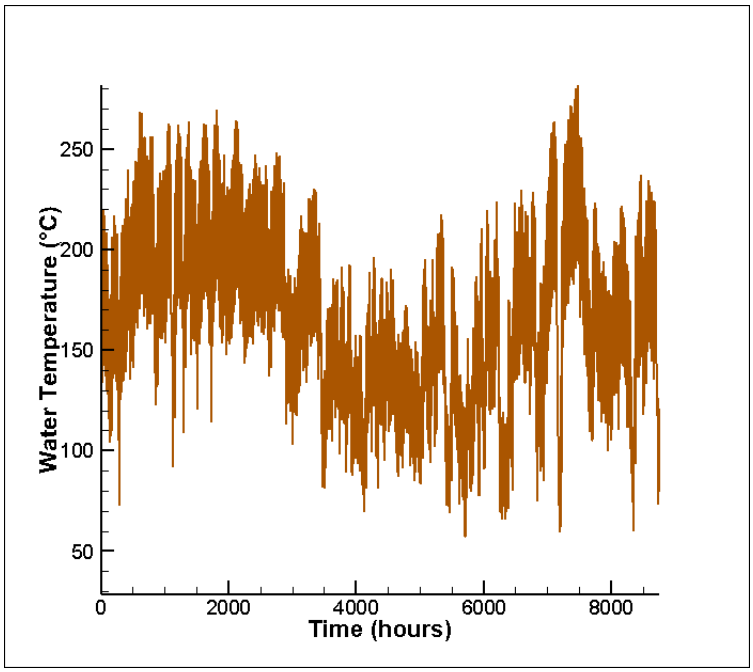

Figure 3.40: Temperature of feed water from heat exchanger to storage tank at a flow rate 2.9 kg/s.

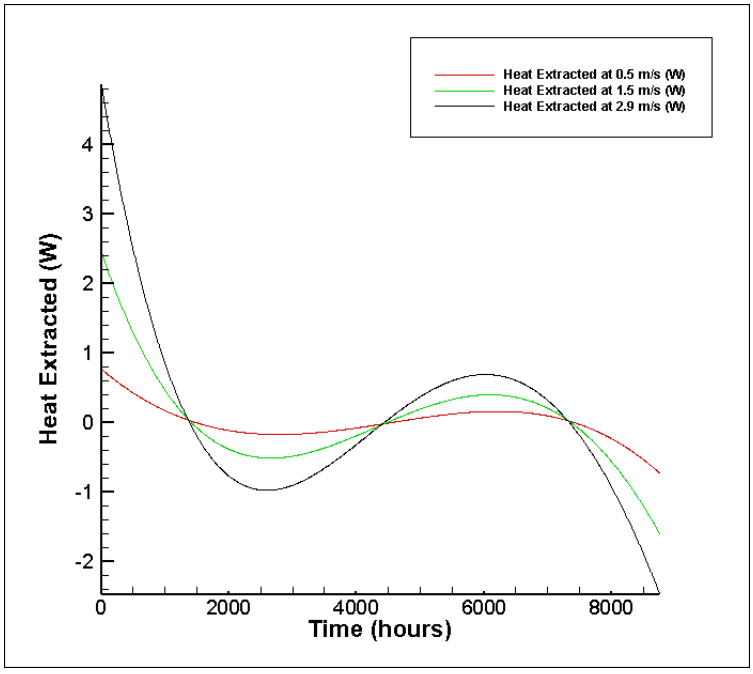

Figure 3.41: Heat extracted by water from HTF in heat exchanger with variation of flow rate of water.

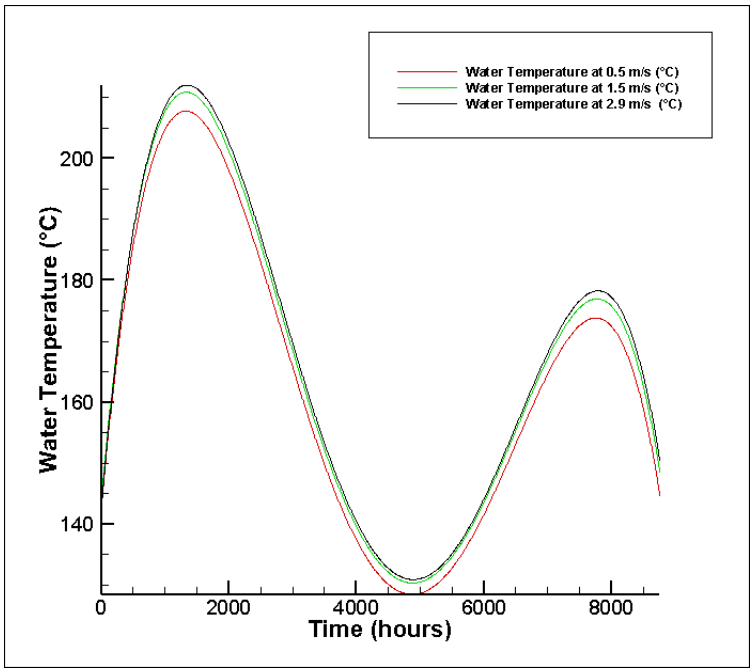

Figure 3.42: Temperature of feed water into storage tank, for 8760 hours, from heat exchanger with variation of flow rate of water.

Chapter 4

Energy Storage

Solar energy is a time-dependent energy resource. Energy needs for a very wide variety of applications are also time dependent but in a different fashion than the solar energy supply. Energy (or product) storage must be considered in the light of a solar process system, the major components of which are the solar collector, storage units, conversion devices (such as air conditioners or engines), loads, auxiliary (supplemental) energy supplies, and control systems. The performance of each of these components is related to that of the others.

The optimum capacity of an energy storage system depends on the expected time dependence of solar radiation availability, the nature of loads to be expected on the process, the degree of reliability needed for the process, the manner in which auxiliary energy is supplied, and an economic analysis that determines how much of the annual load should be carried by solar and how much by the auxiliary energy source.

In passive solar heating, collector and storage components are integrated into the building structure. The performance of storage media in passive heating systems is interdependent with the absorption of energy [32].

4.1 Solar Energy Storage System

The choice of storage media depends on the nature of the process. For water heating, energy storage as sensible heat of stored water is logical. If air heating collectors are used, storage in sensible or latent heat effects in particulate storage units is indicated, such as sensible heat in a pebble bed heat exchanger. In passive heating, storage is provided as sensible heat in building elements. If photovoltaic or photochemical processes are used, storage is logically in the form of chemical energy.

The major characteristics, as discussed by Duffie and Beckman [32], of a thermal energy storage system are:

1. Its capacity per unit volume.

2. The temperature range over which it operates, that is, the temperature at which heat is added to and removed from the system.

3. The means of addition or removal of heat and the temperature differences associated therewith.

4. Temperature stratification in the storage unit.

5. The power requirements for addition or removal of heat.

6. The containers, tanks, or other structural elements associated with the storage system.

7. The means of controlling thermal losses from the storage system.

8. Its cost.

A relationship between the average collector temperature and the temperature at which heat is delivered to the load is given by [32]:

$$\begin{aligned} T\ (collector) - T\ (delivery) = \Delta T\ (transport\ from\ collector\ to\ storage) \\ + \Delta T\ (into\ storage) \\ + \Delta T\ (storage\ loss) \\ + \Delta T\ (out\ of\ storage) \\ + \Delta T\ (into\ application) \\ + \Delta T\ (transport\ from\ storage\ to\ application) \end{aligned}$$

Thus, the temperature of the collector, which determines the useful gain for the collector, is higher than the temperature at which the heat is finally used by the sum of a series of temperature difference driving forces. An objective of system design, and particularly of storage unit design, is to minimize or eliminate these temperature drops within economic constraints.

4.2 Types of Storage

A solar process design may have alternatives in locating the energy storage component. The choice of energy storage very different effects on the operating temperature of the solar collector, collector size, and ultimately cost. These arguments may be substantially modified by requirements for use of auxiliary energy.

The available storage technologies are:

1. Water storage.

2. Stratified storage tank.
3. Packed Bed storage.
4. Storage walls.
5. Seasonal storage.
6. Phase change energy storage.
7. Chemical energy storage.
8. Battery storage.

4.2.1 Water Storage

For many solar systems water is the ideal material in which to store usable heat. Energy is added to and removed from this type of storage unit by transport of the storage medium itself, thus eliminating the temperature drop between transport fluid and storage medium.

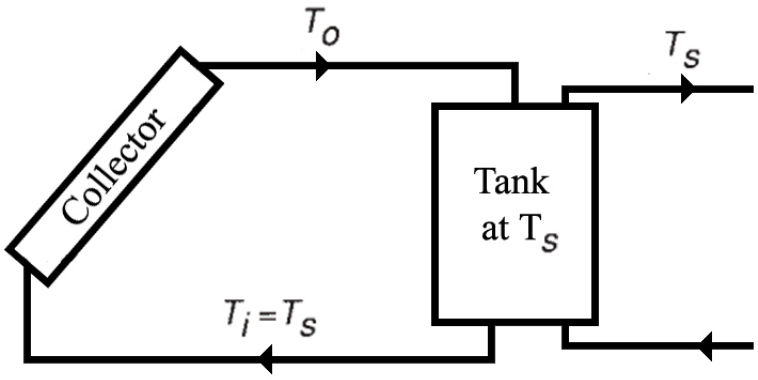

Figure 4.1: A typical system using water tank storage, with water circulation through collector, to add energy, and through the load, to remove energy.

A typical system in which a water tank is used is shown in Figure 4.1. A forced-circulation (pumped) system is shown, but it could be natural circulation. Energy delivery to the load could be across a heat exchanger. Implicit in the following discussion is the idea that flow rates into and out of the tanks, to collector and load, can be determined. The energy storage capacity of a water (or other liquid) storage unit at uniform temperature (i.e., fully mixed, or unstratified) operating over a finite temperature difference is given by:

$$Q_s = (mC_p)_s \Delta T_s \tag{4.1}$$

where Q_s is the total heat capacity for a cycle operating through the temperature range ΔT_s and m is the mass of water in the unit.

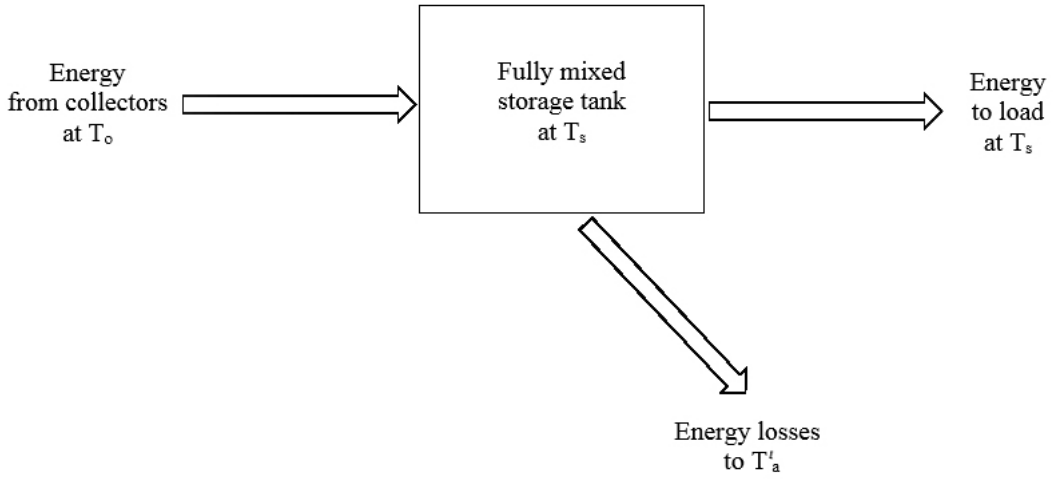

Figure 4.2: Unstratified storage of mass m operating at time-dependent temperature T_s in ambient temperatur T'_a.

An energy balance on the unstratified tank shown in Figure 4.2 is:

$$(mC_p)_s \frac{dT_s}{dt} = \dot{Q}_u - \dot{L}_s - (UA)_s(T_s - T'_a) \tag{4.2}$$

here $\dot{Q}_u$ and $\dot{L}_s$ are rates of addition or removal of energy from the collector and to the load and $T'a$ is the ambient temperature for the tank (which may not be the same as that for a collector supplying energy to the tank).

Using simple Euler integration on Equation 4.2 is usually satisfactory [32] [i.e., rewriting the temperature derivative as (T_s^+ - T_s)/Δt and solving for the tank temperature at the end of a time increment],

$$T_s^+ = T_s + \frac{\Delta t}{(mC_p)_s}\left[Q_u - L_s - (UA)_s(T_s - T'_a)\right] \tag{4.3}$$

Thus the temperature at the end of an hour is calculated from that at the beginning, assuming that Q_u, L_s, and the tank losses do not change during the hour.

4.2.2 Stratified Storage Tank

Water tanks can operate with significant degrees of stratification, that is, with the top of the tank hotter than the bottom. Many stratified tank models have been developed;

they fall into either of two categories as discussed by Duffie and Beckman [32]. In the first, the multinode approach, a tank is modeled as divided into N nodes (sections), with energy balances written for each section of the tank; the result is a set of N differential equations that can be solved for the temperatures of the N nodes as functions of time. In the second, the plug flow approach, segments of liquid at various temperatures are assumed to move through the tank in plug flow, and the models are essentially bookkeeping methods to keep track of the size, temperature, and position of the segments. Each of these approaches has many variations, and the selection of a model depends on the use to which it will be put. None of them lend themselves to hand calculations.

The degree of stratification in a real tank will depend on the design of the tank; the size, location, and design of the inlets and outlets; and flow rates of the entering and leaving streams. It is possible to design tanks with low inlet and outlet velocities that will be highly stratified (Gari and Loehrke [50]; Van Koppen et al. [17]). The effects of stratification on solar process performance can be bracketed by calculating performance with fully mixed tanks and with highly stratified tanks.

Multimode Tank

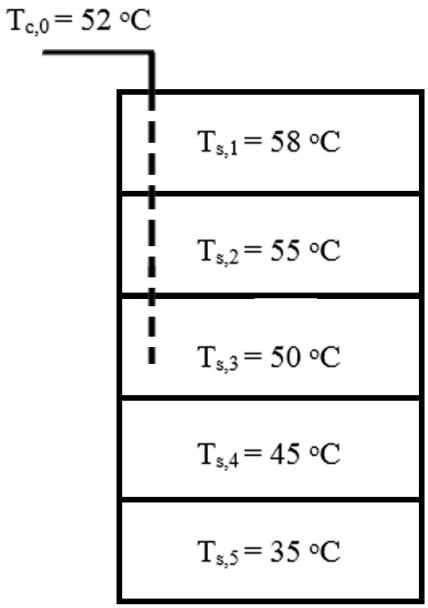

Figure 4.3: A hypothetical five-node tank with $T_{s,2} > T_{c,o} > T_{s,3}$. Water can be considered to enter at node 3 or be distributed among nodes 1, 2, and 3.

To formulate the equations for a multinode tank, it is necessary to make assumptions about how the water entering the tank is distributed to the various nodes. For example, for the five-node tank shown in Figure 4.3, water from the collector enters at a temperature $T_{c,0}$, which lies between $T_{s,2}$ and $T_{s,3}$. It can be assumed that it all finds its way down inside the tank to node 3, where its density nearly matches that of the water in the tank. Alternatively, it can be assumed that the incoming water distributes itself in some way to nodes 1, 2, and 3. In the following discussion, a model is developed that can represent a high degree of stratification; it is assumed that the water in Figure 4.3 finds its way into node 3.

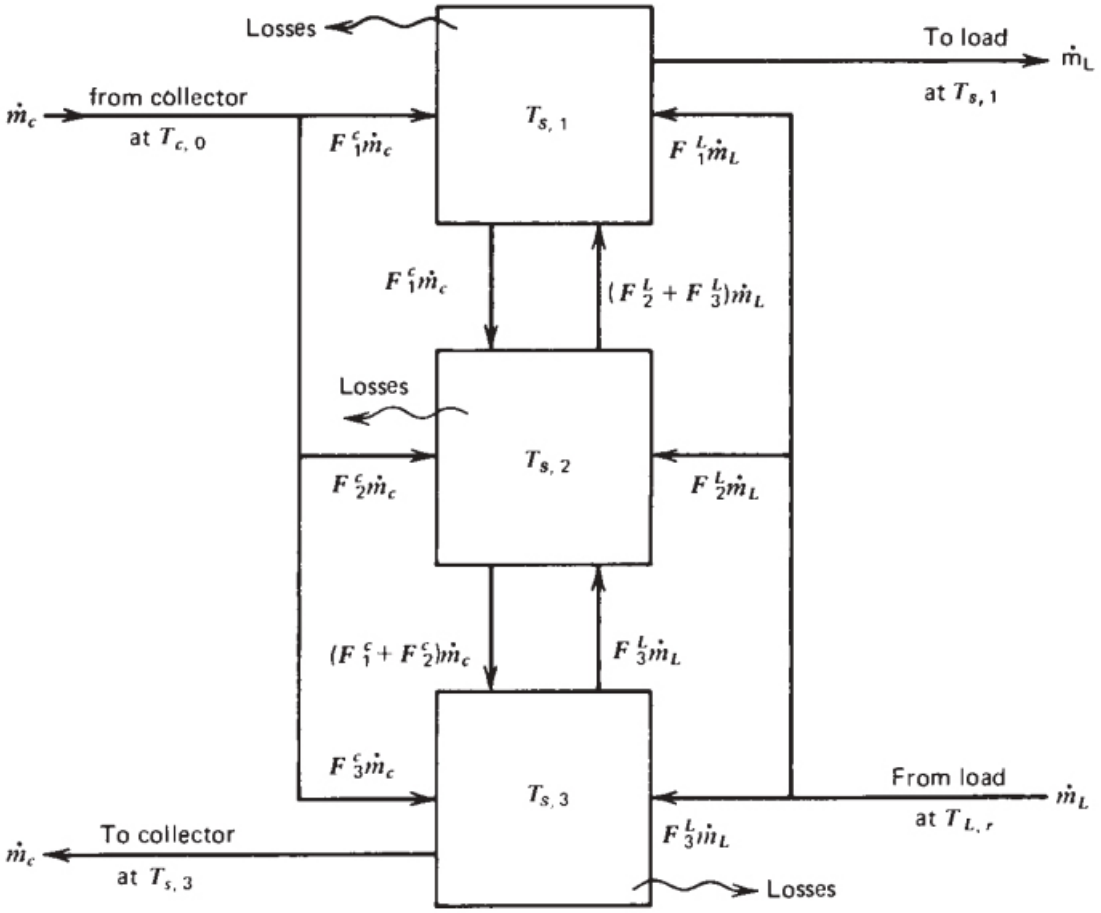

Figure 4.4: Three-node stratified liquid storage tank. Adopted from Duffie and Beckman [32].

Stratification is difficult to evaluate without considering the end use. If the load can use energy at the same efficiency without regard to its temperature level (that is, thermodynamic availability), then maximum stratification would provide the lowest possible temperature near the bottom of the tank and this would maximize collector output. On the other hand, if the quality of the energy to the load is important, then minimizing the destruction of available energy may be the proper criteria for defining maximum stratifi-

cation (although all parts of the system should be considered simultaneously in such an analysis). The following analysis is intended to provide a limiting case in which the bottom of the tank is maintained at a minimum temperature, but other criteria could be used.

For a three-node tank, as shown in Figure 4.4, adopted from Duffie and Beckman [32], the flow to the collector always leaves from the bottom, node 3, and the flow to the load always leaves from the top, node 1. The flow returning from the collector will return to the node that is closest to but less than the collector outlet temperature. Suppose the three node temperatures are 45°C, 35°C, and 25°C, with, of course, the hottest at the top. Return water from the collector lower than 35°C will go to node 3 and between 35°C and 45°C would go to node 2.

A collector control function F_i^c can be defined to determine which node receives water from the collector:

$$F_i^c = \begin{cases} 1, & \text{if } i = 0 \text{ and } T_{c,0} > T_{s,1} \\ 1, & \text{if } T_{s,i-1} \geq T_{c,0} > T_{s,i} \\ 0, & \text{if } i = 0 \text{ or if } i = N+1 \\ 0, & \text{otherwise} \end{cases} \tag{4.4}$$

Note that if the collector is operating, then one and only one control function can be nonzero. Also, a fictitious temperature Ts,0 of the nonexistent node zero is assumed to be a large number. The three branches of the collector return water are controlled by this collector return control function, as shown in Figure 4.4. For the three-node tank of the previous paragraph with return water between 45°C and 35°C, $F_1^c = 0$, $F_2^c = 1$, $F_3^c = 0$.

The liquid returning from the load can be controlled in a similar manner with a load return control function F_i^L,

$$F_i^c = \begin{cases} 1, & \text{if } i = N \text{ and } T_{L,r} < T_{s,N} \\ 1, & \text{if } T_{s,i-1} \geq T_{L,r} > T_{s,i} \\ 0, & \text{if } i = 0 \text{ or if } i = N+1 \\ 0, & \text{otherwise} \end{cases} \tag{4.5}$$

The net flow between nodes can be either up or down depending upon the magnitudes of the collector and load flow rates and the values of the two control functions at any particular instant. It is convenient to define a mixed-flow rate, adopted from Duffie and Beckman [32], that represents the net flow into node i from node i - 1, excluding the effects of flow, if any, directly into the node from the load:

$$\dot{m}_{m,1} = 0 \tag{4.6}$$

$$\dot{m}_{m,i} = \dot{m}_c \sum_{j=1}^{i-1} F_i^c - \dot{m}_L \sum_{j=i+1}^{N} F_j^L \tag{4.7}$$

$$\dot{m}_{m,N+1} = 0 \tag{4.8}$$

With these control functions, an energy balance on node i can be expressed as:

$$m_i \frac{dT_{s,i}}{dt} = \left(\frac{UA}{C_p}\right)_i (T'_a - T_{s,i}) + F_i^c \dot{m}_c (T_{c,o} - T_{s,i}) + F_i^L \dot{m}_L (T_{L,r} - T_{s,i}) + \begin{cases} \dot{m}_{m,i}(T_{s,i} - T_{s,i}), & \text{if } \dot{m}_{m,i} > \\ \dot{m}_{m,i+1}(T_{s,i} - T_{s,i+1}), & \text{if } \dot{m}_{m,i+1} \end{cases}$$

(4.9)

where a term has been added to account for losses from node i to an environment at T'_a.

With a large number of nodes, the tank model given by Equation 4.9 represents a high level of stratification that may not be achievable in actual experiments. There is very little experimental evidence to support the use of this model to represent high stratification, but the model is based on first principles.

As a practical matter, many tanks show some degree of stratification, and it is suggested that three or four nodes may represent a reasonable compromise between conservative design (represented by systems with one-node tanks) and the limiting situation of carefully maintained high degrees of stratification.

Two other factors may be significant. First, stratified tanks will have some tendency to destratify over time due to diffusion and wall conduction. This has been experimentally studied by Lavan and Thompson [51]. Second, some tanks have sources of energy in addition to that in fluids pumped into or out of the tank. If, for example, an auxiliary heater coil were present in one of the nodes, an additional term could be added to Equation 4.9 to account for its effect.

Numerical integration of Equations 4.2 or 4.9 can be accomplished by several techniques that are discussed in texts on numerical methods. The explicit Euler, implicit Crank-Nicholson, predictor-corrector, and Runge–Kutta methods are the most common. Because of the complicated nature of the tank equations when coupled to a load and a collector, particularly with the stratified tank model, a computer must be used to obtain solutions.

Plug Flow

An alternative approach suggested by Kuhn et al. [52] for modeling a stratified storage tank is based on the assumption of plug flow of the fluid up or down in the tank. (The resulting model is not amenable to the step-by-step solutions of a differential equation and is useful only in programs such as TRNSYS (2012).) Increments of volume (segments) of fluid from either the collector (or other heat source) or load enter the tank at

an appropriate location, shifting the position of all existing segments in the tank between the inlet and the return. The size of a segment depends on the flow rate and the time increment used in the computation.

The point at which heated fluid is considered to enter the tank can be at a fixed position or at a variable position. If the fluid is considered to enter at a fixed position, it may be necessary to combine nodes above or below the entry to avoid temperature inversions. If the inlet is considered to be at a variable position (in a manner analogous to that shown in Figure 4.3), the position is selected so as to avoid temperature inversions.

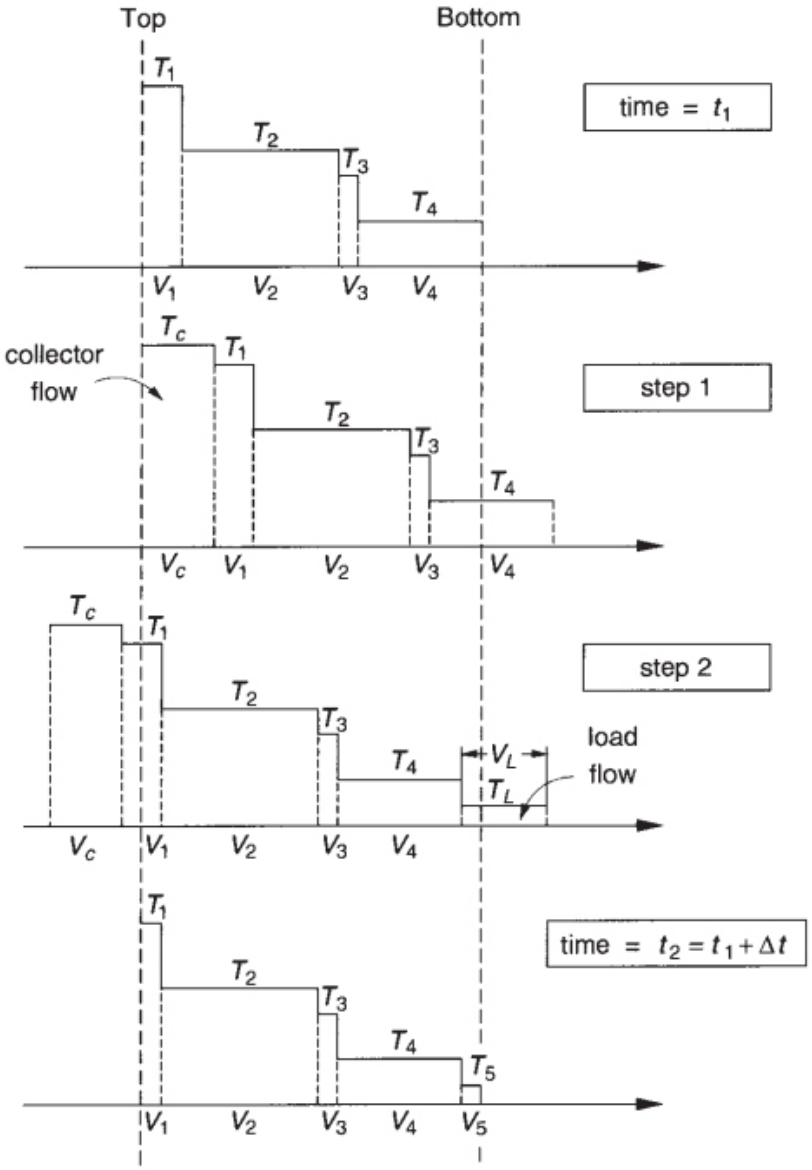

Figure 4.5: An example of the plug flow algebraic tank model. Adapted from Kuhn et al. [52].

Figure 4.5 illustrates the concept of the plug flow tank model. In this example, the

tank is initially divided into four segments of volume V_i (represented on the figure by segments of the horizontal axis) and temperatures T_i without temperature inversions. In one time step, the collector delivers a volume of liquid, V_c, equal to $\dot{m}_c \Delta t/\rho$ at a temperature T_c. Assuming that $T_c > T_L$, a new segment is added at the top of the tank and the existing profile is shifted down. At the same time, a volume of fluid V_L returns from the load, with $V_L = \dot{m}_L \Delta t/\rho$ at a temperature of T_L. (These steps are shown sequentially, although they occur simultaneously.) If $T_L < T_4$, then a segment is added at the bottom of the tank and the whole profile is shifted upward. The net shift of the profile in the tank is volume V_c - V_L or $(\dot{m}_c \ \ \dot{m}_L)\Delta t/\rho$. The segments and/or fractions of segments whose positions fall outside the bounds of the tank are returned to the collector and/or load. The average temperature of the fluid delivered to the load for the example of Figure 4.5 is:

$$T_D = \frac{V_c T_c + (V_L - V_c) T_1}{V_L} \tag{4.10}$$

and the average heat source return temperature $T_R = T_L$.

The plug flow model, in contrast to the differential equations of the type of Equation 4.10, is algebraic. Its use in simulations is primarily a matter of bookkeeping.

This model can represent a somewhat higher degree of stratification than that of multinode differential equation models (TRNSYS, 2012; Kuhn et al., [52]).

The number of nodes needed to adequately predict the performance of a solar storage tank depends upon the application. If the goal is to predict the thermocline (i.e., the temperature distribution) during laboratory testing of tanks with specified periods of charging, discharging, and stand-by, Druck (as reported by Oberndorfer et al. [53]) needed more than 100 nodes to reproduce the measured exit temperatures. Kleinbach et al. [54] compared experimental data (for domestic hot-water-sized systems) with model predictions and found that 10 or fewer nodes were satisfactory in predicting measured performance. Oberndorfer et al. [53] modeled a number of different systems using from 1 to 100 tank nodes and concluded that for annual predictions no more than 10 nodes are necessary and 3 to 5 nodes are usually sufficient. The general conclusion from these studies is that a 1-node tank model (i.e., a fully mixed tank) provides a conservative estimate of annual performance and a 10-node model provides essentially the same system performance estimate as a 100-node model.

4.2.3 Packed Bed Storage

A packed-bed (also called a pebble bed or rock pile) storage unit uses the heat capacity of a bed of loosely packed particulate material to store energy. A fluid, usually air, is circulated through the bed to add or remove energy. A variety of solids may be used, rock being the most widely used material.

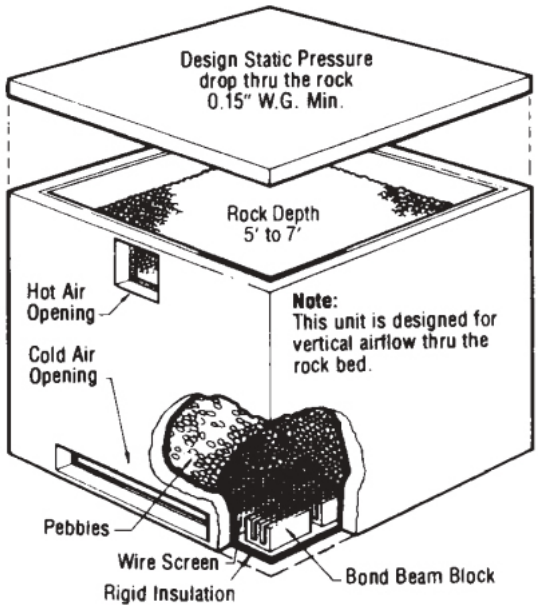

Figure 4.6: A packed-bed storage unit. Courtesy of Solaron Corp [32].

A packed-bed storage unit is shown in Figure 4.6. Essential features include a container, a screen to support the bed, support for the screen, and inlet and outlet ducts. In operation, flow is maintained through the bed in one direction during addition of heat (usually downward) and in the opposite direction during removal of heat.

A major advantage of a packed-bed storage unit is its high degree of stratification. This can be visualized by consideration of a hypothetical situation of a bed initially at a fixed temperature, which has air blown into it at a higher fixed temperature. The heat transfer coefficient–area product between the air and pebbles is high, which means that high-temperature air entering the bed quickly loses its energy to the pebbles. The pebbles near the entrance are heated, but the temperature of the pebbles near the exit remains unchanged and the exit air temperature remains very close to the initial bed temperature. As time progresses a temperature front passes through the bed. By hour 5 the front reaches the end of the bed and the exit air temperature begins to rise.

When the bed is fully charged, its temperature is uniform. Reversing the flow with a new reduced inlet temperature results in a constant outlet temperature at the original inlet temperature for 5 h and then a steadily decreasing temperature until the bed is fully discharged.

A packed bed in a solar heating system does not normally operate with constant inlet temperature. During the day the variable solar radiation, ambient temperature, collector inlet temperature, load requirements, and other time-dependent conditions result in a variable collector outlet temperature.

4.2.4 Storage Walls

In passive heating systems, storage of thermal energy is provided in the walls and roofs of the buildings. A case of particular interest is the collector-storage wall, which is arranged so that solar radiation transmitted through glazing is absorbed on one side of the wall. The temperature of the wall increases as energy is absorbed, and time-dependent temperature gradients are established in the wall. Energy is lost through the glazing and is transferred from the room side of the wall to the room by radiation and convection. Some of these walls may be vented, that is, have openings in the top and bottom through which air can circulate from and to the room by natural convection, providing an additional mechanism for transfer of energy to the room. Figure 4.7 shows a section of such a wall.

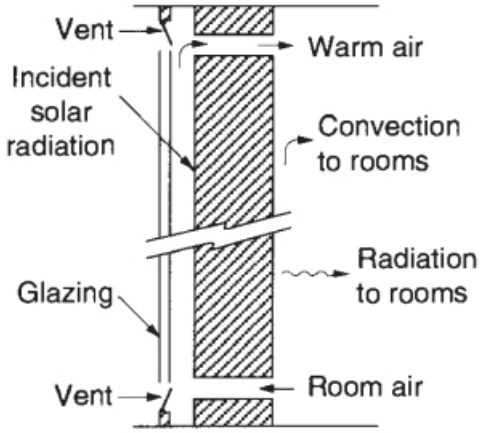

Figure 4.7: Section of a storage wall with glazing and energy-absorbing surface on one surface [32]

The heat transfer coefficient between air in the gap and the wall and glazing depends on whether the vents are open. The analysis for collector-storage walls can be simplified to apply to walls that are not vented or that are not glazed.

4.2.5 Seasonal Storage

Large-scale solar heating systems that supply energy to district heating systems for building and water heating require large-scale storage facilities. These are in most cases in the ground, as there is no other feasible way to gain the necessary capacity. The objective of very large scale storage is to store summer energy for winter use.

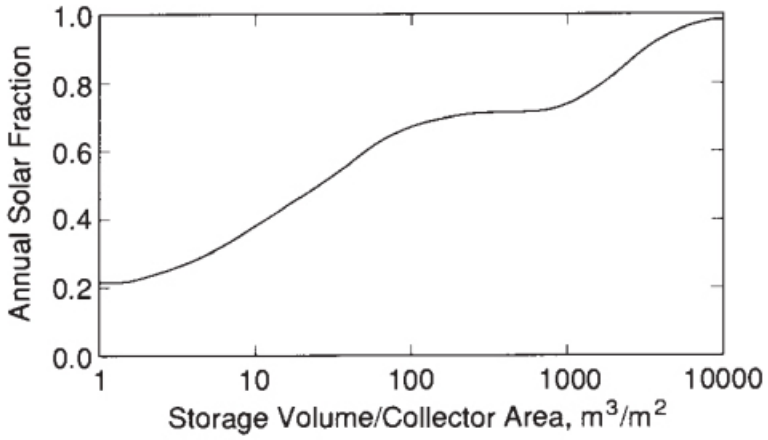

Figure 4.8: Variation of annual fraction of heating loads carried by solar energy in a space heating application with storage capacity per unit collector area. Adapted from Braun [55].

Figure 4.8 shows how annual solar fraction can vary with storage capacity (on a log scale) for building heating. There are two "knees" in the curve; the first is where sufficient energy is stored in a day to carry the loads through the night and the second is where energy is stored in the summer to carry loads in the next winter. Storage capacity per unit collector area must be two to three orders of magnitude larger for seasonal storage than for overnight storage. These factors have led to consideration of very large thermal energy storage systems.

Bankston [56] provides a review of seasonal storage solar heating systems, much of which is concerned with design and performance of the storage units. Several ground storage methods have been explored and/or used, including water-filled tanks, pits, and caverns underground; storage in the ground itself; and storage in aquifers.

Aquifer storage is closely related to ground storage, except that the primary storage medium is water which flows at low rates through the ground. Water is pumped out of and into the ground to heat it and extract energy from it. Water flow also provides a mechanism for heat exchange with the ground itself. As a practical matter, aquifers cannot be insulated. Only aquifers that have low natural flow rates through the storage field can be used.

4.2.6 Phase Change Energy Storage

Materials that undergo a change of phase in a suitable temperature range may be useful for energy storage if several criteria can be satisfied. The phase change must be accompanied by a high latent heat effect, and it must be reversible over a very large number of cycles without serious degradation. The phase change must occur with limited supercooling or superheating, and means must be available to contain the material and transfer

heat in and out. Finally, the cost of the material and its containers must be reasonable. If these criteria can be met, phase change energy storage systems can operate over small temperature ranges, have relatively low volume and mass, and have high storage capacities (relative to energy storage in specific-heat-type systems).

Morrison and Abdel-Khalik [57] developed a model applicable to phase change materials in such containers, where the length in flow direction is L, the cross-sectional area of the material is A, and the wetted perimeter is P. The heat transfer fluid passes through the storage unit in the x direction at the rate m and with inlet temperature T_{fi} as shown in Figure 4.9.

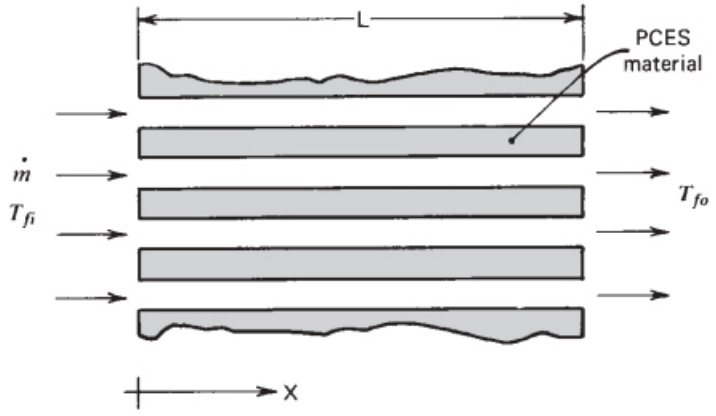

Figure 4.9: Schematic of a phase change storage unit. From Morrison and Abdel-Khalik ([57]).

A model can be based on three assumptions:

1. During flow, axial conduction in the fluid is negligible.
2. The Biot number is low enough that temperature gradients normal to the flow can be neglected.
3. Heat losses from the bed are negligible.

Other practical considerations include corrosion, reactions of the phase change material with containers or other side reactions, vapor pressure, and toxicity. Cost is a major factor in many applications and rules out all but the least expensive materials.

4.2.7 Chemical Energy Storage

An ideal thermochemical reaction for energy storage is an endothermic reaction in which the reaction products are easily separable and do not undergo further reactions. For example, decomposition reactions of the type AB + heat A + B are candidates if the reaction can be reversed to permit recovery of the stored energy. The products A and B

can be stored separately, and thermal losses from the storage units are restricted to sensible heat effects, which are usually small compared to heats of reaction. Unfortunately, there are not very obvious candidates of this type useful for low-temperature solar applications. Reactions in which water vapor is a product have the difficulty that the heat of condensation is usually lost.

Thermal decomposition of metal oxides for energy storage has been considered by Simmons [58]. These reactions may have the advantage that the oxygen evolved can be used for other purposes or discarded and oxygen from the atmosphere used in the reverse reactions. Two examples are the decomposition of potassium oxide,

$$4KO_2 \rightarrow 2K_2O + 3O_2$$

which occurs over a temperature range of 300°C to 800°C with a heat of decomposition of 2.1 MJ/kg, and lead oxide,

$$2PbO_2 \rightarrow 2PbO + O_2$$

which occurs over a temperature range of 300°C to 350°C with a heat of decomposition of 0.26 MJ/kg. There are many practical problems yet to be faced in the use of these reactions.

Processes that produce electrical energy may have storage provided as chemical energy in electrical storage batteries. Several types of battery systems can be considered for these applications, including lead-acid, nickel-iron, and nickel-cadmium batteries. For low discharge rates and moderate charge rates the efficiencies of these systems range from 60 to 80% (ratio of watt-hour output to watt-hour input). It is also possible to electrolyze water with solar-generated electrical energy, to store oxygen and hydrogen, and to recombine in a fuel cell to regain electrical energy (Bacon [59]). These storage systems are characterized by the relatively high cost per kilowatt-hour of storage capacity and can now be considered for low-capacity special applications such as auxiliary power supply for space vehicles, isolated telephone repeater power supplies, instrument power supplies, and so on.

4.2.8 Battery storage

In this section we consider chemical reactions that are specifically designed to store electricity. In recent years there has been considerable work on improving batteries for hybrid electric vehicles. This work is directly applicable to batteries used for energy storage for wind and photovoltaic systems. A detailed discussion of batteries is presented by Bode [60].

The Shepard [61] model is the basis of a number of different battery models. Here we discuss the Shepard model as implemented by Eckstein [62] in the TRNSYS (2012)

simulation program. One problem with all battery models is that a large number of parameters are needed to predict the performance of a specific battery and the only way to accurately obtain values for these parameters is to test the battery.

Accordin[32], the model for each cell requires two equations, one for charging and one for discharging. For charging (when the current I > 0)

$$V = V_{oc} + \frac{1}{k_z} ln\left(\frac{|I|}{I_z} + 1\right) - g_d H + I r_{qd}\left(1 + \frac{m_d H}{Q_d/Q_m - H}\right) \tag{4.11}$$

and for discharging (when the current I < 0)

$$V = V_{oc} - \frac{1}{k_z} ln\left(\frac{|I|}{I_z} + 1\right) - g_c H + I r_{qc}\left(1 + \frac{m_c H}{Q_c/Q_m - H}\right) \tag{4.12}$$

The subscripts c and d represent charging and discharging, respectively. The subscript oc is open circuit and z is a correction for small currents. The parameter H is the fractional depth of discharge and is equal to 1 F, where F is the fractional state of charge and is equal to Q/Q_m. The battery capacity is Q_m (at F = 1 obtainable from the manufacturer) and Q is the actual battery capacity. The cell capacity parameters for charge and discharge are Q_c and Q_d . The internal resistance of the battery is a resistance parameter r_{qc} or r_{qd} times the dimensionless term in the brackets in either Equation 4.11 or 4.12.

The battery model presented here is only one of many possible models. The parameters presented here are for a typical lead-acid battery and may vary considerably for batteries from different manufacturers. When designing a system using this battery model the parameters should be obtained from tests on the actual battery being used.

Chapter 5

Cooling Load

5.1 Introduction

The total heat required to be removed from the space in order to bring it at the desired temperature by the solar absorption cooling system is known as cooling load.

The primary objective is to provide a convenient, consistent and accurate method of calculating these loads and to enable the designer to select suitable solar absorption cooling system that meet the requirement for efficient energy utilization and also considering the economic efficiency. Wherever possible the references and recommendations of ASHRAE Standard 90 and HUD Minimum Property Standards have been included in this Paper. The cooling load obtained by this procedure described herein generally agree within less error.

The purpose of a load estimation is to determine the size of the solar absorption system and its equipment that is required to maintain inside design conditions during Four Season in Bangladesh- Winter, Spring, Summer and Autumn. The design load is based on inside and outside design conditions and it is air conditioning equipment capacity to produce and maintain satisfactory temperature of 25°C and Relative Humidity of 50%. The total heat required to be removed from the space in order to bring it at the desired temperature by the solar absorption cooling system is known as cooling load.

Load calculation is used to accomplish the following objectives:

- Evaluation of the optimum possibilities for load reduction
- Selection of Solar Absorption Cooling system according to requirements
- Partial loads as required for system design,operation and control
- Selection of Solar Collector,Stratified Tank and other accessories

Cooling Load measurement is very important for SAC as the system is chosen from variety of options. Choosing the system is also important considering the economical and working efficiency.

5.2 Overview of the Automobile Lab of IUT

IUT is located at Board Bazar, Gazipur, about 30 kilometres (19 mi) north of Dhaka, the capital city of Bangladesh. Dhaka experiences a hot, wet and humid tropical climate. The total area of IUT is 12 hectares (30 acres). 2 Academic Buildings,3 Labs, Auditorium, Mosque, Admin Building, Student Center , 2 Male Hall, 1 Female Hall and other residence for Teachers and Vice Chancellor.

We selected the Automobile lab portion (**2356'55.7"N 9022'41.2"E**) for SAC system. The reasons to select the automobile labs are

- It has limited useage hour compare to other labs
- The Location of the Lab
- It has no instruments that produces latent heat
- The instruments of this lab is very organized and do not produce heat at all.
- The architecture of lab is very symmetric and has same dimensional windows and doors.

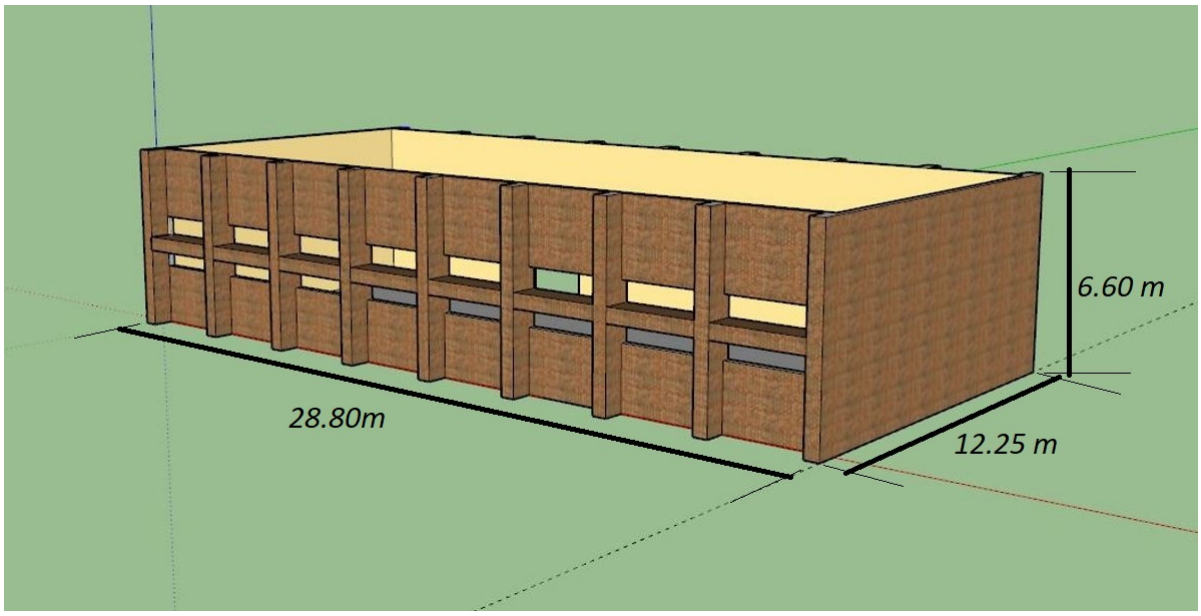

Figure 5.1: Automobile Lab of IUT

The Dimension is as per Figure 5.1 and Important dimensions are on the Table 5.1

ITEM	DIMENSION/NUMBERS
Length	28.80m
Width	12.25m
Height	6.60m
Number of Fan	25
Number of Light	80
Number of Computer	1
Number of Projector	1
Number of Windows	30
Number of Main Doors	2
Number of Side Door	1
Number of Occupants	40
Length of Window	3.10m
Height of Window	.7m
Length of Main Door	3.10m
Height of Main Door	2.85m
Length of Side Door	1.54m
Height of Side Door	2.08m

Table 5.1: LAB OVERVIEW

The main doors are south faced , 16 windows are north Faced and 14 windows are south faced. The only side door is west faced and it is partition door with other lab and complete shaded so it has only conduction heat transfer and infiltration. While all the windows and main doors have radiation,conduction and infiltration.

The information can be divided as per calculation

1. Internal Load
    - Occupants : 40 people
    - Appliances : Computer and Projector
    - Products
    - Lighting Equipment : 80 fluorescent lamp
    - Power Equipment : 25 fans
2. External Load
    - Heat gain through Glass : 30 Windows
    - Heat gain through Walls : Four open walls
    - Heat gain through Roofs : Open Roof
    - Heat gain through Radiation
3. Heat gain from Ventilation and Infiltration

5.3 Weather and Temperature

The climate in the Bangladesh inherent tropical with warm and and sunny winter season which lasts from November until February. It's characterized by a short spring - from March to May, and a long season of rains which goes from June to October. About 80% of all these rains are falling from May to mid-October. As a result, rain over the entire Ganga and Brahmaputra valley leads to submergence of wide areas.

The duration of the dry season here is from November to March. For this country the time of monsoon ends in October. Sometimes the rain can last until November because of an overdue cyclone, what is more likely for the southeastern part of the country.

We have collected data for one complete year that is 8760 hours from Bangladesh Meteorological Department as on figure 5.2. This data contains the radiance, temperature, wind speed pv data as well.

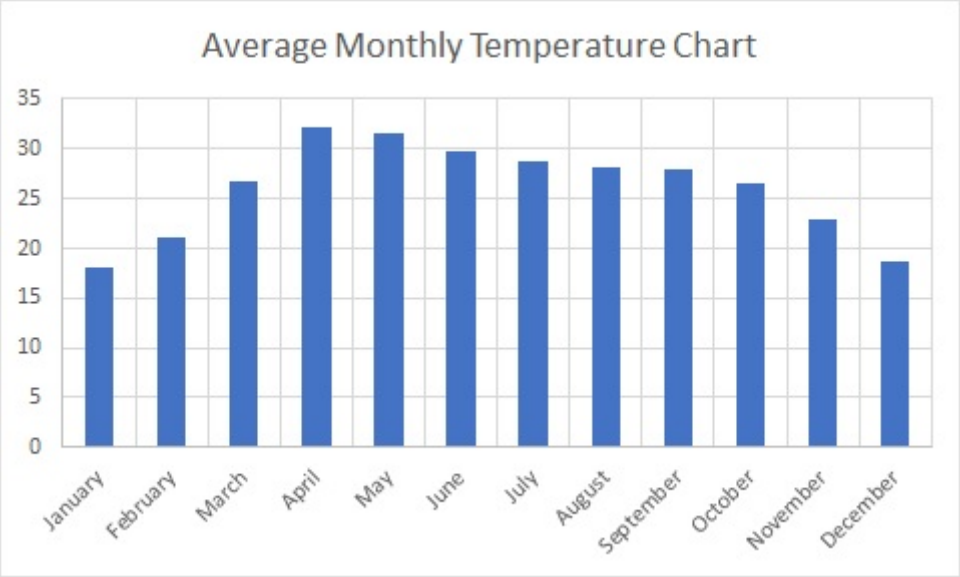

Figure 5.2: Average Monthly Temperature Data from BMD

5.3.1 Winter

For winter season, which begins in December, lukewarm sunny days and chilly nights are more common. In cities like Saidpur and Rangpur in the far north the minimum temperature in January (the coldest month) is 11C and the maximum - around 23C.

Data	December	January	February
Max average t°	+24° C (76° F)	+23° C (73° F)	+25° C (78° F)
Min average t°	+10° C (50° F)	+9° C (48° F)	+10.5° C (51° F)
Sundial in the day	10 hours	10 hours	10.5 hours
Rainy days	0 days	0 days	0 days

Table 5.2: Winter Data

Maximum Value in Winter
Maximum t°: +31.973° C (89.5514° F)
Minimum t°: +8.014° C (47° F)
Sundial in the day: 10.5 hours
Rainy days: 0 days

5.3.2 Spring

From the end of February until the end of March it's very hot in Bangladesh and constant humidity additionally exhausts. Maximal heat point is going to be in April. This season is also characterized by stormy northwest winds, which, among other things, brings showers of hail. As a rule, these unusual thunderstorms may occur in the afternoon and sometimes continue at night.

Data	March	April	May
Max average t°	+31.5° C (89° F)	+35° C (96° F)	+36° C (97° F)
Min average t°	+15° C (59° F)	+20.5° C (69° F)	+24° C (76° F)
Sundial in the day	10.5 hours	9.5 hours	9 hours
Rainy days	2 days	8 days	12 days

Table 5.3: Spring Data

Maximum Value in Spring
Maximum t°: +42.771° C (97° F)
Minimum t°: +15.292° C (59.5° F)
Sundial in the day: 10.5 hours
Rainy days: 12 days

5.3.3 Summer

In June a monsoon usually begins in Bangladesh. Rainfall especially abundant in July, continuing until September - October. The rainiest area - southeast (Chittagong). At the same time, the southwestern regions (for example - Jessur) can be called arid. Air humidity during this period is extremely high everywhere.During this period, there're no state holidays which are celebrated in the country.

Data	June	July	August
Max average t°	+34.5° C (94° F)	+32.5° C (91° F)	+32° C (90° F)
Min average t°	+26° C (78° F)	+25.5° C (77° F)	+26° C (78° F)
Sundial in the day	8 hours	6 hours	6.5 hours
Rainy days	13 days	15 days	14 days

Table 5.4: Summer Data

Maximum Value in Summer
Maximum t°: +35.326° C (95.5868° F)
Minimum t°: +25.176° C (77.3° F)
Sundial in the day: 10.5 hours
Rainy days: 12 days

5.3.4 Autumn

The spill of two great rivers often provokes floods this season. The results are overflowed roads and flooded houses. The end of monsoon rains (October) is marked by approaching of strong winds. Usually, cyclones happen in October - and sometimes they lasts until November. Although November is a hot month more often, but not to the extreme. The average maximum air temperature this period is 30 C, and mostly sunny weather.

Data	September	October	November
Max average t°	+32° C (89° F)	+31.5° C (88° F)	+28° C (83° F)
Min average t°	+25° C (77° F)	+21.5° C (71° F)	+14° C (57° F)
Sundial in the day	7 hours	9 hours	10 hours
Rainy days	12 days	6 days	1 days

Table 5.5: Autumn Data

Maximum Value in Autumn
Maximum t°: +32.887° C (91.1966° F)
Minimum t°: +13.862° C (57° F)
Sundial in the day: 10.5 hours
Rainy days: 12 days

All the calculation is done considering four season of Bangladesh. We calculated the cooling load according to the maximum temperature during seasons. All the maximum temperature of the collected data from Bangladesh Meteorological Department is separated in each weather. As we considered the SAC working under maximum critical condition so at average state it will work smoothly and efficiently. So all the cooling load variable calculation is divided into four section for four session.

5.4 Components of a cooling load

In the system there are three distinct but related heat flow rates, each of which varies with time :

- Heat Gain
- Cooling Load
- Heat Extraction

Heat Gain is the rate at which heat enters or is generated within a space at a given instant of time.There are two gain is classified.They are the manner in which heat enters the space and the type of heat gain.The manner in which a load source enters a space is indicated as follows:

1. Solar radiation through transparent surfaces such as windows
2. Heat conduction through exterior walls and roofs
3. Heat conduction through interior partitions,ceilings and floors
4. Heat generated within the space by occupants,light,appliances,equipment and processes
5. Loads as a result of ventilation and infiltration of outdoor air
6. Other miscellaneous heat gains

The types of heat gain are sensible and latent. Proper selection of cooling and humidifying equipment is required by determining whether the heat gain is sensible or latent. Sensible heat gain is the direct addition of heat to an enclosure, apart from any change in the moisture content, by any or all of the mechanisms of conduction, convection and radiation. When moisture is added to the space.

As constant humidity ratio is to be maintained in the system. then water vapor must be condensed out in the cooling apparatus at a rate equal to its rate of addition in the space. The amount of energy required to do this is essentially equal to the product of the rate of condensation per hour and the latent heat of condensation. This product is called the latent heat gain.

The proper design of an air conditioning system requires the determination of the sensible heat gain in the space, the latent heat gain in the space, and a value for the total load, sensible plus latent, of the outdoor air used for ventilation.

As a further example, the infiltration of outdoor air with a high dry-bulb temperature and a high humidity ratio, and the corresponding escape of room air at a lower dry-bulb

temperature and a lower humidity ratio, would increase both the sensible heat gain and the latent heat gain of the space.

The sensible cooling load is defined as the rate at which heat must be removed from the space to maintain the room air temperature at a constant value. The summation of all instantaneous sensible heat gains at a specific time does not necessarily equal the sensible cooling load for the space at that time. The latent load, however, is essentially an instantaneous cooling load. That part of the sensible heat gain which occurs by radiation is partially absorbed by the surfaces and contents of the space and is not felt by the room air until some time later. The radiant energy must first be absorbed by the surfaces that enclose the space, such as walls and floor, and by furniture and other objects.As soon as these surfaces and objects become warmer than the air,some heat will be transferred to the air in the room by convection. The heat storage capacity of the building components and items, such as walls, floors and furniture, governs the rate at which their surface temperatures increase for a given radiant input. Thus,the interior heat storage capacity governs the relationship between the radiant portion of the sensible heat gain and how it contributes to the cooling load. The thermal storage effect is important in determining the cooling equipment capacity.

5.4.1 Types of Calculations

The calculation can be divided into three section

1. Internal Load
    - Occupants
    - Appliances
    - Products
    - Lighting Equipment
    - Power Equipment
2. External Load
    - Heat gain through Glass
    - Heat gain through Walls
    - Heat gain through Roofs
    - Heat gain through Radiation
3. Heat gain from Ventilation and Infiltration

5.5 Heat gain from occupants

The human body generates heat through the process of metabolism an releases it by radiation from skin or clothing and by by convection and evaporation from the skin,clothing

and the breathing process. That portion of the load due to evaporation of moisture is latent and the rest is sensible.

Degree of Activity	Typical Application	SH /person Watts	LH /person in Watts
Standing,light work,typing	Laboratory	90	95

Table 5.6: Rate of Heat Gain from Occupants of Conditioned Spaces for Adjusted Group [63]

Occupants Equation

$$q_s = No.of people \ \times Sensible\ Heat\ Gain \ \times Cooling\ Load\ Factor \tag{5.1}$$

$$q_l = No.of people \ \times Latent\ Heat\ Gain \tag{5.2}$$

Equation 5.1 is for sensible heat gain and equation 5.2 is for latent heat gain

Conditions

- 40 people
- Standing,light work,typing at Laboratory
- CLF value for 8 hours in a space and average hours after entry into space is .535

If we put the values in equation 5.1 we get

$q_s = 40 \ \times 90 \ \times .535 \ =$ **1926 W**
$q_l = 40 \ \times 95 \ =$ **3800 W**

Total Heat Gain from Occupants = **5726 W**

5.6 Heat gain from appliances

The Internal equipment are another source of heat gain for cooling loads.In a cooling load estimate, heat gain from all appliances-electrical, gas, or steam-should be taken into account. Because of the variety of appliances, applications, schedules, use, and installations,estimates can be very subjective. Often, the only information available about heat gain from equipment is that on its name-plate.

There are many instruments and models of automobile components in the Lab. Along with three vehicles and few car engines with other components. None of them create any

form of heat as all of this are for study and overhauling purposes. Only 24 types of experiments is done here. All of this experiments are study based of different components of the Automobile system.

There is one computer and one projector used for class purpose and their rate of sensible heat gain are respectively 200W and 600W.

So total heat gain from appliances
$q_s = 200 + 600 = \mathbf{800\ W}$

5.7 Heat gain from lighting equipment

The electricity which is supplied produces heat along with the generation of light. Some energy is convected to the air in the conditioned space and some is radited to surrounding surfaces to be convected to the space air at a later time. All of this load is sensible heat. Heat gain from lights in modern office or production areas may be of significant amount. The heat emitted from lights to the room depends on

- Type of lights and their construction
- Location of the light equipment
- Light level in the room

light level in the room

The light level in a room depends primarily on type of activity. For typical office work the level may be in the range 500 - 1000 lux. The lux is the SI unit of illuminance and luminous emittance - measuring luminous flux per unit area and recommended Light Levels in Rooms

Lighting Equation

$$q_s = n \times q_i \times F_u \times F_s \times CLF \tag{5.3}$$

Here,
n Number of lights
q_i Total lamp wattage
F_u fraction of $q_i inuse$
F_s Special ballast allowance factor for fluorescent fixtures
CLF Cooling load factor

Conditions

- The number of lights is 80
- Lamp Wattage is 60 Watt

- No. of Lamps per fixture 1
- Recessed lights are not vented
- Low air supply rate - less than $0.5cfm/ft^2$ of floor area.
- 6 in. Concrete Floor $75lb/ft^2$
- Low ventilation rate - minimum required to handle cooling load.Supply through floor,wall or ceiling diffuser. Ceiling space not vented

If we put the values of F_u=1, F_s=1.30, CLF=0.64 as per the conditions [63] in equation 5.3 we get

$q_s = 80 \times 60 \times 1 \times 1.30 \times 0.64 =$ **3993.6 W**

5.8 Heat gain from power equipment

Instantaneous sensible h eat g ain fr om equip ment op erated by electric motors in a conditioned space is calculated as

$$q_s = SensibleHeatGain \times F_l \times CoolingLoadFactor. \tag{5.4}$$

Here,
F_l Load Factor

The motor use factor may be applied when motor use is known to be intermittent, with significant non use during all hours of operation (e.g., overhead door operator). F or conventional applications, its value is 1.0. The motor load factor is the fraction of the rated load delivered under the conditions of the cooling load estimate.It is assumed that both the motor and driven equipment are in the conditioned space. Unless the manufacturer's technical literature indicates otherwise, motor heat gain normally should be equally divided between radiant and convective components for the subsequent cooling load calculation.

For 25 Fans of Shaded Pole of Nominal rpm of 1500 Full load motor efficiency in percent 36 the value is 900 Btu/hr, the value of Load factor is 1 as the motors are small and CLF value is also 1 as the cooling system is not on 24hr a day [63].
Putting the value on equation 5.4 we find,
$q_s = 25 \times 900 \times 1 \times 1 = 22500Btu/hr =$ **6594.075 W**

5.9 Heat gain due to Ventilation

Ventilation is the intentional introduction of outdoor air into a space and is mainly used to control indoor air quality by diluting and displacing indoor pollutants; it can also be

used for purposes of thermal comfort or dehumidification.

The intentional introduction of outdoor air can be categorized as either mechanical ventilation, or natural ventilation [64]. Mechanical ventilation uses fans to drive the flow of outdoor air into a building. This may be accomplished by pressurization (in the case of positively pressurized buildings), or by depressurization (in the case of exhaust ventilation systems).

It has been shown that outdoor air enters a structure by means of both infiltration and ventilation. Because air is composed of a mix-ture of dry air and moisture particles, the heat gain produced by the entering air will be expressed in terms of both its sensible heat gain and its latent heat gain in Btu per hour.

The sensible and latent heat gain resulting from entering air rep- resents only a small portion of the total heat gain involved in deter- mining the design cooling load of a structure. For many applications, however, the calculation of this portion of the heat gain is crucial to a well-designed system. The following formulas, adapted from ASHRAE materials, are used for making these calculations [63].

Ventilation Equation

$$q_{ventilation} = m_v Cp_m(T_o - T_i) + m_v h_{fg}(W_o - W_i) \tag{5.5}$$

Here,

m_v Mass flow rate of ventilated air
h_{fg}latent heat of vaporization of water
Cp_m Average specific heat of moist air
$T_o Outdoor drybulb temperature$
$T_i Indoor drybulb temperature$
$W_o Outdoor Humidity Ratio$
$W_i Indoor Humidity Ratio$

Conditions

- 1.5 L/s is air requirement per person for Classroom [64].

Title	Winter	Spring	Summer	Autumn
m_v	1.111	1.119	1.14	1.157
T_o	31.973 °	42.771 °	35.326 °	32.887 °
T_i	25 °	25 °	25 °	25 °
W_o	.022331	.042839	.030859	.026191
W_i	.102	.102	.102	.102

Table 5.7: Indoor and Outdoor dry bulb and humidity ratio

Putting value of m_v, T_o, T_i, W_o and W_i for four different seasons on equation 5.5 from table 5.7 we get,

$q_{ventilation,winter} = \mathbf{38206.24\ W}$
$q_{ventilation,spring} = \mathbf{102427.8217\ W}$
$q_{ventilation,summer} = \mathbf{64997.48\ W}$
$q_{ventilation,autumn} = \mathbf{49120.54\ W}$

5.10 Heat gain due to Infiltration

Infiltration is the unintentional or accidental introduction of outside air into a building, typically through cracks in the building envelope and through use of doors for passage [64]. Infiltration is sometimes called air leakage. The leakage of room air out of a building, intentionally or not, is called exfiltration. Infiltration is caused by wind, negative pressurization of the building, and by air buoyancy forces known commonly as the stack effect.

Infiltration Equation

$$q_{infiltration} = V_o \rho_o Cp_m (T_o - T_i) + V_o \rho_o h_{fg} (W_o - W_i) \tag{5.6}$$

Here,
V_o Volumetric flow rate of outdoor air
ρ_o Specific Volume of outdoor air
Cp_m Average specific heat of moist air
$T_o Outdoor dry bulb temperature$
$T_i Indoor dry bulb temperature$
$W_o Outdoor Humidity Ratio$
$W_i Indoor Humidity Ratio$

Condition

- Air Changes per hour half

- $V_o = Length \times Width \times Height \times Ac/60$

Like ventilation we are using table 5.7 for data and putting the values on equation 5.6 we get,

$q_{infiltration,winter} = \mathbf{12867.48\ W}$
$q_{infiltration,spring} = \mathbf{32888.33\ W}$
$q_{infiltration,summer} = \mathbf{20632.97\ W}$
$q_{infiltration,autumn} = \mathbf{16231.57\ W}$

5.11 Sensible heat gain through Glass and Door areas

The heat gain components through glass consists of solar radiation and conduction. Solar radiation is considered in two parts - direct and diffuse (or scatter). Diffuse radiation is the solar radiation that is absorbed, stored and scattered in the atmosphere. The glass can be in the sun (direct and diffuse radiation) or in the shade (diffuse or scatter radiation). Conduction heat gain occurs due to the difference in temperature on either side of the glass. Conduction heat gain is positive if the outdoor air temperature is greater than indoor air temperature and it is negative (heat loss from the space) if the indoor air temperature is greater.//

Direct solar radiation is the vector component of the absolute (total) solar radiation that is perpendicular to the glass surface. The Solar Cooling Load (SCL) Factor for a window is based on this value. So for any given hour, the SCL values for windows with different azimuth and tilt angles will have different SCLs although the absolute solar radiation is the same for all windows.//

Direct solar radiation is the vector component of the absolute (total) solar radiation that is perpendicular to the glass surface. The Solar Cooling Load (SCL) Factor for a window is based on this value. So for any given hour, the SCL values for windows with different azimuth and tilt angles will have different SCLs although the absolute solar radiation is the same for all windows.//

Shading Coefficient (SC) is the ratio of the solar heat through a given glass type under specific conditions to the solar heat gain through a standard reference unshaded glass that was used to determine Solar Cooling Load (SCL) factors.//

Heat gain from Glass Conduction

$$q_{gc} = U \times Area \times CLTD \tag{5.7}$$

Putting the value of Glass window area from table 5.1 2.17 m^2 (23.35769 ft^2) and U = .97 and CLTD value 12, 27, 14 and 14 for respectively winter, spring, summer and autumn for total 30 windows on equation 5.7 we get [63].

$q_{gcwinter}$ = **2415.07 W**
$q_{gcspring}$ = **5433.90 W**
$q_{gcsummer}$ = **2817.58 W**
$q_{gcautumn}$ = **2817.58 W**

Heat gain from Glass Solar Radiation

$$q_{gr} = A \times SC \times SHGF \times CLF \tag{5.8}$$

Solar Heat Gain from radiation for 16 windows on north side and 14 windows on south side. The area of each window is 2.17 m^2 (23.35769 ft^2) and SC=.98. The value of CLF for north is .84 and south is .65 [63]. The value of SHGF is from table 5.8

SHGF	NORTH	SOUTH
Winter	38	86
Spring	38	86
Summer	46	59.67
Autumn	31	181.67

Table 5.8: Solar Heat Gain Factor Table for 24 Deg North Latitudes [63]

$q_{gr,n,w} =$ **2488.46 W**
$q_{gr,n,sp} =$ **3426.15 W**
$q_{gr,n,su} =$ **3893.51 W**
$q_{gr,n,au} =$ **2795.01 W**
$q_{gr,s,w} =$ **13345.86 W**
$q_{gr,s,sp} =$ **5249.97 W**
$q_{gr,s,su} =$ **3276.3 W**
$q_{gr,s,au} =$ **11090.23 W**

Heat gain from Door Conduction

$$q_d = U \times Area \times CLTD \tag{5.9}$$

Putting the value for area of main door and side door which are respectively 8.835 m^2 (95.099149 ft^2) and 3.2032 m^2 (34.4789578 ft^2). The value of U=1.639 and CLTD value of winter, spring, summer and autumn which are respectively 12, 27, 14 and 14 on equation 5.9 we get [63],

$q_{dcwinter} =$ **1215.08 W**
$q_{dcspring} =$ **2733.94 W**
$q_{dcsummer} =$ **1412.56 W**
$q_{dcautumn} =$ **1412.56 W**

5.12 Sensible heat gain through outside walls and roofs

Walls and Roofs can have an important effect on interior comfort conditions in both the residential and non-residential sectors. Walls and roofs come into direct contact with the exterior environmental conditions. The effect on the interior of the building can be seen in HVAC run time, interior temperatures, energy use. As an answer to these concerns, FSEC can help determine what is useful for both energy efficiency and comfort.

Roofs Insulation: Insulation in the attic is important because the attic is a large source of heat gain from the roof. In addition, many buildings have their ducts located in the unconditioned attic space.

Color: Light colored roofs in such a hot and humid environment is highly recommended. Testing has revealed that a white ceramic tile or white metal roof is best. These types of roofs will last 30-40 year compared to the 15 years that is typical of asphalt shingle roofs. These white reflective roofs can lower attic temperatures by up to 25-30 degrees F. Many commercial buildings with central AC have ducts in the attic where there is a significant amount of heat gain. The white roof lowers the attic temperature greatly increasing the air distribution efficiency of the HVAC system.

$$q_{roof} = U \times A \times CLTD \tag{5.10}$$

$$CLTD_{corr} = \big[(CLTD + LM) + (78 - T_r) + (T_o - 85)\big] \times$$

f(5.11)

Walls : Several factors can be utilized to reduce energy consumption and improve interior comfort conditions. Light colored exterior walls can help to reduce interior temperatures by reducing solar heat gain. In addition, shade trees and bushes can reduce this heat gain.

The portion of the air conditioning and heating use due to gains and losses through walls in most commercial buildings is small compared to internal gains. Therefore, going to extremes on wall insulation is not usually of the highest priority. However, some minimal insulation is recommended to reduce peak loads. For buildings in very cold climates, more heavily insulated walls and windows are generally necessary. Windows are important features of walls.

$$q_{wall} = U \times A \times CLTD \tag{5.12}$$

$$CLTD_{corr} = (CLTD + LM) \times K + (78 - T_r) + (T_o - 85) \tag{5.13}$$

Here, K Color adjustment factor
LM Latitude-month correction
f Factor for atic fan and ducts

The value of U for Wall = .413 and for roof= .167. The area of roof, north wall, south wall, east wall and west wall are respectively 352.8 m^2, 155.36 m^2, 142.03 m^2, 80.85 m^2, 77.6468 m^2. The color adjustment factor for wall is .65 and f is .75 [63]. The adjusted CLTD value from

Season	Winter	Spring	Summer	Autumn
Roof	35.6625	49.5	49.1	39.89
North	11.7	20.45	20.986	13.346
South	26.75	24.35	20.986	28.9466
West	19.6	30.85	30.086	23.7466
East	17.65	28.9	28.136	21.7966

Table 5.9: CLTD correction from equations 5.11 and 5.13 [63]

Putting the Value of U, A and CLTD on equation 5.10 and 5.12 we get,

ITEM	Winter	Spring	Summer	Autumn
Occupants	5726 W	5726 W	5726 W	5726 W
Appliances	800 W	800 W	800 W	800 W
Motor	6594.075 W	6594.075	6594.075	6594.075
Lighting	3993.6 W	3993.6 W	3993.6 W	3993.6 W
SHG,North	2488.46 W	3426.15 W	3893.51 W	2795.01
SHG,South	13345.86 W	5249.97 W	3276.3 W	11090.23 W
Roof	6628.24 W	9200.07 W	9125.73 W	7413.97 W
Wall,North	2368.19 W	4139.26 W	4247.75 W	2701.22 W
Wall,South	4949.88 W	4505.78 W	3883.3 W	5356.35 W
Wall,West	1982.75 W	3120.81 W	3043.52 W	2402.23 W
Wall,East	1859.15 W	3044.16 W	2963.69 W	2295.93 W
Glass,conduction	2415.07 W	5433.90 W	2817.58 W	2817.58 W
Door	1215.08 W	2733.94 W	1412.56 W	1412.56 W
Ventilation	38206.24 W	102427.8217 W	64997.48 W	49120.54 W
Infiltration	12867.48 W	32888.33 W	20632.97 W	16231.57 W
TON	29.98 Ton	54.95 Ton	39.07 Ton	34.33 Ton

Table 5.11: Total Cooling Load

Season	Winter	Spring	Summer	Autumn
Roof	6628.24 W	9200.07 W	9125.73 W	7413.97 W
North	2368.19 W	4139.26 W	4247.75 W	2701.22 W
South	4949.88 W	4505.78 W	3883.3 W	5356.35 W
West	1982.75 W	3120.81 W	3043.52 W	2402.23 W
East	1859.15 W	3044.16 W	2963.69 W	2295.93 W

Table 5.10: Cooling load for roof from 5.10 and for walls from 5.12 [63]

5.13 Total cooling load

Chapter 6

Air Conditioning System

6.1 Solar Energy in Air conditioning systems

A simplest way to utilize solar energy for cooling involves connecting a conventional vapor compression chiller to a PV power supply system. A more complex technology involves driving sorption chillers by heat generated at a solar collector system. Heat from collectors may also be used for desiccative and evaporative cooling (DEC) systems.

A vapor compression chiller driven by direct current generated by PV modules is a relatively simple solution, but it requires using a battery. This limits the size and rating of such a system. As a result, this technology is used mainly in small scale applications, often in portable devices used to store medicines or food in tropical areas. Figure 6.1 shows a schematic of a vapor compression chiller driven by electricity generated by PV modules. This electricity is used to power a direct current motor that drives the chiller compressor. The cycle of the refrigerant is a typical cycle of a vapor compression chiller.

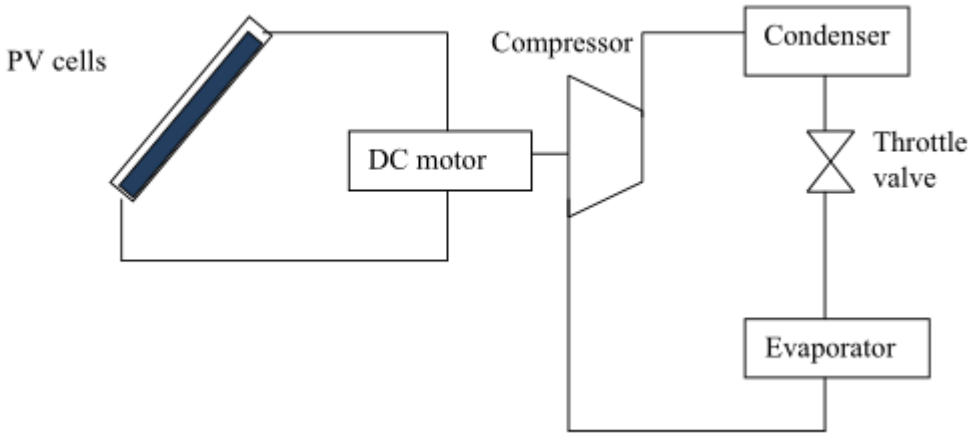

Figure 6.1: Vapor compression chiller driven by PV modules

Except for PV technology, solar thermal collectors coupled to sorption chillers are also seen as a very promising solution. Sorption chillers are divided into absorption and adsorption technology. The general principle of operation is similar in both cases. Heat is removed from a colder heat sink and discharged to the warmer one thanks to a driving energy supplied in the form of heat. In cooling technologies, a phenomenon is called absorption if the refrigerant is absorbed in a liquid called absorbent (refrigerant can be in gaseous and liquid phase), while adsorption involves refrigerant being absorbed in a solid medium called adsorbent (refrigerant can be also in gaseous and liquid phase). Refrigerant absorption or adsorption occurs at low pressure and low temperature. Reverse process (i.e., desorption of a rich solution) occurs at higher pressure and high temperature. In this way, the compression process is carried out. In a desorber (also called a generator), compressed refrigerant vapor is released. Then, just like in the case of an electrically-driven cooling device (refrigerator), the refrigerant vapor is flowing into the condenser, where it releases heat at a constant temperature. The created condensate flows through a throttling (expansion) valve, where it decompresses and cools down. Then, cooled down and decompressed refrigerant is supplied to the evaporator, where it takes heat from the low temperature heat source (cooling this source down). This causes the refrigerant to evaporate; vapor flows into absorber/adsorber, and the cycle is repeated.

Absorption chillers may operate continuously while adsorption devices operate in cycles. In absorption chillers, lithium bromide and water are the most typical working pairs, while in adsorption devices following pairs of adsorber-refrigerant are typically used: silica gelewater, activated carbone ammonia, or methanol, and zeolites-ammonia.

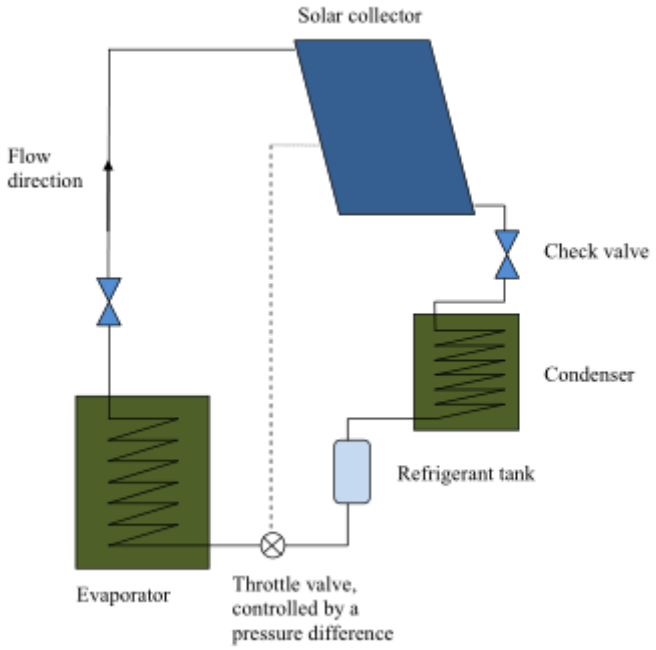

Figure 6.2: Schematic of a solar-driven adsorption chiller.

In the adsorption chiller shown in Figure 6.2, the role of adsorber and desorber is played by solar collectors filled with adsorbent. During the day, solar collectors work as desorbers. They absorb solar radiation and heat the refrigerant that evaporates out of the adsorbent. Then a refrigerant vapor flows to the condenser. There it condenses, releases heat, and as a liquid enters the refrigerant tank. During the night, when there is no solar radiation, temperature and pressure in the collector are dropping. It may also happen during the day, if insolation conditions are changed and solar irradiance reduces considerably. If the collector pressure drops to a level below the evaporator pressure, then the throttling valve controlled by the pressure difference enables the flow of refrigerant into the evaporator. There it evaporates and collects heat from the low-temperature heat source (directly or indirectly, through a cooling medium), thus cooling it down. Then the refrigerant as vapor is absorbed by the adsorbent. When solar radiation appears again with sufficiently high irradiance, the collector turns back into the desorber. All this means that in the considered system cooling takes place during nighttime (when the refrigerant evaporates in the evaporator). If there is no cooling demand during the night, the cooling energy must be stored for later use (e.g., during the daytime). It may be stored in ice blocks, hence the name of such equipment: ice generators.

6.2 Absorption Air Conditioning

Absorption air conditioning is compatible with solar energy since a large fraction of the energy required is thermal energy at temperatures that currently available flat-plate collectors can provide. Solar absorption air conditioning has been the subject of investigation by a number of researchers [65] [66].

Absorption refrigeration systems utilize heat as the source of energy for refrigeration compared to Electrical energy used in conventional vapor compression systems. These systems achieve the cooling effect by evaporating the refrigerant and then releasing heat into the surroundings while condensation, in a way very similar to vapor compression systems. The key difference between conventional systems and absorption systems is that in conventional systems a compressor is required to create the pressure difference which is the driving force of circulating the refrigerant, while in absorption systems, an absorber and generator chamber is used to generate and circulate water vapor that mostly works as the refrigerant in these systems (Except in $NH_3 - H_20$ systems where NH_3 is the refrigerant).

Figure 6.3 shows a schematic of an absorption refrigeration system. Absorption refrigeration differs from vapor-compression air conditioning only in the method of compressing the refrigerant (left of the dashed line in Figure 6.4). In absorption air-conditioning systems, the pressurization is accomplished by first dissolving the refrigerant in a liquid (the absorbent) in the absorber section, then pumping the solution to a high pressure with an ordinary liquid pump.

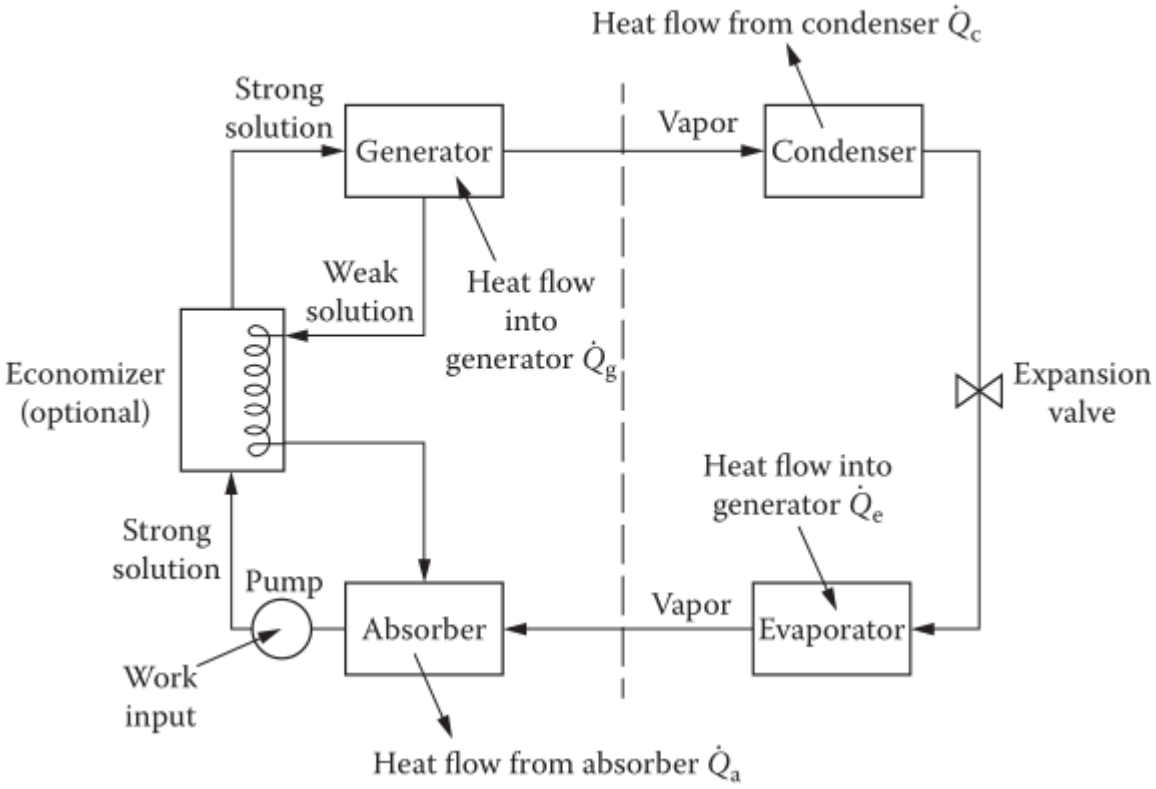

Figure 6.3: Schematic of an absorption refrigeration system.

The low I boiling refrigerant is then driven from solution by the addition of heat in the generator. By this means, the refrigerant vapor is compressed without the large input of high-grade shaft work that the vapor-compression air conditioning demands. The effective performance of an absorption cycle depends on the two materials that comprise the refrigerant–absorbent pair. Desirable characteristics for the refrigerant–absorbent pair are as follow.

1. The absence of a solid-phase absorbent.
2. A refrigerant more volatile than the absorbent so that separation from the absorbent occurs easily in the generator.
3. An absorbent that has a strong affinity for the refrigerant under conditions in which absorption takes place.
4. A high degree of stability for long-term operations
5. Nontoxic and nonflammable fluids for residential applications. This requirement is less critical in industrial refrigeration.

6. A refrigerant that has a large latent heat so that the circulation rate can be kept low.

7. A low fluid viscosity that improves heat and mass transfer and reduces pumping power.

8. Fluids that must not cause long-term environmental effects.

Lithium bromide–water ($LiBr$–H_2O) and ammonia–water (NH_3–H_2O) are the two pairs that meet most of the requirements. In the $LiBr$–H_2O system, water is the refrigerant and LiBr is the absorber, while in the ammonia– water system, ammonia is the refrigerant and water is the absorber. Because the $LiBr$–H_2O system has high volatility ratio, it can operate at lower pressures and, therefore, at the lower generator temperatures achievable by flat-plate collectors. A disadvantage of this system is that the pair tends to form solids. $LiBr$ has a tendency to crystallize when air cooled, and the system cannot be operated at or below the freezing point of water. Therefore, the $LiBr$–H_2O system is operated at evaporator temperatures of 5°C or higher. Using a mixture of $LiBr$ with some other salt as the absorbent can overcome the crystallization problem. The ammonia–water system has the advantage that it can be operated down to very low temperatures. However, for temperatures much below 0°C, water vapor must be removed from ammonia as much as possible to prevent ice crystals from forming. This requires a rectifying column after the boiler. Also, ammonia is a safety Code Group B2 fluid which restricts its use indoors . Other refrigerant–absorbent pairs include [66]:

- Ammonia–salt
- Methylamine–salt
- Alcohol–salt
- Ammonia–organic solvent
- Sulfur dioxide–organic solvent
- Halogenated hydrocarbons–organic solvent
- Water–alkali nitrate
- Ammonia–water–salt

The COP values for absorption air conditioning range from 0.5 for a small, single-stage unit to 0.85 for a double-stage, steam-fired unit. These values are approximately 15% of the COP values that can be achieved by a vapor-compression air conditioner. It is difficult to directly compare the COP of an absorption air conditioner with that of a vapor-compression air conditioner because the efficiency of electric power generation or transmission is not included in the COP of the vapor-compression air conditioning.

6.3 Working Principle of Double effect Absorption Chiller

The components of the double effect system are Low pressure generator (LPG) , high pressure generator(HPG), absorber, condenser, evaporator, pumps , two solution heat exchangers and various sorts of valves.

At the HPG, heat is supplied from the storage tank which is absorbed by the $LiBr–H_2O$ solution to generate primary vapor. The concentration of the $LiBr–H_2O$ solution increases as the primary vapor is generated. This primary vapor enters into the LPG and gets changed into liquid form, giving the heat of condensation to the solution in the LPG. Thus, the solution in the LPG absorbs this heat and generates secondary vapor. As a result, the most concentrated solution is produced inside the LPG, which then moves on to the absorber.

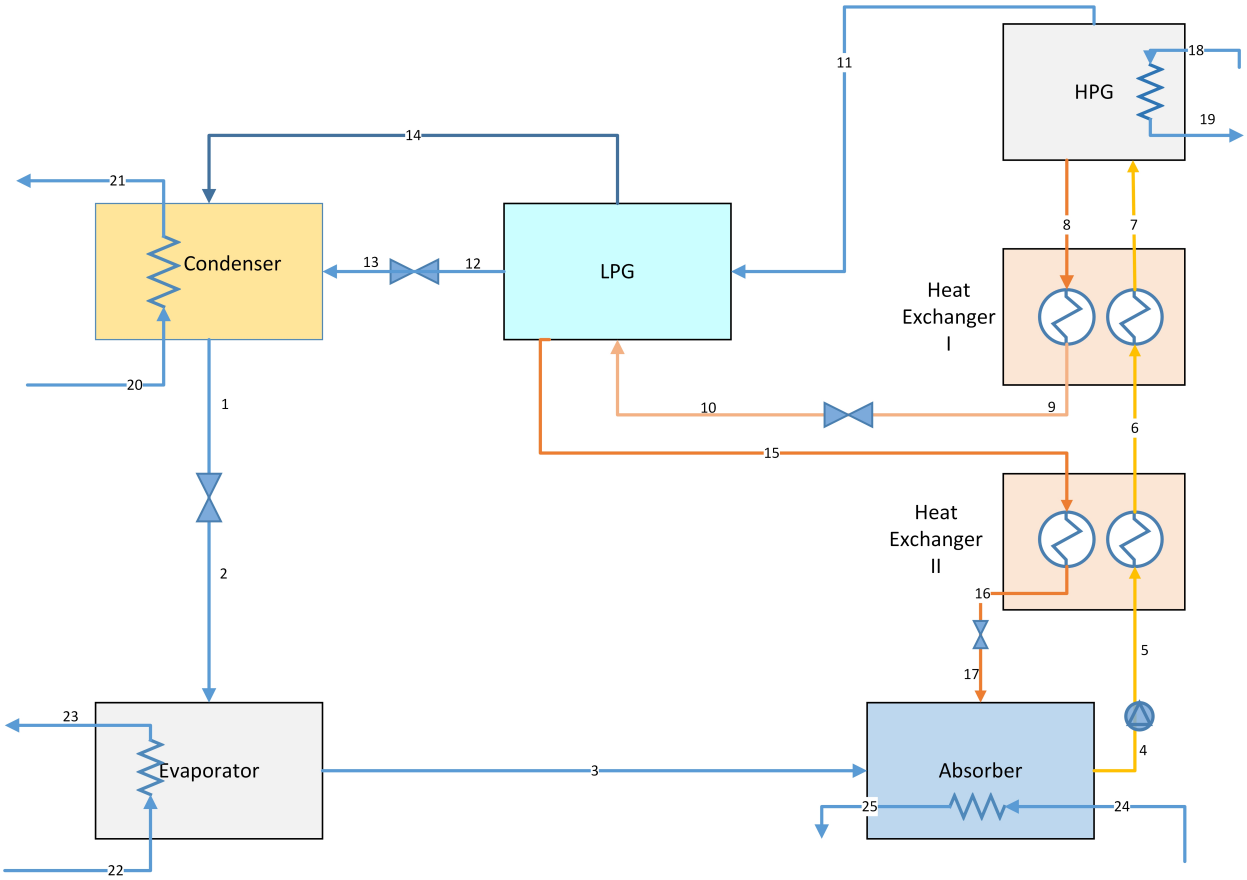

Figure 6.4: Schematic of a double effect $LiBr - H_20$ absorption chiller.

The secondary vapor, along with the condensed water from the LPG enters into the condenser where heat rejection takes place. After condensation, the total amount of liquid refrigerant leaving the condenser is the sum of the refrigerant coming from the LPG and HPG. The liquid refrigerant is then sent to the evaporator, where it changes phase to vapor in low pressure. The refrigerant absorbs the heat of vaporization from

the chilled water loop that carries the unwanted heat from the space that is to be cooled. In the absorber, vapor comes in contact with the concentrated solution from the generators that comes through the solution heat exchangers. The solution absorbs the vapor spontaneously, producing heat and creating a vacuum in the chamber, which is how low pressures are obtained inside the evaporator. From the absorber, $LiBr–H_2O$ solution is sent back the LPG and HPG separately and the cycle is repeated.

6.4 Mathematical Model

A simple model to describe the performance characteristics of absorption chillers, based on the earlier works of other authors, was proposed in Hellmann et al. [67]. The heat transfer equations (which implicitly also include the internal mass transfer) in the four major components relate the transferred heat loads to the driving temperature differences encountered in the heat exchangers (Eq. (1)).

$$Q_E = UA_E\ Z_E\ (t_E - T_E) \tag{6.1}$$

$$Q_C = UA_C\ Z_C\ (T_C - t_C) \tag{6.2}$$

$$Q_A = UA_A\ Z_A\ (T_A - t_A) \tag{6.3}$$

$$Q_G = UA_G\ Z_G\ (t_G - T_G) \tag{6.4}$$

The internal temperatures of the four heat exchangers can be combined using Duhring's rule for the dissolution field of aqueous lithium bromide

$$T_G\ - T_A\ = B\ (T_C - T_E) \tag{6.5}$$

where B is an average solution concentration in the generator and the absorber. Determining the relation between the external temperatures,

$$\frac{Q_G}{UA_G\ Z_G} + \frac{Q_A}{UA_A\ Z_A} + B\ (\frac{Q_C}{UA_C\ Z_C} + \frac{Q_E}{UA_E\ Z_E}) = t_G\ - t_A\ - B\ (t_C\ - t_E) = \Delta\Delta t \tag{6.6}$$

This equation indicates the total of the heat flows exchanged between an absorption chiller and the ambient scale with a characteristic temperature difference $\Delta\Delta t$. When a serial flow from the absorber to the condenser with a constant mass flow rate is assumed,Eq. 6.6 is not appropriate for specifying the actual operating conditions because the absorber outlet temperature is not commonly specified in the manufacturers' data. Therefore, the characteristic temperature difference is reduced to:

$$\Delta\Delta t\ = t_G\ - t_{AC}\ - B(t_{AC}\ - t_E)$$

$$t_{AC}\ = \frac{1}{2}\ (t_{cw,i}\ + t_{cw,o}) \tag{6.7}$$

To eliminate the heat loads of the generator, absorber and condenser from Eq. 6.7, the energy balances of the four major components are introduced:

$$Q_E = m_{ref}\ (h_{vaporE} - h_{liquidC}) \tag{6.8}$$

$$Q_C = m_{ref}\ (h_{vaporG} - h_{liquidC}) \tag{6.9}$$

$$Q_A = m_{ref}\ h_{vaporE} + m_{strong}\ h_{strongG} - m_{weak}\ h_{weakA} - Q_{hex} \tag{6.10}$$

$$Q_G = m_{ref}\ h_{vaporG} + m_{strong}\ h_{strongG} - m_{weak}\ h_{weakA} - Q_{hex} \tag{6.11}$$

where Q_{hex} stands for the heat exchanged in the solution heat exchanger between the strong and the weak solution streams. The heat loads of the condenser, absorber and generator can be expressed as function of the evaporator load as follows

$$Q_C = \frac{h_{vaporG} - h_{liquidC}}{h_{vaporE} - h_{liquidC}}\ Q_E = C\ Q_E \tag{6.12}$$

$$Q_E = \frac{h_{vaporE} - h_{strongG}}{h_{vaporE} - h_{liquidC}}\ Q_E + m_{weak}\ (h_{strongG} - h_{weakA}) - Q_{hex} \tag{6.13}$$

$$\begin{aligned} Q_G &= \frac{h_{vaporG} - h_{strongG}}{h_{vaporE} - h_{liquidC}}\ Q_E + m_{weak}\ (h_{strongG} - h_{weakA}) - Q_{hex} \\ &= G\ Q_E + Q_{loss} \end{aligned} \tag{6.14}$$

where Q_{loss} is an equivalent for the solution heat exchanger loss, that is, the heat that is required in the generator for heating and that is rejected in the absorber for cooling the solution streams to the appropriate internal equilibrium temperatures. After substituting these heat loads in Eq. 6.7, we obtain simple expressions to calculate the cooling capacity and the COP:

$$COP = \frac{Q_E}{Q_G} = \frac{Q_E}{G\ Q_E + Q_{loss}} = \frac{\Delta\Delta t - \Delta\Delta t_{min}}{G\ \Delta\Delta t + (\frac{1}{n} - G)\ \Delta\Delta t_{min}} \tag{6.15}$$

with :

$$s = \frac{1}{\frac{G}{UA_G\ Z_G} + \frac{A}{UA_A\ Z_A} + B\ (\frac{C}{UA_C\ Z_C} + \frac{1}{UA_E\ Z_E})}$$

$$\alpha = \frac{(\frac{1}{UA_G\ Z_G} + \frac{1}{UA_A\ Z_A})}{\frac{G}{UA_G\ Z_G} + \frac{A}{UA_A\ Z_A} + B\ (\frac{C}{UA_C\ Z_C} + \frac{1}{UA_E\ Z_E})}$$

In order to solve this set of equations, Kuhn and Ziegler [68] developed an approach, in which a numerical fit was carried out to improve the results of the characteristic equation method. These authors used the following arbitrary characteristic temperature function:

$$\Delta\Delta t' = t_G + a\ t_{AC} + e\ t_E \tag{6.16}$$

They also defined a linear characteristic equation:

$$Q_E \ = s' \ \Delta\Delta t' \ + r \tag{6.17}$$

Insertion of $\Delta\Delta t$ in the characteristic equation yields

$$Q_E \ = s' \ t_G \ + s' \ a \ t_{AC} \ + s' \ e \ t_E \ + r \tag{6.18}$$

6.5 Absorption system modelling

In order to model the chiller, a linear regression analysis was conducted on a commercially available chiller model designed by BROAD INC. The data points were extracted from the performance curves provided by the manufacturer's catalogue.

Parameters	Unit	Double effect Chiller
Chilled water temperature (inlet/outlet)	°C	14/7
Cooling water temperature (inlet/outlet)	°C	30/37
Hot water temperature (inlet/outlet)	°C	180/165
Hot water mass flow rate	gpm	58
Cooling capacity	TR	66
Pump electricity consumption	kW	2.1
COP	-	1.41

Table 6.1: Technical Specifications of 66TR Double-effect chiller selected from BROAD INC

The performance curves portrayed the variance of the cooling capacity with the cooling water and chilled water temperatures as well as the relation of COP as a function of the output cooling capacity and external temperatures at the different components e.g. evaporator, condenser, generator and absorber. The performance curves are shown below.

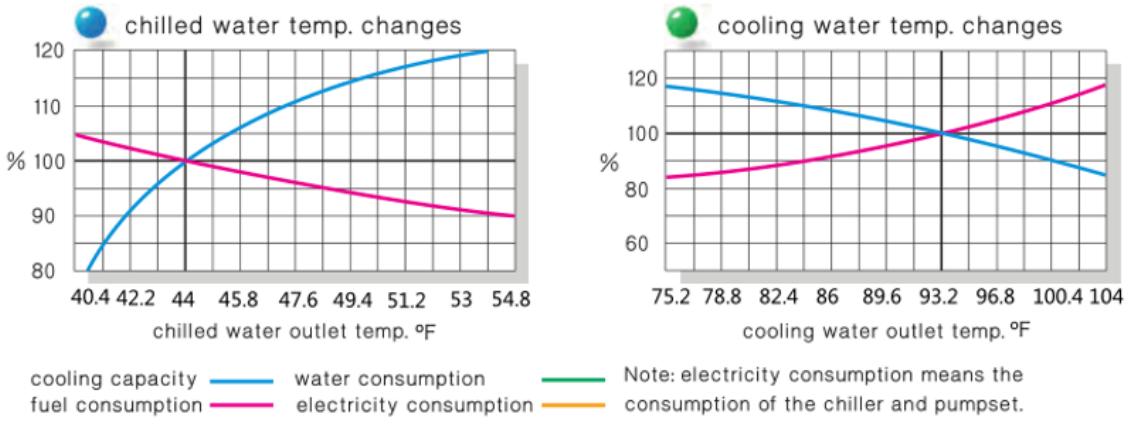

Figure 6.5: Source of data points from Manufacturer's Catalogue

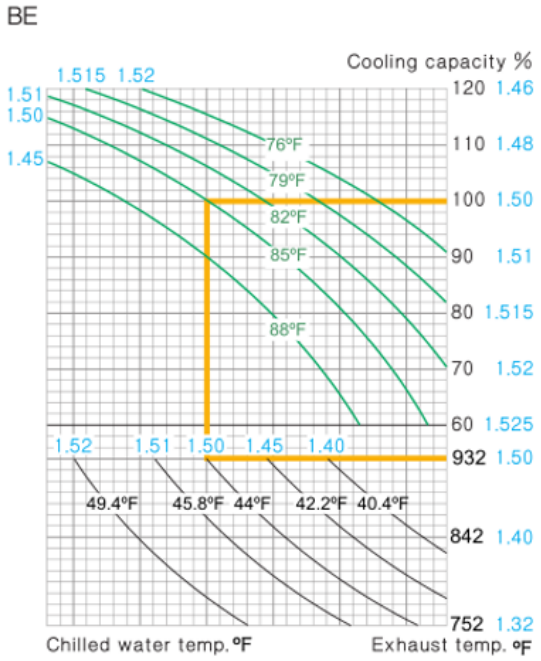

Figure 6.6: Source of data points from Manufacturer's Catalogue

6.5.1 Linear Regression Analysis

After carrying out a linear regression operation on 140 data points extracted from the load curves the final results were obtained. The R squared value was found to be 0.945 and the coefficients of the temperature variables along with the intercept of the linear model was calculated.

Multiple R	0.972445003
R Square	0.945649284
Intercept	-657.2481225
Coefficient of t_G	5.758565946
Coefficient of t_{AC}	-8.593567514
Coefficient of t_G	17.1275222

Table 6.2: Linear Regression results on 140 data points of the 66 TR double effect chiller

The coefficients and the intercept will be used to form the final equation that will predict the cooling capacity.

6.5.2 Line Fit Plot

The line fit plot representing the predicted cooling capacity in comparison with the actual cooling capacity depending on the arbitrary temperature function $\Delta\Delta t$ was plotted. The plot represents the linear model based on the results of the regression.

The data points used here was taken from the performance curves. The cooing capacity variation with the change in external temperatures were taken as real values and the predicted values are calculated using the linear model developed afer carrying out the regression. The plot is shown below.

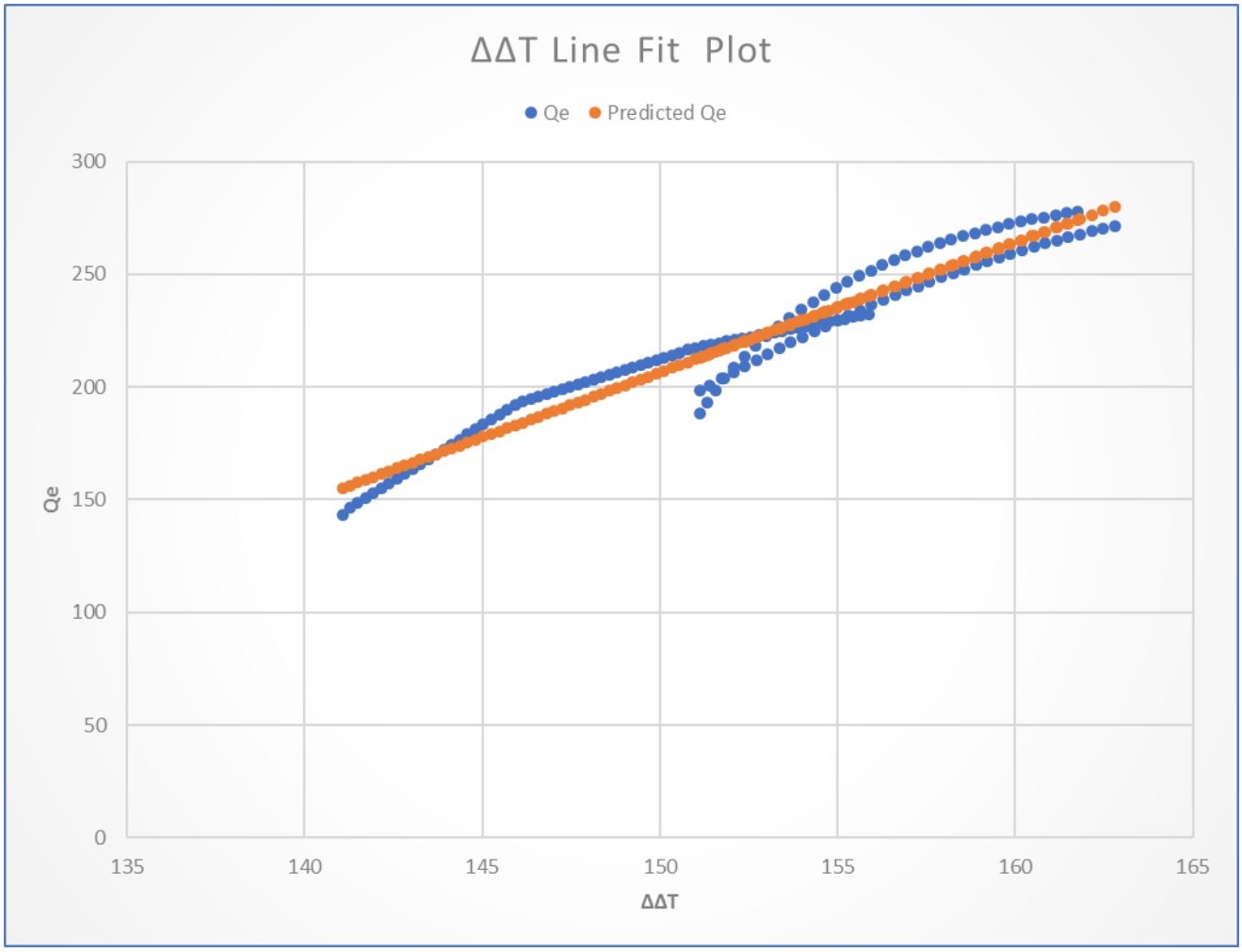

Figure 6.7: Line Fit plot showing the predicted cooling capacity versus the actual cooling capacity against the arbitrary temperature difference function

6.6 Results

Final equation that predicts the chiller capacity if the temperatures at the generator, absorber-condenser and evaporator are known:

$$Q_E = 5.759t_G - 8.594t_{AC} + 17.128t_E - 657.248 \tag{6.19}$$

Based on the final temperatures of water from the storage tank, equation 6.19 was used to calculate the cooling capacities and driving heat input for 8760 hours. The peak cooling capacity reaches up to 158.5 KW and driving input up to 111.14 KW. The following load curves depict the comparison between these two parameters over the course of 1 year.

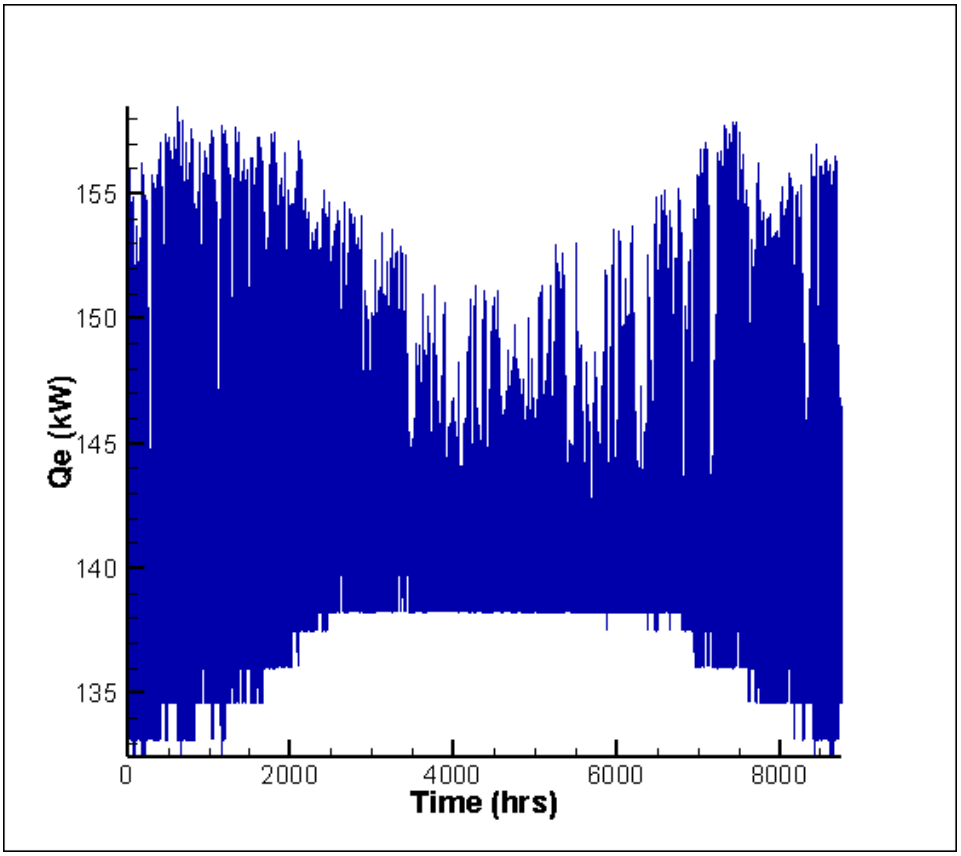

Figure 6.8: 8760 hrs representation of output cooling capacity of the chiller

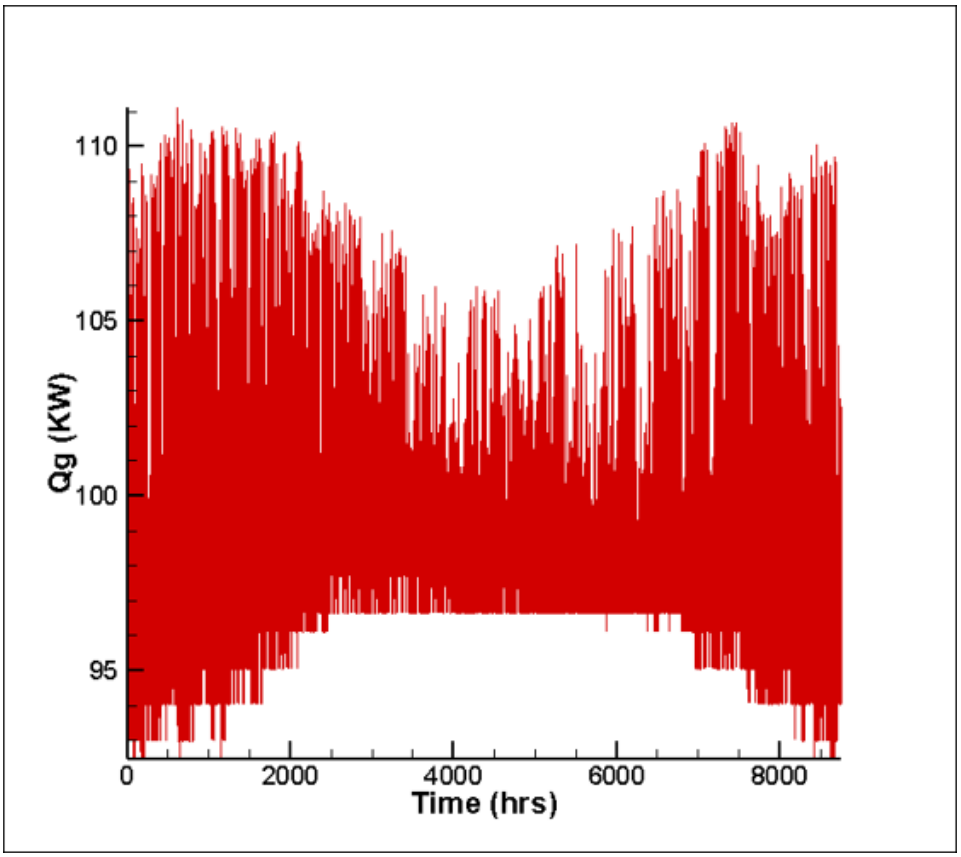

Figure 6.9: 8760 hrs representation of driving heat input required by the chiller

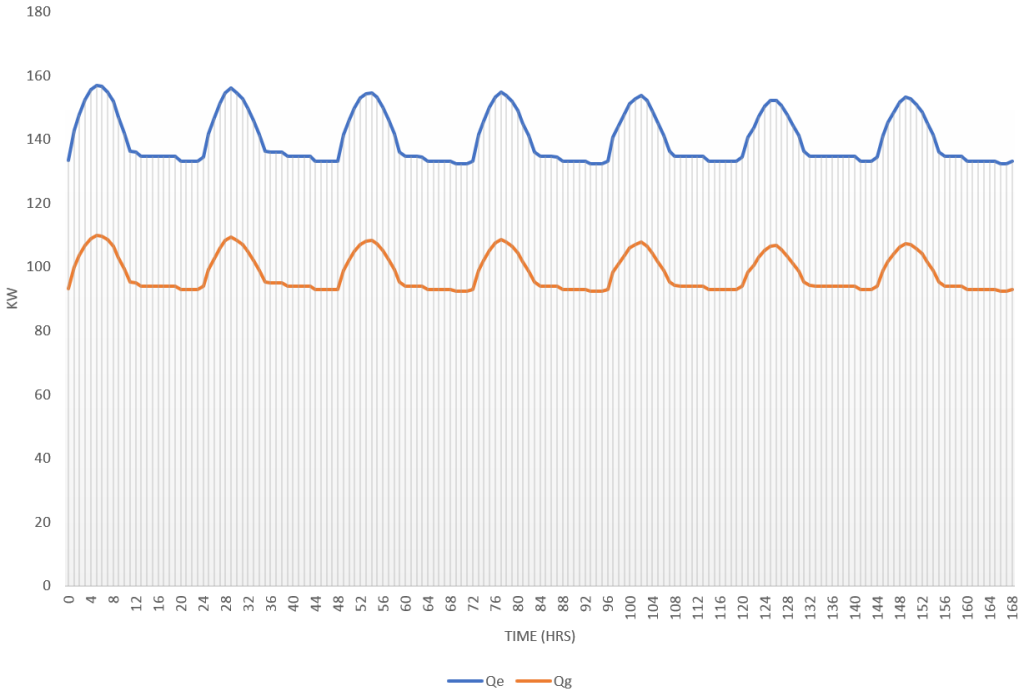

Figure 6.10: Comparison of Q_e and Q_g values on a typical week in January

6.6.1 Auxiliary Heater Requirement

Throughout the course of the year, there are a few months starting from the middle of May to the end of July where the beam solar radiation drops down due to the monsoons bringing in clouds. At this time, the overall heat absorbed at the collectors fall below average. As a result, an auxiliary heat source is required for the chiller in order to be in operation. A typical gas burner with a simple control unit that monitors the temperature at the storage tank and compares it with the temperature requirement of the chiller is sufficient for compensating this situation.

Following figure represents the time period the auxiliary needs to be turned on and the heat requirement from the auxiliary heater for meeting the cooling demand.

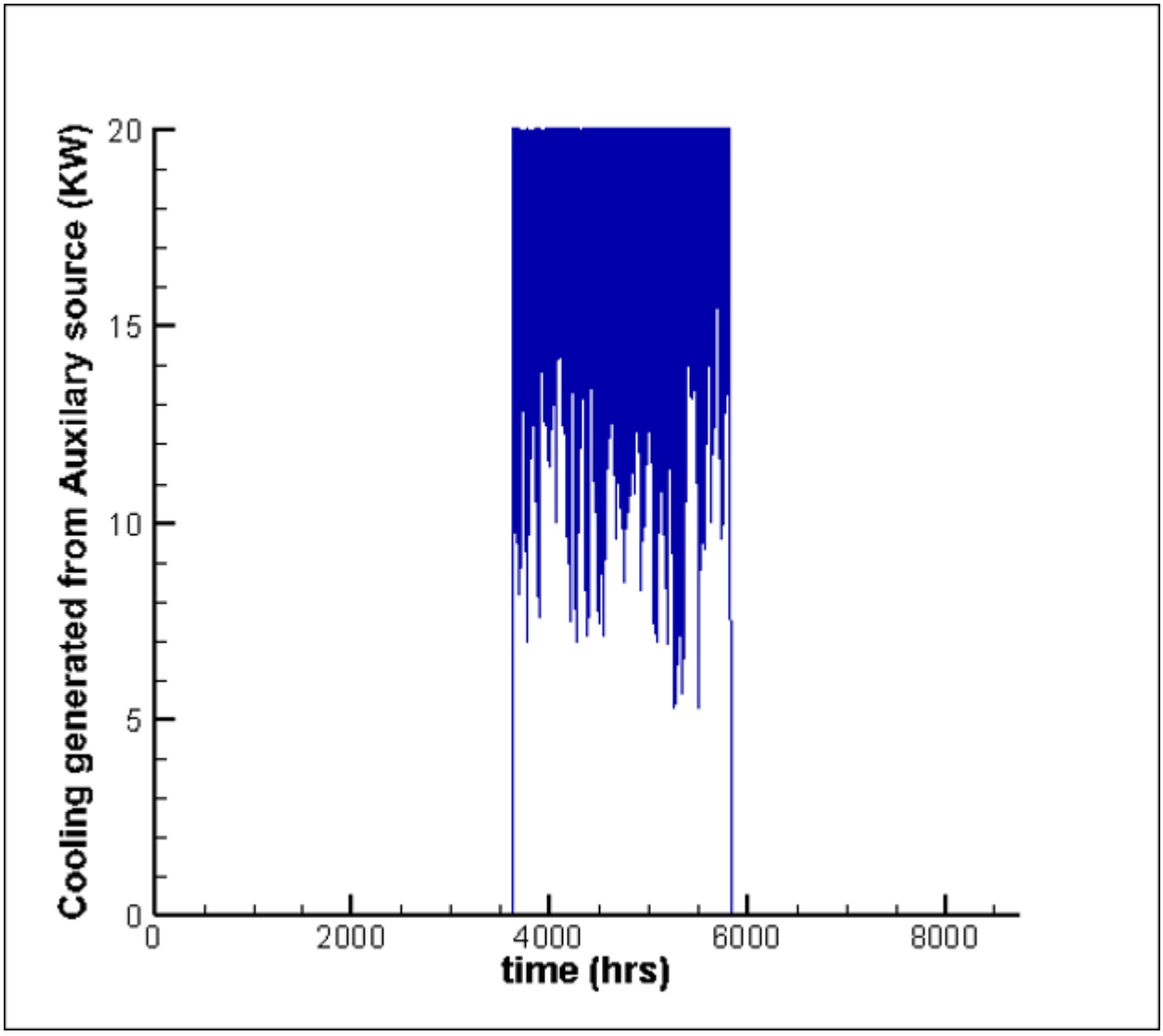

Figure 6.11: Auxiliary Source requirement for meeting cooling demand

6.6.2 Modelled chiller Specifications

SPECIFICATIONS	SIMULATED RESULTS
Chiller Peak Capacity	158.5 KW (45.1 TR)
Chiller Peak Heat Requirement	111.114 KW
Rated COP	1.4
Solar Fraction	75%
Auxiliary Heater Requirement	2208 hrs

Table 6.3: Specifications of modelled chiller

6.6.3 Solar Fraction

The final solar fraction for the double effect chiller coupled with evacuated flat plate collector was found to be 75% and the rest 25% would have to be supplied from the auxiliary source.

Chapter 7

Conclusion

In this study, a Double effect chiller coupled with evacuated flat plate collectors and a thermal storage tank was simulated for meeting the cooling demands of the laboratory. The proposed chiller could reach a peak capacity of 45 Tonnes of refrigeration, and with a COP of 1.4, the system achieved a solar fraction of 75%. The electricity consumption was minimal with only 2.1 kW required by the pump.
However, due to space limitations on the roof of the laboratory, no more than 60 solar collectors could be integrated, which resulted in a lower solar fraction. The incident solar radiation on the collectors dropped heavily in the monsoon season, which resulted in the consistent use of the auxiliary heat source in that period of the year. Optimizing the inlet and outlet temperatures at the different chiller components and combining it with the collectors through an enhanced thermal storage facility could lead to better overall performances and achieve a higher solar fraction.

Air conditioning systems take up to 48% of global energy consumption and are highly responsible for increasing the hydrocarbon footprint across the globe. Renewable energy systems like Solar Absorption Cooling have the potential to shift this imbalance in the field of air conditioning, despite being relatively expensive and difficult to implement on the current status quo. This project creates a grounding for future research for the integration of solar powered air conditioning in places where it is still very foreign and consequently have an impact on a global scale on the long run. SAC systems commercially available on the market are mostly large systems of more than 100 Tonnes which eliminates a lot of possibilities like implementing this technology on regular households, and financially too expensive for non-industrial applications. This project enlightens the fact that small units are also feasible with relatively low fossil fuel or electricity requirements, setting aside the substantial amount of initial investment. Despite the expected hurdles, a successful system has been proposed for further design and optimization, and a pathway has been paved that leads to cleaner sources of air conditioning for the future.

Bibliography

[1] Abdul Ghafoor and Anjum Munir. Worldwide overview of solar thermal cooling technologies. *Renewable and Sustainable Energy Reviews*, 43:763–774, 2015.

[2] Carlos Infante Ferreira and Dong-Seon Kim. Techno-economic review of solar cooling technologies based on location-specific data. *International Journal of Refrigeration*, 39:23–37, 2014.

[3] WS Loh, II El-Sharkawy, Kim Choon Ng, and Bidyut Baran Saha. Adsorption cooling cycles for alternative adsorbent/adsorbate pairs working at partial vacuum and pressurized conditions. *Applied Thermal Engineering*, 29(4):793–798, 2009.

[4] Christian Keil, Stefan Plura, Michael Radspieler, and Christian Schweigler. Application of customized absorption heat pumps for utilization of low-grade heat sources. *Applied Thermal Engineering*, 28(16):2070–2076, 2008.

[5] Byongjoo Kim and Jongil Park. Dynamic simulation of a single-effect ammonia–water absorption chiller. *International Journal of Refrigeration*, 30(3):535–545, 2007.

[6] RM Lazzarin, A Gasparella, and GA Longo. Ammonia-water absorption machines for refrigeration: theoretical and real performances. *International journal of refrigeration*, 19(4):239–246, 1996.

[7] Chad B Dorgan, Steven P Leight, and Charles E Dorgan. *Application guide for absorption cooling/refrigeration using recovered heat*. American Society of Heating, Refrigerating, and Air-Conditioning Engineers, 1995.

[8] Gearoid Foley and Richard Sweetser. Emerging role for absorption chillers in integrated energy systems in america. *Advanced Energy Systems*, 2002.

[9] $Sayigh_1992. Solar Air Conditioning and Refrigeration, page\ iv, 1992.$

[10] P Lamp and F Ziegler. European research on solar-assisted air conditioning. *International Journal of Refrigeration*, 21(2):89–99, 1998.

[11] X.q. Zhai, M. Qu, Yue. Li, and R.z. Wang. A review for research and new design options of solar absorption cooling systems. *Renewable and Sustainable Energy Reviews*, 15(9):4416–4423, 2011.

[12] D.s. Kim and C.a. Infante Ferreira. Solar refrigeration options – a state-of-the-art review. *International Journal of Refrigeration*, 31(1):3–15, 2008.

[13] Pongsid Srikhirin, Satha Aphornratana, and Supachart Chungpaibulpatana. A review of absorption refrigeration technologies. *Renewable and Sustainable Energy Reviews*, 5(4):343–372, 2001.

[14] G.a. Florides, S.a. Kalogirou, S.a. Tassou, and L.c. Wrobel. Modelling, simulation and warming impact assessment of a domestic-size absorption solar cooling system. *Applied Thermal Engineering*, 22(12):1313–1325, 2002.

[15] Rabah Gomri. Investigation of the potential of application of single effect and multiple effect absorption cooling systems. *Energy Conversion and Management*, 51(8):1629–1636, 2010.

[16] George OG Löf and Richard Alton Tybout. The design and cost of optimized systems for residential heating and cooling by solar energy. *Solar Energy*, 16(1):9–18, 1974.

[17] CWJ Van Koppen, JP Simon Thomas, and WR Veltkamp. The actual benefits of thermally stratified storage in a small and a medium size solar system. In *Sun II*, pages 576–580, 1979.

[18] A Al-Karaghouli, I Abood, and NI Al-Hamdani. The solar energy research center building thermal performance evaluation during the summer season. *Energy Conversion and Management*, 32(5):409–417, 1991.

[19] R Best and N Ortega. Solar refrigeration and cooling. *Renewable Energy*, 16(1-4):685–690, 1999.

[20] A Syed, M Izquierdo, P Rodriguez, G Maidment, J Missenden, A Lecuona, and R Tozer. A novel experimental investigation of a solar cooling system in madrid. *International Journal of refrigeration*, 28(6):859–871, 2005.

[21] F Storkenmaier, M Harm, C Schweigler, F Ziegler, J Albers, P Kohlenbach, and T Sengewald. Small-capacity water/libr absorption chiller for solar cooling and waste-heat driven cooling. In *Proceedings of International Congress of Refrigeration, Washington DC, USA*, 2003.

[22] Klaus Hennecke, Ahmet Lokurlu, Matthias Rommel, and Frank Späte. Solare prozesswärme für industrie, meerwasserentsalzung und solarchemie. *Jahrestagung des Forschungs-Verbunds Sonnenenergie in Kooperation mit der Landesinitiative Zukunfts-Energien NRW*, 22(23.09):2005, 2005.

[23] Francesco Calise, Adolfo Palombo, and Laura Vanoli. Design and dynamic simulation of a novel polygeneration system fed by vegetable oil and by solar energy. *Energy Conversion and Management*, 60:204–213, 2012.

[24] M.j. Tierney. Options for solar-assisted refrigeration—trough collectors and double-effect chillers. *Renewable Energy*, 32(2):183–199, 2007.

[25] Osama Ayadi, Marcello Aprile, and Mario Motta. Solar cooling systems utilizing concentrating solar collectors - an overview. *Energy Procedia*, 30:875–883, 2012.

[26] Francesco Calise. High temperature solar heating and cooling systems for different mediterranean climates: Dynamic simulation and economic assessment. *Applied Thermal Engineering*, 32:108–124, 2012.

[27] Annamaria Buonomano, Francesco Calise, Adolfo Palombo, and Maria Vicidomini. Energy and economic analysis of geothermal–solar trigeneration systems: A case study for a hotel building in ischia. *Applied Energy*, 138:224–241, 2015.

[28] Ali Shirazi, Robert A. Taylor, Stephen D. White, and Graham L. Morrison. A systematic parametric study and feasibility assessment of solar-assisted single-effect, double-effect, and triple-effect absorption chillers for heating and cooling applications. *Energy Conversion and Management*, 114:258–277, 2016.

[29] William B Stine. Power from the sun: principles of high temperature solar thermal technology. *NASA STI/Recon Technical Report N*, 88, 1987.

[30] Soteris A Kalogirou. *Solar energy engineering: processes and systems*. Academic Press, 2013.

[31] Ali Shirazi, Robert A Taylor, Graham L Morrison, and Stephen D White. Solar-powered absorption chillers: A comprehensive and critical review. *Energy conversion and management*, 171:59–81, 2018.

[32] John A Duffie and William A Beckman. *Solar engineering of thermal processes*. John Wiley & Sons, 2013.

[33] Roland Winston. Principles of solar concentrators of a novel design. *Solar Energy*, 16(2):89–95, 1974.

[34] CB Eaton and HA Blum. The use of moderate vacuum environments as a means of increasing the collection efficiencies and operating temperatures of flat-plate solar collectors. *Solar Energy*, 17(3):151–158, 1975.

[35] N Benz and T Beikircher. High efficiency evacuated flat-plate solar collector for process steam production. *Solar Energy*, 65(2):111–118, 1999.

[36] Cristoforo Benvenuti. Evacuable flat panel solar collector, October 12 2010. US Patent 7,810,491.

[37] R Moss and Stan Shire. Design and performance of evacuated solar collector microchannel plates. In *EuroSun Conference, Aix-les-Bains, France*, 2014.

[38] GSF Shire, RW Moss, Paul Henshall, Farid Arya, PC Eames, and Trevor Hyde. Development of an efficient low-and medium-temperature vacuum flat-plate solar thermal collector. In *Renewable Energy in the Service of Mankind Vol II*, pages 859–866. Springer, 2016.

[39] G Francia. Pilot plants of solar steam generating stations. *Solar Energy*, 12(1):51–64, 1968.

[40] Jeffrey Gordon. *Solar energy: the state of the art: ISES position papers*. Earthscan, 2001.

[41] WT Xie, YJ Dai, RZ Wang, and K Sumathy. Concentrated solar energy applications using fresnel lenses: A review. *Renewable and Sustainable Energy Reviews*, 15(6):2588–2606, 2011.

[42] Paul Henshall, Roger Moss, Farid Arya, Philip C Eames, Stan Shire, and Trevor Hyde. An evacuated enclosure design for solar thermal energy applications. 2014.

[43] Sadık Kakaç, Ramesh K Shah, and Win Aung. Handbook of single-phase convective heat transfer. 1987.

[44] Marco Lorenzini, Gian Luca Morini, et al. Poiseuille and nusselt numbers for laminar flow in microchannels with rounded corners. 2009.

[45] Rudolf Richter, Martin Bachmann, Wouter Dorigo, and A Muller. Influence of the adjacency effect on ground reflectance measurements. *IEEE Geoscience and Remote Sensing Letters*, 3(4):565–569, 2006.

[46] PI Cooper. The absorption of radiation in solar stills. *Solar energy*, 12(3):333–346, 1969.

[47] SA Klein. Calculation of monthly average insolation on tilted surfaces. *Solar energy*, 19(4):325–329, 1977.

[48] Hoyt Clarke Hottel. Performance of flat-plate solar heat collectors. *Trans. ASME 64*, 91, 1942.

[49] Khaled Zelzouli, Amenallah Guizani, Ramzi Sebai, and Chakib Kerkeni. Solar thermal systems performances versus flat plate solar collectors connected in series. *Engineering*, 4(12):881, 2012.

[50] HN Gari and RI Loehrke. A controlled buoyant jet for enhancing stratification in a liquid storage tank. *Journal of Fluids Engineering*, 104(4):475–481, 1982.

[51] Zalman Lavan and James Thompson. Experimental study of thermally stratified hot water storage tanks. *Solar energy*, 19(5):519–524, 1977.

[52] JK Kuhn, GF von Fuchs, AW Warren, and AP Zob. Developing and upgrading of solar system thermal energy storage simulation models. technical progress report, march 1, 1978-august 31, 1978. Technical report, Boeing Computer Services Co., Seattle, WA (USA), 1979.

[53] G Oberndorfer, WA Beckman, and SA Klein. Sensitivity of annual solar fraction of solar space and water heating systems to tank and collector heat exchanger model parameters. Technical report, Univ. of Wisconsin, Madison, WI (US), 1999.

[54] Eberhard Markus Kleinbach, WA Beckman, and SA Klein. Performance study of one-dimensional models for stratified thermal storage tanks. *Solar energy*, 50(2):155–166, 1993.

[55] James Edward Braun, SA Klein, and JW Mitchell. Seasonal storage of energy in solar heating. *Solar Energy*, 26(5):403–411, 1981.

[56] Neil Winterton. Chlorine: the only green element–towards a wider acceptance of its role in natural cycles. *Green Chemistry*, 2(5):173–225, 2000.

[57] DJ Morrison and SI Abdel-Khalik. Effects of phase-change energy storage on the performance of air-based and liquid-based solar heating systems. *Solar Energy*, 20(1):57–67, 1978.

[58] John A Simmons. Reversible oxidation of metal oxides for thermal energy storage. In *Sharing the Sun: Solar Technology in the Seventies, Volume 8*, volume 8, pages 219–225, 1976.

[59] FT Bacon. British patent 667 298. *The manuscript of this paper was received on 8 October*, 1964.

[60] Hans Bode. Lead-acid batteries. 1977.

[61] Clarence M Shepherd. Design of primary and secondary cells ii. an equation describing battery discharge. *Journal of the Electrochemical Society*, 112(7):657–664, 1965.

[62] Jürgen Helmut Eckstein. *Detailed modelling of photovoltaic system components*. PhD thesis, 1990.

[63] Faye C McQuiston, Jeffrey D Spitler, et al. *Cooling and heating load calculation manual*. 1992.

[64] ASHRAE Handbook. Fundamentals volume of the ashrae handbook, 2005.

[65] J. C. V. Chinnappa and N. E. Wijeysundera. Simulation of solar-powered ammonia-water integrated hybrid cooling system. *Journal of Solar Energy Engineering*, 114(2):125–127, Jan 1992.

[66] R.a. Macriss, T.s. Zawacki, M.t. Kouo, and D.m. Sneed. Analysis of advanced conceptual designs for single-family-size absorption chillers. Jan 1978.

[67] HM Hellmann, C Schweigler, and F Ziegler. The characteristic equation of sorption chillers. In *Proc. of the Int. Sorption Heat Pump Conf.(ISHPC 1999), Munich*, volume 24, page 26, 1999.

[68] A Kühn, S Petersen, F Ziegler, P Kohlenbach, M Harm, and C Schweigler. Operational results of a 10 kw absorption chiller for low-grade driving heat. In *Proc. of the Int. Sorption Heat Pump Conf., June 22*, volume 24, 2005.

Appendix A

Values for Hour Angle ω

Hour	**Hour Angle, ω**
01 00	-165^o
02 00	-150^o
03 00	-135^o
04 00	-120^o
05 00	-105^o
06 00	-090^o
07 00	-075^o
08 00	-060^o
09 00	-045^o
10 00	-030^o
11 00	-015^o
12 00	000^o
13 00	+015^o
14 00	+030^o
15 00	+045^o
16 00	+060^o
17 00	+075^o
18 00	+090^o
19 00	+105^o
20 00	+120^o
21 00	+135^o
22 00	+150^o
23 00	+165^o

Table A.1: Variation of Hour Angle